Innovation, Sciences et Développement économique Canada
Office de la Propriété Intellectuelle du Canada

Innovation, Science and Economic Development Canada
Canadian Intellectual Property Office

CA 2960294 C 2023/11/21

(11)(21) 2 960 294

(12) BREVET CANADIEN
CANADIAN PATENT

(13) C

(86) Date de dépôt PCT/PCT Filing Date: 2015/10/05
(87) Date publication PCT/PCT Publication Date: 2016/04/07
(45) Date de délivrance/Issue Date: 2023/11/21
(85) Entrée phase nationale/National Entry: 2017/03/03
(86) N° demande PCT/PCT Application No.: US 2015/053930
(87) N° publication PCT/PCT Publication No.: 2016/054621
(30) Priorité/Priority: 2014/10/03 (US62/059,663)

(51) Cl.Int./Int.Cl. *C07F 7/12* (2006.01)

(72) Inventeurs/Inventors:
PENA HUESO, JOSE, ADRIAN, US;
OSMALOV, DAVID, US;
DONG, JIAN, US;
USREY, MONICA, US;
POLLINA, MICHAEL, US;
DU, PENG, US;
ZHOU, LIU, US;
...

(73) Propriétaire/Owner:
SILATRONIX, INC., US

(74) Agent: GOWLING WLG (CANADA) LLP

(54) Titre : SILANES FONCTIONNALISES ET COMPOSITIONS D'ELECTROLYTES ET DISPOSITIFS ELECTROCHIMIQUES LES CONTENANT
(54) Title: FUNCTIONALIZED SILANES AND ELECTROLYTE COMPOSITIONS AND ELECTROCHEMICAL DEVICES CONTAINING THEM

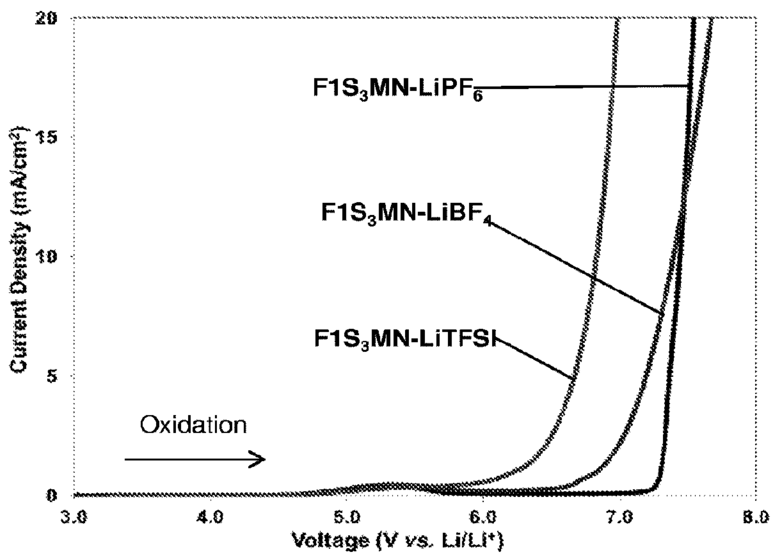

(57) Abrégé/Abstract:
Described are compounds of the structure R4-$_a$-Si-(Sp-Y)$_a$-Z$_b$, wherein "a" is integer from 1 to 4; "b" is an integer from 0 to (3 x a); "Z," which is absent when "b "R" or formula (II), wherein each "R" is halogen, C_{1-6} linear or branched alkyl, alkenyl, or alkynyl or C_{1-6}

(72) **Inventeurs(suite)/Inventors(continued)**: JOHNSON, TOBIAS, US; GILBERT, DEBORAH, US; WEST, ROBERT, US

(57) **Abrégé(suite)/Abstract(continued)**:
linear or branched halo-alkyl, halo-alkenyl, or halo-alkynyl; each "Sp" C_{1-15} linear or branched alkylenyl or CMS linear or branched halo-alkylenyl; and each "Y" an organic polar group. Also described are electrolyte compositions containing one or more of these compounds.

CA 02960294 2017-03-03

(12) INTERNATIONAL APPLICATION PUBLISHED UNDER THE PATENT COOPERATION TREATY (PCT)

(19) World Intellectual Property Organization
International Bureau

(43) International Publication Date
7 April 2016 (07.04.2016)

(10) International Publication Number
WO 2016/054621 A1

(51) International Patent Classification: *C07F 7/12* (2006.01)

(21) International Application Number: PCT/US2015/053930

(22) International Filing Date: 5 October 2015 (05.10.2015)

(25) Filing Language: English

(26) Publication Language: English

(30) Priority Data: 62/059,663 3 October 2014 (03.10.2014) US

(71) Applicant: **SILATRONIX, INC.** [US/US]; 3587 Anderson Street, Suite 108, Madison, MA 53704 (US).

(72) Inventors: **PENA HUESO, Jose, Adrian**; 4701 Sheboygan Avenue, Apt. 107, Madison, WI 53705 (US). **OSMALOV, David**; 4805 Wallace Avenue, Monona, WI 53716 (US). **DONG, Jian**; 2409 Denby Court, Fort Collins, CO 80526 (US). **USREY, Monica**; 330 Marinette Trail, Madison, WI 53705 (US). **POLLINA, Michael**; 7975 Millstream Ct., Elkridge, MD 20175 (US). **DU, Peng**; 525 Kelvington Drive, #4, Sun Prairie, WI 53590 (US). **ZHOU, Liu**; 3826 Manito Ct., Middleton, WI 53562 (US). **JOHNSON, Tobias**; 917 Burning Wood Way, Madison, WI 53704 (US). **GILBERT, Deborah**; 2735 Sunflower DrIve, Fitchburg, WI 53711 (US). **WEST, Robert**; 305 Nautilus Drive, Madison, WI 53705 (US).

(74) Agents: **SARA, Charles S.** et al.; Dewitt Ross & Stevens S.C., 2 East Mifflin Street, Suite 600, Madison, WI 53703-2865 (US).

(81) Designated States *(unless otherwise indicated, for every kind of national protection available)*: AE, AG, AL, AM, AO, AT, AU, AZ, BA, BB, BG, BH, BN, BR, BW, BY, BZ, CA, CH, CL, CN, CO, CR, CU, CZ, DE, DK, DM, DO, DZ, EC, EE, EG, ES, FI, GB, GD, GE, GH, GM, GT, HN, HR, HU, ID, IL, IN, IR, IS, JP, KE, KG, KN, KP, KR, KZ, LA, LC, LK, LR, LS, LU, LY, MA, MD, ME, MG, MK, MN, MW, MX, MY, MZ, NA, NG, NI, NO, NZ, OM, PA, PE, PG, PH, PL, PT, QA, RO, RS, RU, RW, SA, SC, SD, SE, SG, SK, SL, SM, ST, SV, SY, TH, TJ, TM, TN, TR, TT, TZ, UA, UG, US, UZ, VC, VN, ZA, ZM, ZW.

[Continued on next page]

(54) Title: FUNCTIONALIZED SILANES AND ELECTROLYTE COMPOSITIONS AND ELECTROCHEMICAL DEVICES CONTAINING THEM

(57) Abstract: Described are compounds of the structure $R4-_a-Si-(Sp-Y)_a-Z_b$, wherein "a" is integer from 1 to 4; "b" is an integer from 0 to (3 x a); "Z," which is absent when "b "R" or formula (II), wherein each "R" is halogen, C_{1-6} linear or branched alkyl, alkenyl, or alkynyl or C_{1-6} linear or branched halo-alkyl, halo-alkenyl, or halo-alkynyl; each "Sp" C_{1-15} linear or branched alkylenyl or CMS linear or branched halo-alkylenyl; and each "Y" an organic polar group. Also described are electrolyte compositions containing one or more of these compounds.

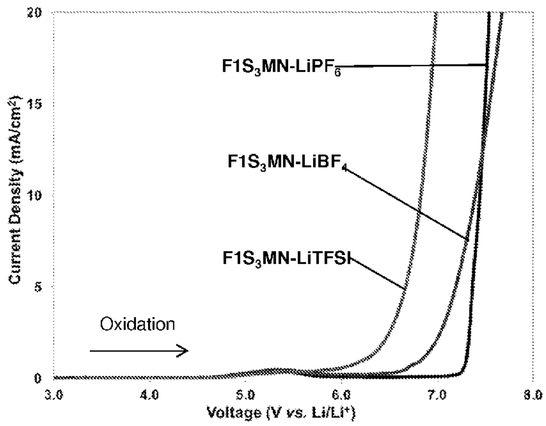

FIG. 1A

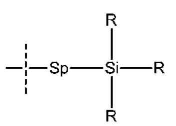

(II)

WO 2016/054621 A1

WO 2016/054621 A1

(84) Designated States *(unless otherwise indicated, for every kind of regional protection available)*: ARIPO (BW, GH, GM, KE, LR, LS, MW, MZ, NA, RW, SD, SL, ST, SZ, TZ, UG, ZM, ZW), Eurasian (AM, AZ, BY, KG, KZ, RU, TJ, TM), European (AL, AT, BE, BG, CH, CY, CZ, DE, DK, EE, ES, FI, FR, GB, GR, HR, HU, IE, IS, IT, LT, LU, LV, MC, MK, MT, NL, NO, PL, PT, RO, RS, SE, SI, SK, SM, TR), OAPI (BF, BJ, CF, CG, CI, CM, GA, GN, GQ, GW, KM, ML, MR, NE, SN, TD, TG).

Declarations under Rule 4.17:

— *of inventorship (Rule 4.17(iv))*

Published:

— *with international search report (Art. 21(3))*

— *before the expiration of the time limit for amending the claims and to be republished in the event of receipt of amendments (Rule 48.2(h))*

FUNCTIONALIZED SILANES AND ELECTROLYTE COMPOSITIONS AND ELECTROCHEMICAL DEVICES CONTAINING THEM

BACKGROUND

Liquid electrolytes in Li-ion batteries conventionally comprise a lithium salt, usually $LiPF_6$, in an organic solvent blend of ethylene carbonate (EC) and one or more co-solvents such as dimethyl carbonate (DMC), diethyl carbonate (DEC), or ethylmethyl carbonate (EMC). Unfortunately, $LiPF_6$ is unstable in these carbonate solvents above 60 °C, as well as at charge voltages above 4.3 volts. Operation of a Li-ion battery above these temperatures or voltages results in rapid degradation of electrode materials and battery performance. In addition, current Li-ion electrolyte solvents exhibit flashpoints around 35°C, and are the major source of the energy released during an extreme Li-ion cell failure. Given these significant limitations, current electrolytes are impeding the development of advanced Li-ion batteries for all uses, including portable products, electric drive vehicles (EDVs), and utility scale use. A dramatic reduction in battery failure rate is also required for large scale Li-ion batteries to effectively serve applications in EDVs and grid storage.

Thus, there is a long-felt and unmet need for improved electrolyte solutions in energy storage devices such as Li-ion batteries.

Date Reçue/Date Received 2022-05-30

SUMMARY OF THE INVENTION

Disclosed herein are organosilicon (OS) compounds for use as electrolyte solvents in electrochemical devices, among other uses.

In general, OS compounds are environmentally friendly, non-flammable, high temperature-resistant materials. These characteristics make OS materials well-suited for use as electrolyte solvents, binders, and coatings in energy storage devices. OS-based electrolytes are compatible with all lithium (Li) based electrochemical systems, including primary and rechargeable batteries, (i.e. Li-ion, Li-air), and capacitors (i.e. super/ultra-capacitors). The process of designing OS-based electrolytes into a Li battery involves limited changes in the cell design, and these electrolytes can be incorporated into production operations with existing manufacturing processes and equipment.

The OS compounds described herein can be used as liquid electrolyte solvents that replace the carbonate based solvent system in traditional Li-ion batteries. The OS-based solvents provide significant improvements in performance and abuse tolerance in Li-ion batteries, including increased thermal stability for longer life at elevated temperatures, increased electrolyte flash points for improved safety, increased voltage stability to allow use of high voltage cathode materials and achieve higher energy density, reduced battery failure rates for consistency with the requirements for large scale Li batteries used in EDV and grid storage applications, and compatibility with materials currently in use in Li-ion batteries for ease of adoption in current designs. Electrical double-layer capacitor (EDLC) devices have also demonstrated functionality with OS based electrolytes. The OS compounds described herein can be used in OS-based electrolyte blends to meet the requirements of specific applications in the industrial, military, and consumer product devices.

The objects and advantages of the compounds and electrolyte formulations will appear more fully from the following detailed description and accompanying drawings.

Thus, disclosed herein are:

1. A compound selected from the group consisting of:

$$(R)_{4-a}\text{---}Si\text{---}(Sp\text{---}Y)_a\text{---}Z_b \quad \text{(Formula I)}$$

wherein:

"a" is an integer from 1 to 4; "b" is an integer from 0 to (3 x a);

"Z," which is absent when "b" = 0, is selected from the group consisting of "R" and

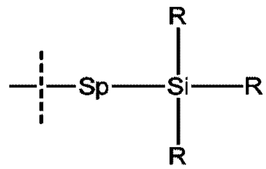
(Formula II);

where each “R” is independently selected from the group consisting of halogen, C_{1-6} linear or branched alkyl, alkenyl, or alkynyl and C_{1-6} linear or branched halo-alkyl, halo-alkenyl, or halo-alkynyl;

each “Sp” in Formulas I and II is independently selected from the group consisting of C_{1-15} linear or branched alkylenyl and C_{1-15} linear or branched halo-alkylenyl; and

each “Y” in Formula I is independently selected from the group consisting of an organic polar group.

2. The compound of Claim 1, wherein each “Y” is independently an organic polar group selected from the group consisting of:

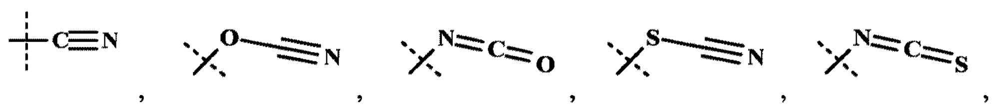

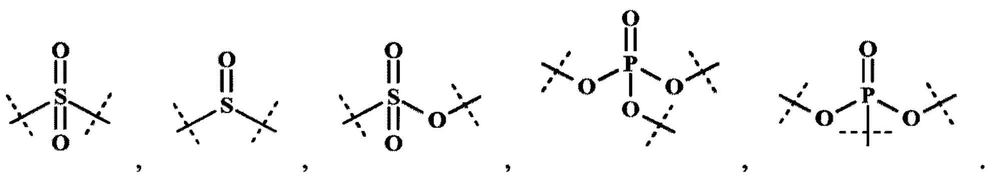

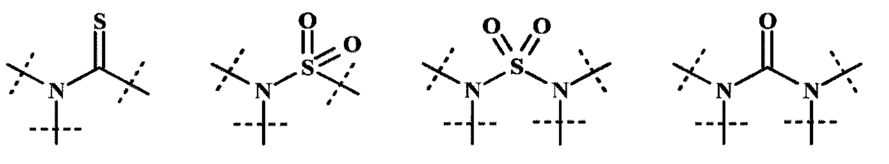

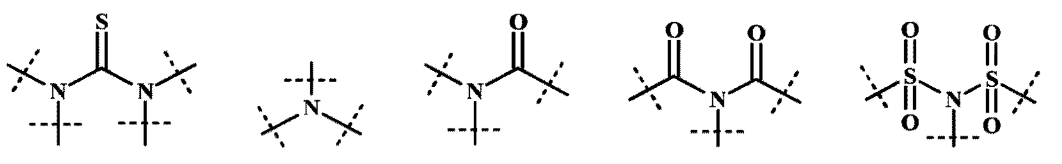

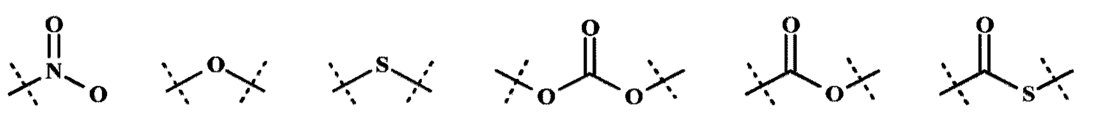

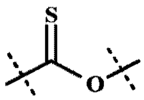 , 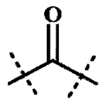 , 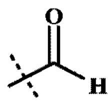 , 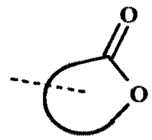 , 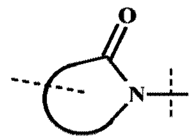 , 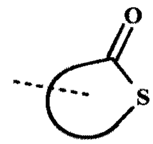 ,

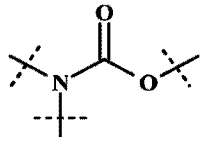 , 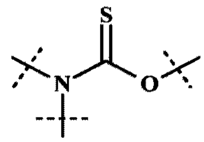 , 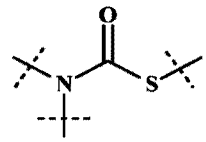 , 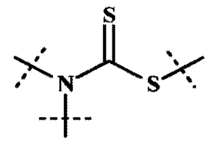 , and

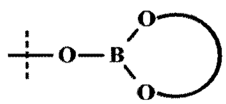 ,

wherein a curved bond denotes a C_{2-6} akylene bridging moiety.

3. The compound of Claim 2, wherein each "Y" is independently an organic polar group selected from the group consisting of:

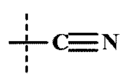 , 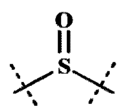 , and 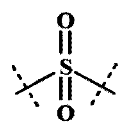 .

4. The compound of Claim 3, wherein each "R" is independently selected from the group consisting of fluorine and C_{1-6} linear or branched fluoro-alkyl, fluoro-alkenyl, or fluoro-alkynyl; and

each "Sp" in Formulas I and II is independently selected from the group consisting of C_{1-15} linear or branched fluoro-alkylenyl.

5. The compound of any one of Claims 1-4, wherein "a" is 1, and "b" is 0 to 3.

6. The compound according to Claim 5, wherein "b" is 1 and "Z" is "-R".

7. The compound according to Claim 5, wherein at least one "R" is fluorine, and each "Sp" is independently selected from the group consisting of C_{1-6} linear alkylene and C_{1-6} linear fluoro-alkylene.

8. The compound of any one of Claims 1-4, wherein "a" is 2, and "b" is 0 to 6.

9. The compound according to Claim 7, wherein "b" is 1 and "Z" is "R".

10. The compound according to Claim 7, wherein at least one "R" is fluorine, and each "Sp" is independently selected from the group consisting of C_{1-6} linear alkylene.

11. The compound of any one of Claims 1-4, wherein "a" is 3, and "b" is 0 to 9.

12. The compound according to Claim 11, wherein "b" is 1 and "Z" is "R".

13. The compound according to Claim 11, wherein at least one "R" is fluorine, and each "Sp" is independently selected from the group consisting of C_{1-6} linear alkylene.

14. The compound of any one of Claims 1-4, wherein "a" is 4, and "b" is 0 to 12.

15. The compound according to Claim 14, wherein "b" is 1 and "Z" is "R".

16. The compound according to Claim 14, wherein at least one "R" is fluorine, and each "Sp" is independently selected from the group consisting of C_{1-6} linear alkylene.

17. The compound of any one of Claims 1-4, wherein at least one "R" is fluorine.

18. An electrolyte composition comprising a compound as recited in any one of Claims 1-4, in combination with a salt.

19. The electrolyte composition of Claim 18, wherein the salt is a lithium-containing salt.

20. An electrochemical device comprising an electrolyte composition as recited in Claim 18.

In more limited versions of the compounds, each "Y" is independently an organic polar group selected from the group consisting of:

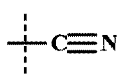

,
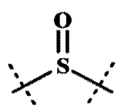

,
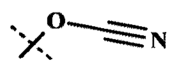

,
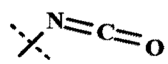

,
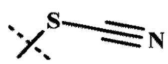

,

, and
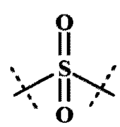

.

Additionally, each "Y" may optionally and independently be an organic polar group selected from the group consisting of:
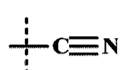

,
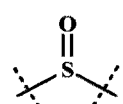

,
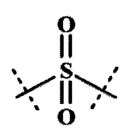

.

In an alternative version of the compounds, "a" is 1, and "b" is 0 to 2; optionally "b" is 1 and "Z" is R. In this version, an optional embodiment is for at least one "R" to be fluorine, and each "Sp" is independently selected from the group consisting of C_{1-6} linear or branched alkylene which could be fluorinated.

In another alternative version of the compounds, "a" is 2, and "b" is 0 to 6; optionally "b" is 1 and "Z" is R. In this version, an optional embodiment is for at least one "R" to be fluorine, and each "Sp" is independently selected from the group consisting of C_{1-6} linear or branched alkylene which could be fluorinated.

In yet another alternative version of the compounds, "a" is 3, and "b" is 0 to 9; optionally "b" is 1 and "Z" is R. In this version, an optional embodiment is for at least one "R" to be fluorine, and each "Sp" is independently selected from the group consisting of C_{1-6} linear or branched alkylene which could be fluorinated.

In still another alternative version of the compounds, "a" is 4, and "b" is 0 to 12; optionally, "b" is 1 and "Z" is R. In this version, an optional embodiment is for at least one "R" to be fluorine, and each "Sp" is independently selected from the group consisting of C_{1-6} linear or branched alkylene which could be fluorinated.

Also disclosed herein is an electrolyte composition comprising a compound as herein, in combination with a salt. Lithium-containing salts are preferred. Also disclosed herein is an electrochemical device comprising the electrolyte composition.

Due to the nature of the subscripts "a" and "b", the following generic structures are explicitly within the scope of the compounds disclosed and claimed herein:

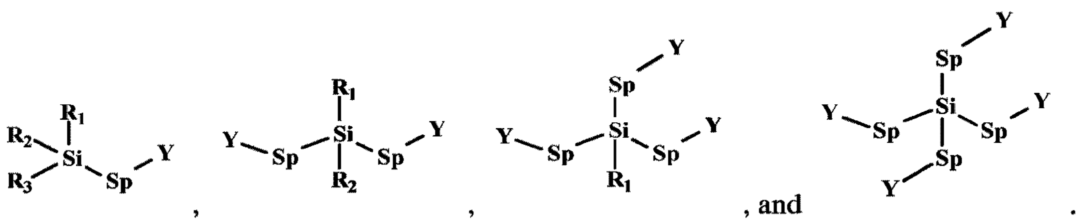

The various R groups are as defined above for "R"; Sp is as defined above, Y is as defined above. Preferably, in all versions of the compounds, Y is an organic polar group that can coordinate Li^+.

When the polar group Y has a valency of two (2) or more it will have more than one site for substitution. Thus, there can be more than one silicon atom bonded to Y through a spacer group, as noted in the definition for Z above. Thus, the following structures are also explicitly within the scope of the compounds disclosed and claimed herein:

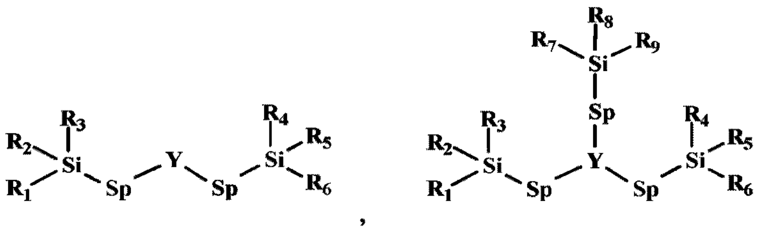

, etc.

In all versions of the compounds, "halogen," includes fluoro, chloro, bromo, and iodo. Fluoro and chloro are the preferred halogen substituents. The term "salt" is used herein in its conventional chemical sense to mean ionic compounds that result from the neutralization reaction of an acid and a base. As used herein, salt is purposefully defined broadly to include all salts, including, but not limited to sodium salts, lithium salts, magnesium salts, borate salts, phosphate salts, and the like. Non-limiting examples include sodium hexafluorophosphate, sodium perchlorate, sodium bis-trifluoromethanesulfonimide, magnesium hexafluorophosphate, magnesium perchlorate, magnesium bis-trifluoromethanesulfonimide, magnesium tetrafluoroborate, magnesium trifluoromethyl sulfonate, tetraethylammonium tetrafluoroborate (TEA-TFB), tetrabutylphosphonium tetrafluoroborate, tetrabutylphosphonium hexafluorophosphate, tetrabutylammonium tetrafluoroborate, tetraethylammonium hexafluorophosphate, tetraethylammonium perchlorate, and tetraethylammonium bistrifluoromethanesulfonimidate. The term "lithium-containing salt" explicitly includes, but is not limited to, $LiClO_4$, $LiBF_4$, $LiAsF_6$, $LiPF_6$, $LiCF_3SO_3$, $Li(CF_3SO_2)_2N$, $Li(CF_3SO_2)_3C$, $LiN(SO_2C_2F_5)_2$, lithium alkyl fluorophosphates and lithium bis(chelato)borates.

Also disclosed herein are electrolyte compositions comprising one or more organosilicon compounds as recited in the preceding paragraphs. Also disclosed herein are electrochemical devices comprising such electrolyte compositions. The compounds disclosed herein are highly useful for formulating electrolytes for use in charge-storage devices of all kinds (*e.g.*, cells, batteries, capacitors, and the like).

The organosilicon solvent molecules disclosed herein have remarkable and unexpected thermal stability as compared to conventional carbonate solvents. Even when formulated into electrolyte compositions including lithium salts such as $LiPF_6$, the organosilicon solvents exhibit remarkable resistance to breakdown during high-temperature exposure and operation. As shown in the examples and figures, several variations of the organosilicon solvent molecules disclosed herein have demonstrated thermostability in the presence of $LiPF_6$ at temperatures up to and exceeding 175°C. These data demonstrate the intrinsic benefit of silicon as an essential stabilizing element within the organosilicon molecular design. Variations of molecules disclosed herein include non-fluorinated, fluorinated, multi-fluorinated, multi-functional, and alternate alkyl structures, as well as many different Li^+ coordinating functionalities. The functional groups include nitriles, carbonates, sulfones, and esters among many others. Both gas phase and liquid phase decomposition were measured by EI-MS and NMR respectively to determine breakdown of electrolytes with organosilicon solvent plus 1M $LiPF_6$ salt after exposure to 175°C for 60 minutes. There was no significant gas or liquid phase decomposition of OS solvents observed.

Numerical ranges as used herein shall include every number and subset of numbers contained within that range, whether specifically disclosed or not. Further, these numerical ranges shall be construed as providing support for a claim directed to any number or subset of numbers in that range. For example, a disclosure of from 1 to 10 shall be construed as supporting a range of from 2 to 8, from 3 to 7, from 1 to 9, from 3.6 to 4.6, from 3.5 to 9.9, and so forth.

All references to singular characteristics or limitations of the present invention shall include the corresponding plural characteristic or limitation, and vice-versa, unless otherwise specified or clearly implied to the contrary by the context in which the reference is made. The indefinite article "a" shall mean "at least one," unless explicitly limited to the singular.

All combinations of method or process steps as used herein can be performed in any order, unless otherwise specified or clearly implied to the contrary by the context in which the referenced combination is made.

BRIEF DESCRIPTION OF THE DRAWINGS

FIG. 1A depict the oxidation stability of $F1S_3MN$ with $LiPF_6$, $LiBF_4$, or LiTFSI in current density (mA/cm^2) versus voltage (V vs. Li/Li^+). FIG. 1B depicts a close-up of the same data shown in FIG. 1A.

FIG. 2A and FIG. 2B depict duplicate runs to measure the reduction stability of $F1S_3MN$ with $LiPF_6$, $LiBF_4$, or LiTFSI in current density (mA/cm^2) versus voltage (V vs. Li/Li^+).

FIG. 3A depicts the oxidation stability of $F1S_3MN$ or $F1S_3M2$ with 1M $LiPF_6$ in current density (mA/cm^2) versus voltage (V vs. Li/Li^+). FIG. 3B depicts a close-up of the same data shown in FIG. 3A.

FIG. 4 depicts the reduction stability of $F1S_3MN$ or $F1S_3M2$ with 1M $LiPF_6$ in current density (mA/cm^2) versus voltage (V vs. Li/Li^+).

FIGS. 5A and 5B depict the thermal stability of $F1S_3MN$ with $LiPF_6$. FIG. 5A depicts a close-up of the same data shown in FIG. 5B.

FIG. 6 depicts the thermal stability of $F1S_3M2$ with $LiPF_6$.

FIG. 7 depicts the thermal stability of $F1S_3MN$ with LiTFSI.

FIG. 8 depicts the thermal stability of $F1S_3MN$ with $LiBF_4$.

FIG. 9 depicts the thermal stability of neat $F1S_3MN$.

FIG. 10 depicts the thermal stability of $DF1S_3MN$ with 20% EC and VC/LiBOB.

FIG. 11 depicts the enhanced stability of $F1S_3MN$ electrolytes compared to carbonate control electrolyte heated with de-lithiated NCA cathode.

FIG. 12 depicts the discharge capacity of cells containing various electrolyte solvents at a variety of C-rates at 30°C.

FIG. 13 depicts the construction of a test cell.

FIG. 14 depicts the discharge capacity of cells containing the same electrolyte solvents shown in FIG. 12 at a variety of C-rates at 55°C.

FIG. 15 depicts the construction of an EDLC device.

FIG. 16 depicts the performance of an EDLC device containing $DF1S_2MN$ electrolyte with TEA-BF_4.

FIG. 17 depicts the performance of an EDLC device containing various electrolyte solvents with TBP-PF_6.

FIG. 18 depicts the oxidation stability of 1ND1N with 1M $LiPF_6$ or 1M LiTFSI in current density (mA/cm^2) versus voltage (V vs. Li/Li^+).

FIG. 19 depicts the reduction stability of 1ND1N with 1M $LiPF_6$ or 1M LiTFSI in current density (mA/cm^2) versus voltage (V vs. Li/Li^+).

FIGS. 20A and 20B depict current density (mA/cm^2) versus voltage (V vs. Li/Li^+) for cycling scans with 1ND1N and 1M $LiPF_6$ or 1M LiTFSI from 0 to 6 V and from 6 to 0 V. FIG. 20A depicts a first cycle. FIG. 20B depicts a second cycle.

FIG. 21A depicts the oxidation stability of $F1S_3MN$ or 1ND1N with 1M $LiPF_6$ in current density (mA/cm^2) versus voltage (V vs. Li/Li^+). FIG. 21B depicts a close-up of the same data shown in FIG. 21A.

FIG. 22A depicts the oxidation stability of $F1S_3MN$ or 1ND1N with 1M LiTFSI in current density (mA/cm^2) versus voltage (V vs. Li/Li^+). FIG. 22B depicts a close-up of the same data shown in FIG. 22A.

FIG. 23 is a mass spectrum illustrating the thermal stability of neat 1ND1N.

FIG. 24 is a mass spectrum illustrating the thermal stability of 1ND1N with $LiPF_6$.

FIG. 25A depicts a close-up of the mass spectrum profile as described with respect to FIG. 24 from 24-30 m/z. FIG. 25B depicts a close-up of the mass spectrum profile as described with respect to FIG. 24 from 49-55 m/z.

FIG. 26 depicts the thermal stability of 1ND1N with LiTFSI, vinylene carbonate (VC) and lithium bis(oxalato)borate (LiBOB).

FIG. 27 depicts the thermal stability of 1ND1N with $LiBF_4$.

FIG. 28 depicts the discharge capacity of cells containing various electrolytes at a variety of C-rates.

FIG. 29 depicts the discharge capacity of cells containing various other electrolyte solvents comparing the first cycle to the 50^{th} cycle.

FIG. 30A depicts the discharge capacity of cells containing a 1ND1N-$LiPF_6$-based electrolyte at a variety of C-rates. FIG. 30B depicts the discharge capacity of cells containing a 1ND1N-LiTFSI-based electrolyte at a variety of C-rates.

FIG. 31 is the ^{1}H-NMR spectrum (in $CDCl_3$) of 1ND1N with peak assignments.

FIG. 32 is the ^{1}H-NMR spectrum (in $CDCl_3$) of F1S_3MN with peak assignments.

FIG. 33 is the ^{1}H-NMR spectrum (in $CDCl_3$) of DF1S_2MN with peak assignments.

FIG. 34 is the ^{1}H-NMR spectrum (in $CDCl_3$) of DF1S_3MN with peak assignments.

FIG. 35 is the ^{1}H-NMR spectrum (in $CDCl_3$) of F1S_3cMN with peak assignments.

FIG. 36 is the ^{1}H-NMR spectrum (in $CDCl_3$) of 1S_3MN with peak assignments.

FIG. 37 depicts the gas phase decomposition of F1S_3MC, F1S_3cMN, and 1S_3DN with 1M $LiPF_6$ after 60 min at 175°C. The figure shows no significant gas phase decomposition up to 175°C.

FIG. 38 depicts the gas phase decomposition of DF1S_2MN, TF1S_2MN and TF1S_3MN with 1M $LiPF_6$ after 60 min at 175°C. The figure shows no significant gas phase decomposition up to 175°C.

DETAILED DESCRIPTION OF THE INVENTION

Throughout the description, a number of shorthand abbreviations will be used to designate various organosilicon compounds more easily. The following conventions are used:

The F*n*S*n*MN compounds have the general formula:

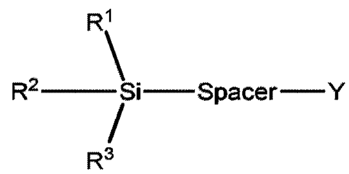

wherein R^1, R^2, and R^3 are the same or different and are independently selected from the group consisting of C_1 to C_6 linear or branched alkyl, alkenyl, alkynyl, or halogen (preferably F), "spacer" is a C_1 to C_6 linear or branched alkylene (preferably C_1 to C_6 linear divalent alkylene). and Y is a polar organic moiety as described earlier.

The compounds disclosed herein can be made by a number of different routes. A general approach that can be used to fabricate the compounds is as follows:

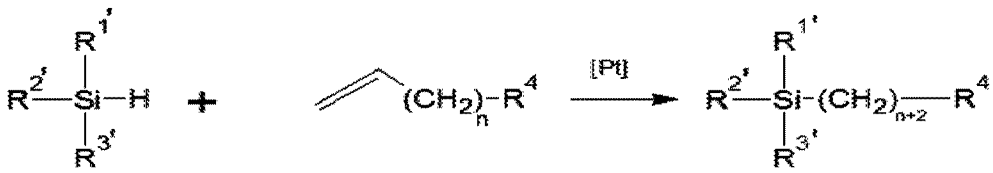

R^{1}, R^{2}, R^{3} =′ alkyl, halogen
(i.e. Cl)

The R^1, R^2, and R^3 groups are as defined for R herein; R^4 has the same definition as Y; "n" is a positive integer.

The compounds disclosed herein can also be fabricated via the following approach:

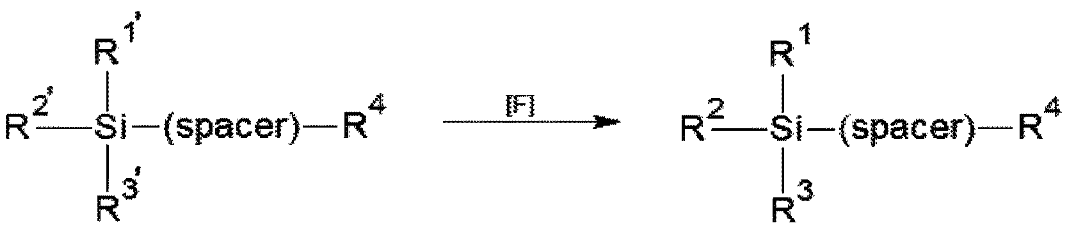

$R^{1'}, R^{2'}, R^{3'}$ = alkyl, chloride
R^{1}, R^{2}, R^{3} = alkyl, fluoride

Again, the R^1, R^2, and R^3 groups are as defined for R herein; R^4 has the same definition as Y.

The compounds disclosed herein are also made by a number of specific routes, including the following reaction schemes:

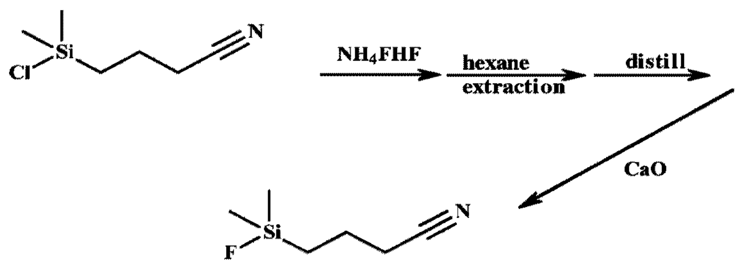

and

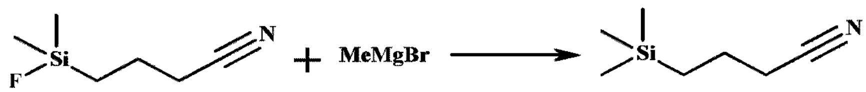

and

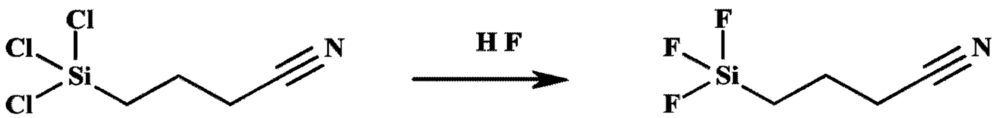

and

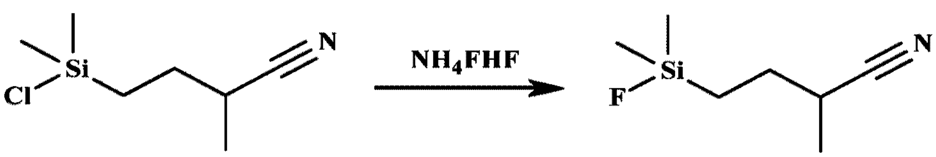

and

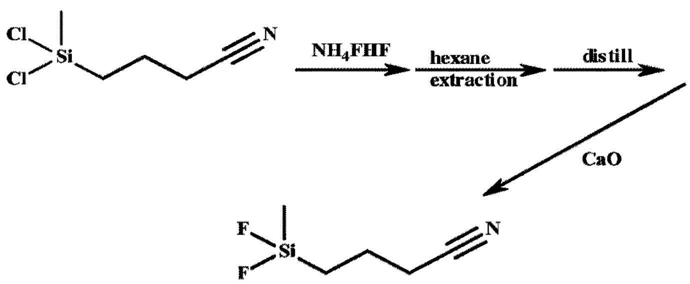

and

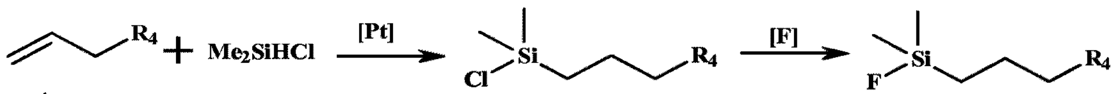

(R^4 as defined above for Y),

and

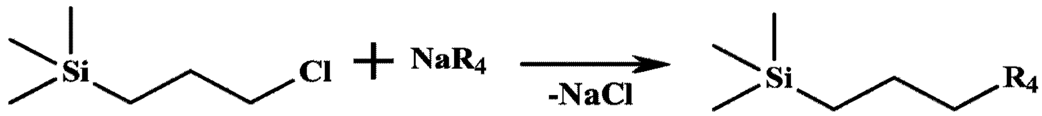

(R^4 as defined above for Y), and

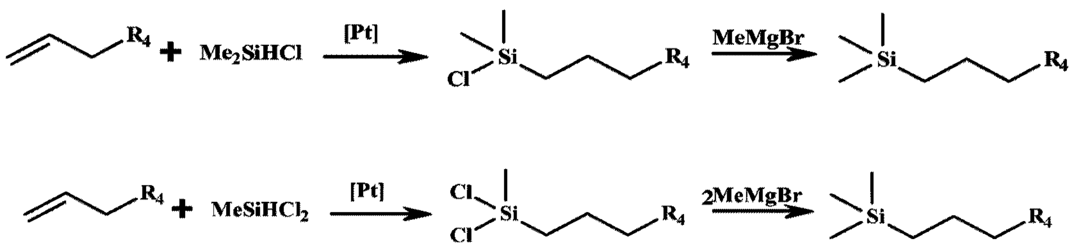

(R^4 as defined above for Y).

LiTFSI, bis(trifluoromethane)sulfonimide lithium salt (Sigma-Aldrich catalog no. 449504), is a commercial product supplied by several international suppliers:

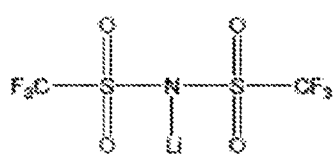

.

The elements and method steps described herein can be used in any combination whether explicitly described or not.

All combinations of method steps as used herein can be performed in any order, unless otherwise specified or clearly implied to the contrary by the context in which the referenced combination is made.

As used herein, the singular forms “a,” “an,” and “the” include plural referents unless the content clearly dictates otherwise.

It is understood that the compounds and compositions disclosed herein are not confined to the particular construction and arrangement of parts herein illustrated and described, but embraces such modified forms thereof as come within the scope of the claims.

The presently disclosed compounds are organosilicon compounds having a shared structural feature in the form of a one or more terminal or internal polar organic substituents or moieties. As used herein, the term “polar organic substituent” and “polar organic moiety” are used interchangeable. The terms explicitly include, but are not limited to, the following functional groups:

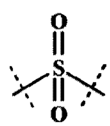
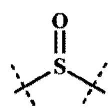
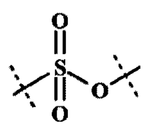
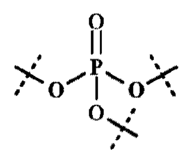
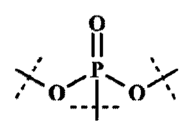

sulfones, sulfoxides, sulfonates, phosphates, phosphonates,

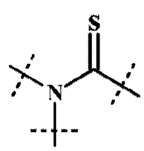
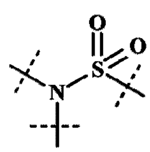
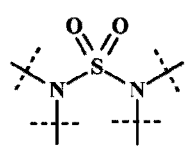
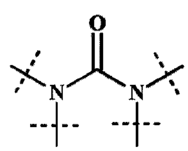
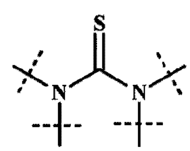

thioamides, sulfonamides, sulfamides, carbamides, thiocarbamides,

Date Reçue/Date Received 2023-10-02

 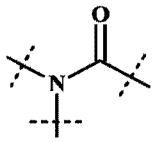 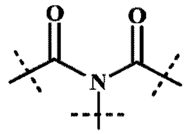 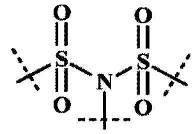 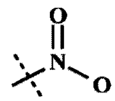 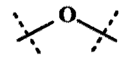

amines, amides, imides, sulfonimides, nitro, ethers,

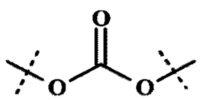 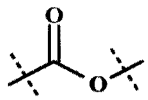 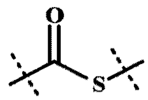 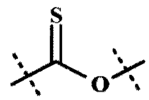 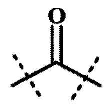 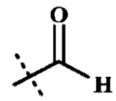

carbonates, esters, thioesters, thionoesters, ketones, aldehydes,

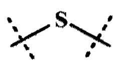 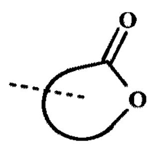 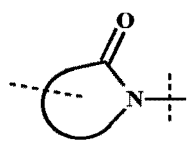 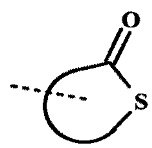

thioethers lactones, lactams, thiolactones,

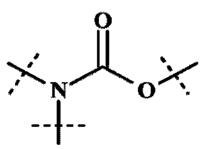 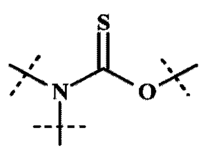 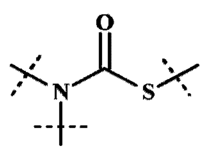 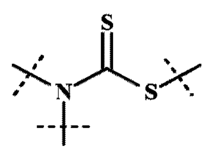

carbamates, O-thiocarbamates, S-thiocarbamates, dithiocarbamates, and

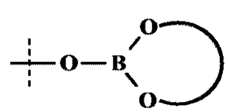

cyclic borates.

Included among the preferred compounds are the following structures:

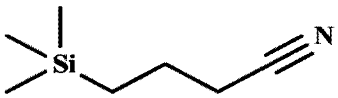

$1S_3MN$
4-(trimethylsilyl)butanenitrile
3-cyanopropyltrimethylsilane

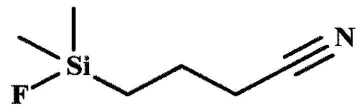

$F1S_3MN$
4-(fluorodimethylsilyl)butanenitrile
3-cyanopropyldimethylfluorosilane

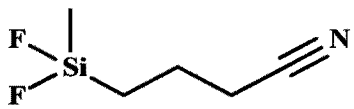

$DF1S_3MN$
4-(difluoromethylsilyl)butanenitrile
3-cyanopropylmethyldifluorosilane

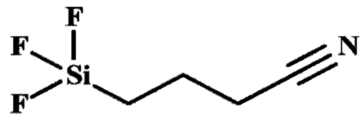

$TF1S_3MN$
4-(trifluorosilyl)butanenitrile
3-cyanopropyltrifluorosilane

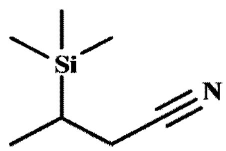

$iso1S_3MN$
3-(trimethylsilyl)butanenitrile

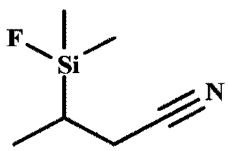

$isoF1S_3MN$
3-(fluorodimethylsilyl)butanenitrile

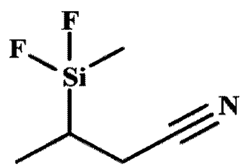

$isoDF1S_3MN$
3-(difluoromethylsilyl)butanenitrile

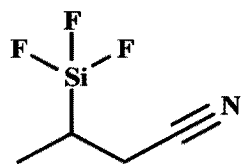

$isoTF1S_3MN$
3-(trifluorosilyl)butanenitrile

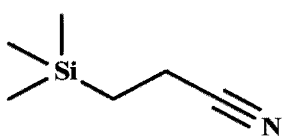

$1S_2MN$
3-(trimethylsilyl)propanenitrile
2-cyanoethyltrimethylsilane

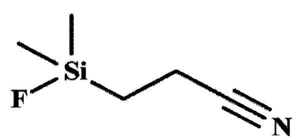

$F1S_2MN$
3-(fluorodimethylsilyl)propanenitrile
2-cyanoethyldimethylfluorosilane

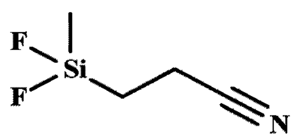

DF1S$_2$MN
3-(difluoromethylsilyl)propanenitrile
2-cyanoethylmethyldifluorosilane

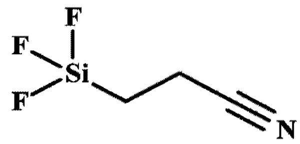

TF1S$_2$MN
3-(trifluorosilyl)propanenitrile
2-cyanoethyltrifluorosilane

The above structures are all depicted with a terminal cyano group. This is for purposes of brevity only. The analogous compounds having internal and/or terminal polar moieties as described above in place of the cyano moiety are explicitly within the scope of the disclosure. Likewise, the halogenated compounds are depicted above as fluorinated compounds. The analogous compounds having other halogen substituents (chlorine, bromine, and/or iodine) in place of fluorine atoms are explicitly within the scope of the present disclosure. For each compound listed, two alternative systematic names are provided (the first of each pair of names designates the fundamental core as a nitrile; the second designated the fundamental cores as silane.) Additionally, each compound has been given a short-hand designation in which DF = difluoro, TF = trifluoro, and "S*n*" designates the alkylene spacer between the silicon atom and the terminal cyanate, isocyanate, or thiocyanate moiety and "n" represents the number of carbon atoms in the spacer. The physical properties of selected organosilicon (OS) compounds are presented in Table 1.

The synthesis of the analogous sulfones can be accomplished using the following illustrative synthesis of the compounds designated, 1NMS, F1S$_3$MS, and DF1S$_3$MS. Note that other sulfones falling within the broader disclosure contained herein can be made by the same route by simply altering accordingly the starting reagents.

The synthesis of 1NMS proceeded as follows: 2-(Methylsulfonyl)ethanol was mixed with 0.5 mol equivalents of hexamethyldisilazane and about 1% mol equivalents of $Al(H_2PO_4)_3$ as catalyst, without solvent. The mixture was kept at about 80°C overnight and distilled twice to get pure 1NMS.

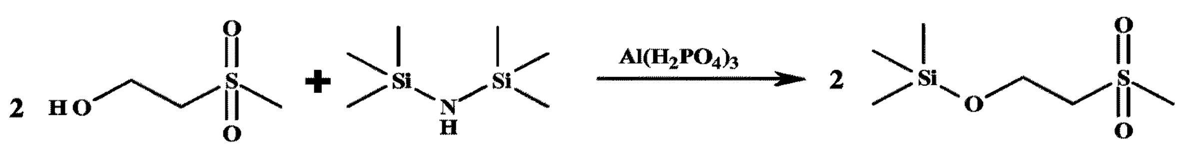

1NMS

The synthesis of F1S3MS proceeded as follows: Allylmethylsulfide was dissolved in ethanol and mixed with 4 mol equivalents of H_2O_2. Approximately 3% mol equivalents of ammonium heptamolybdate was added as catalyst for oxidation. The next day the solution was neutralized with $NaHCO_3$ solution and extracted with CH_2Cl_2, the water fraction was discarded, and the organic layer evaporated and distilled to yield allylmethylsulfone. Allylmethylsulfone was hydrosilylated with dimethylchlorosilane using Karstedt's catalyst. The product was fluorinated using NaFHF at about 150°C, filtered, distilled twice, and dried over a molecular sieve to yield pure F1S3MS

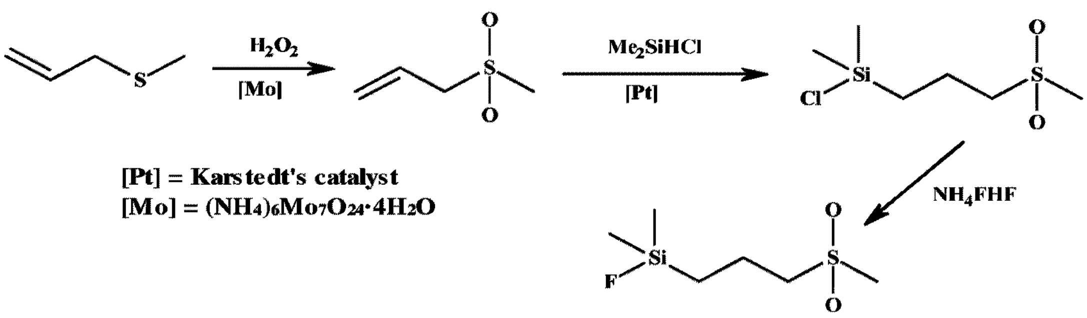

F1S3MS

The synthesis of DF1S3MS proceeded as follows: 3-mercaptopropylmethyldimethoxysilane was dissolved in ethanol and mixed with one (1) mol equivalent of NaOH in water. One (1) mol equivalent of Me_2SO_4 was then added to the mixture and refluxed overnight. The solid was filtered off. The crude product was oxidized with 4 mol equivalents of H_2O_2 and 3% mol equivalents of ammonium heptamolybdate. The solvent was evaporated and 2 mol equivalents of HF in water was added. The product was extracted with CH_2Cl_2 and distilled.

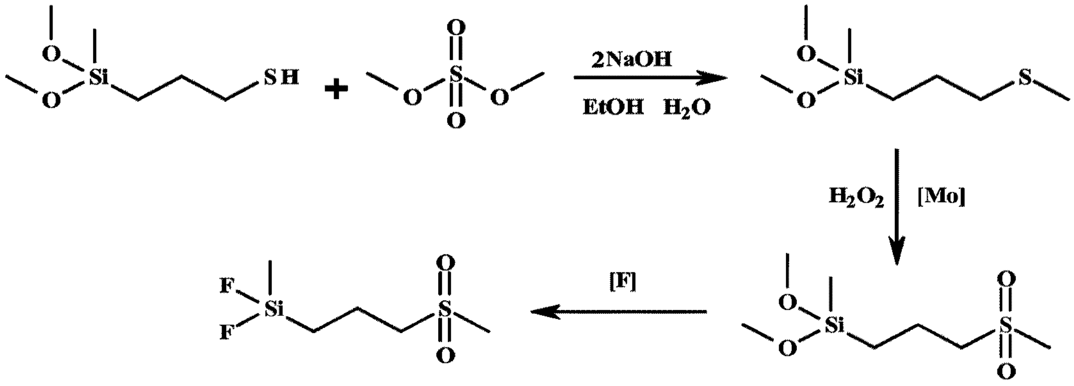

DF1S3MS

Additional characterization data for these sulfone compounds is contained in the appendix, attached hereto.

As shown in Table 1, Reduced viscosity, higher conductivity, and lower flash point with added fluorine and reduced spacer length. $DF1S_2MN$ has lowest viscosity and highest conductivity.

Table 1. Physical Properties (with 20% EC, additives, 1M $LiPF_6$)	Neat Solvent Properties					Electrolyte Properties (w/1M $LiPF_6$) at 30 °C			
						No co-solvent		20% EC	
OS	MW	Diel	FP °C	BP °C	Den. g/mL	Cond. mS/cm	Vis. cP	Cond. mS/cm	Vis. cP
$1S_2MN$	127	12.3	52	n/a	0.83	2.6	7.7	n/a	n/a
$1S_3MN$	141	12.6	72	200	0.81	1.6	9.4	Phase sep. with EC	Phase sep. with EC
$F1S_3MN$	145	16.8	82	249	0.93	2.8	8.0	4.2	8.5
$DF1S_3MN$	149	18.2	78	202	1.09	3.5	7.9	4.8	8.3
$DF1S_2MN$	135	19.5	64	182	1.10	5.0	6.8	5.7	7.6
$TF1S_3MN$	153	16.7	68	n/a	1.22	3.0	10.2	4.0	9.5
$TF1S_2MN$	139	n/a	64	n/a	1.30	n/a	n/a	n/a	n/a
$DPF1S_3MN$	201	12.5	118	206	0.91	0.44	43	n/a	n/a

Key:

Date Reçue/Date Received 2023-10-02

$TF1S_3MN$

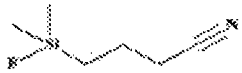

$F1S_3MN$

$DF1S_3MN$

$1S_2MN$

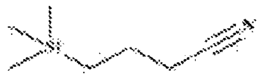

$1S_3MN$

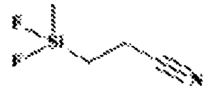

$DF1S_2MN$

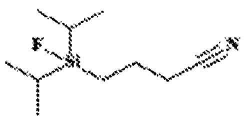

$DPF1S_3MN$

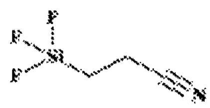

TFS_2MN

The physical properties of neat 1ND2, 1ND1, 1ND1N, $F1S_3MN$, $DPF1S_3MN$, $F1S_3MC$, $F1S_3ME$, $F1S_3MA$, $F1S_3MS$, 1NMS, $F1S_3M2$, and $F1S_{3c}MN$ as well as electrolyte solutions containing these solvents, are shown in Table 2:

Table 2: Physical Properties of Solvents and Electrolytes

OS	Neat Solvent Properties					Electrolyte Properties (w/1M $LiPF_6$) at 30 °C			
						No co-solvent		20% EC	
	MW	Diel.	Flash °C	BP °C	Density g/mL	Cond. mS/cm	Vis. cP	Cond. mS/cm	Vis. cP
1ND2	296	6.4	138	288	1.07	n/a	n/a	3.6	12
1ND1	208	8.1	85	n/a	0.94	n/a	n/a	4.5	5.1
1ND1N	198	30	168	n/a	1.03	1.3	29	1.9	33
$F1S_3MN$	145	16.8	82	249	0.93	2.8	8.0	4.2	8.5
$DPF1S_3MN$	201	12.5	118	206	0.91	0.44	43	n/a	n/a
$F1S_3MC$	194	4.9	86	188	1.02	0.62	11.4	2.1	10.5

F1S$_3$ME	178	6.6	66	170	0.96	1.8	7.2	n/a	n/a
F1S$_3$MA	163	4.8	n/a	155	0.85	n/a	n/a	n/a	n/a
F1S$_3$MS	198	29.4	158	245	1.11	0.3	177	1.0	65
1NMS	196	19.6	48	290	1.06	n/a	n/a	1.5	37
F1S$_3$M2	238	7.2	112	233	n/a	n/a	n/a	3.0	14.0
F1S$_3$cMN	159	16.6	80	n/a	n/a	n/a	n/a	2.6	10.6

Key:

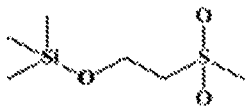

1NMS

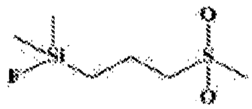

F1S$_3$MS

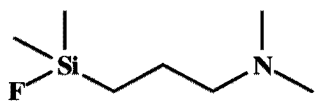

F1S$_3$MA

F1S$_3$MN

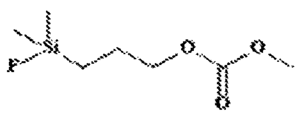

F1S$_3$MC

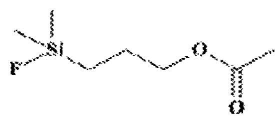

F1S$_3$ME

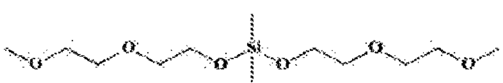

1ND2

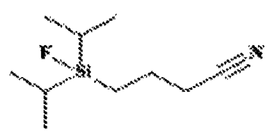

DPF1S$_3$MN

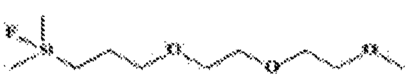

F1S$_3$M2

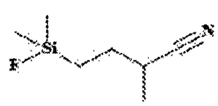

F1S$_3$cMN

1ND1

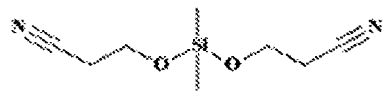

1ND1N

In addition to the organosilicon compounds disclosed herein, the present electrolyte compositions may include conventional non-silicon co-solvents. For example, the present electrolyte compositions may include nitriles and carbonates, such as acetonitrile, ethylene carbonate (EC), dimethyl carbonate (DMC), diethyl carbonate (DEC), or ethylmethyl carbonate (EMC). The instant electrolyte compositions may include non-silicon co-solvents at a wide range of concentrations, including but not limited to, about 1 wt% to about 40 wt%. Examples of suitable co-solvent concentrations include about 1 wt%, about 5 wt%, about 10 wt%, about 15 wt%, about 20 wt%, about 25 wt%, about 30 wt%, about 40 wt% or a range between and including any of the preceding amounts.

EXAMPLES

F1S$_3$MN Synthesis:

Scheme 1 depicts a synthesis scheme for F1S$_3$MN. [F] indicates a fluorinating agent, such as HF, NH_4FHF, or other fluorinating agent. NH_4FHF is preferably used as a fluorinating agent for laboratory scale synthesis. If HF is used, the only byproduct is HCl. The synthesized F1S$_3$MN compound is washed from the solid salt with hexane, distilled, dried with CaO, and distilled again.

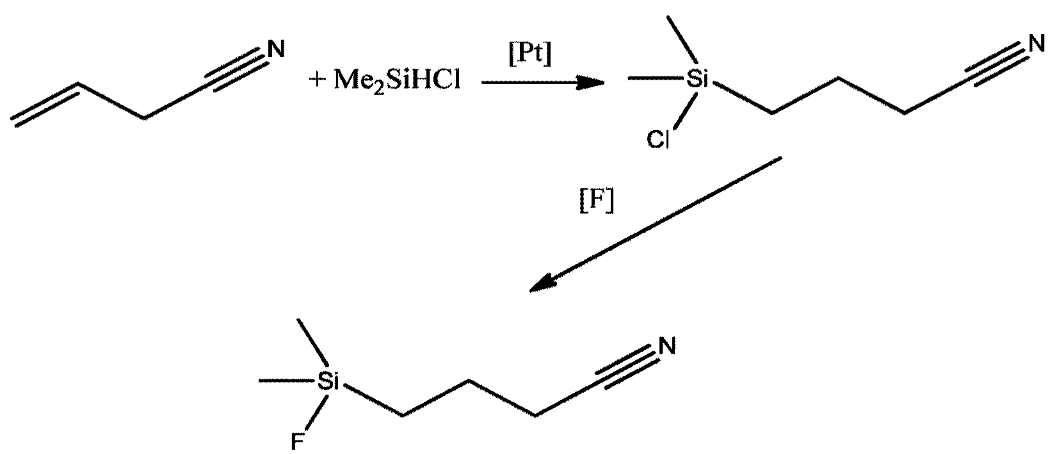

F1S$_3$MN

Scheme 1

Scheme 2 depicts a synthesis scheme for F1S$_3$MN using NH_4FHF as a fluorinating agent. Using Karstedt's catalyst (Platinum(0)-1,3-divinyl-1,1,3,3-tetramethyldisiloxane complex solution, Cat. No. 479519, Sigma-Aldrich, St. Louis, MO), about 3% substitution on the secondary carbon occurs, generating isoF1S$_3$MN. The isoF1S$_3$MN has a lower boiling point than F1S$_3$MN, and most of it can be separated by fractional distillation.

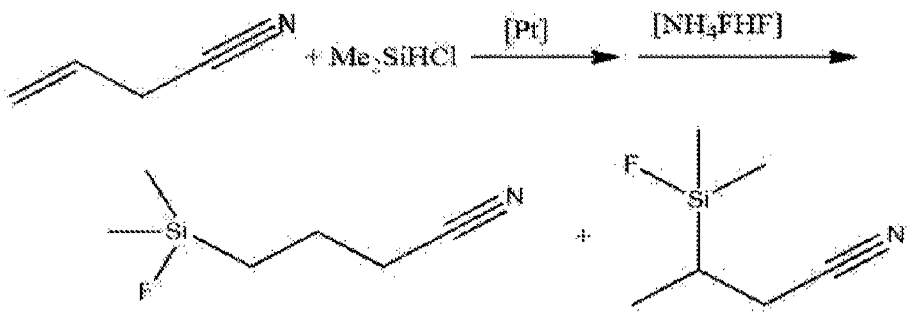

F1S$_3$MN isoF1S$_3$MN

Scheme 2

Scheme 3 depicts an alternative, shorter synthesis scheme for F1S$_3$MN using a Cl1S$_3$MN intermediate. The Cl1S$_3$MN intermediate can be obtained by Gelest, Inc. (Product Code SIC2452.0, 11 East Steel Road, Morrisville, PA). Use of the Cl1S$_3$MN intermediate reduces the time spent during synthesis.

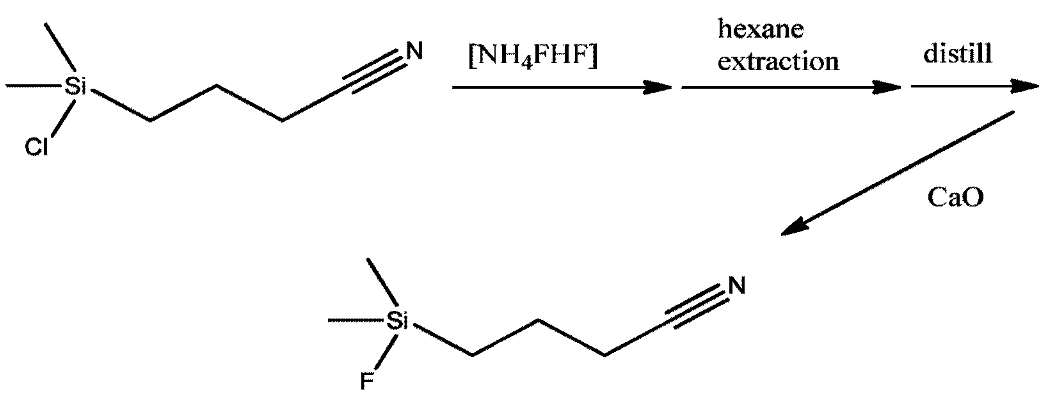

F1S$_3$MN

Scheme 3

Scheme 4 depicts yet another synthesis scheme for $F1S_3MN$. As with Scheme 1, [F] indicates a fluorinating agent, such as HF, NH_4FHF, or other fluorinating agent. The use of HF as fluorinating agent in this synthesis scheme will not give solid byproducts, so there is no need of hexane extraction and filtration of solid. The only byproduct is HCl.

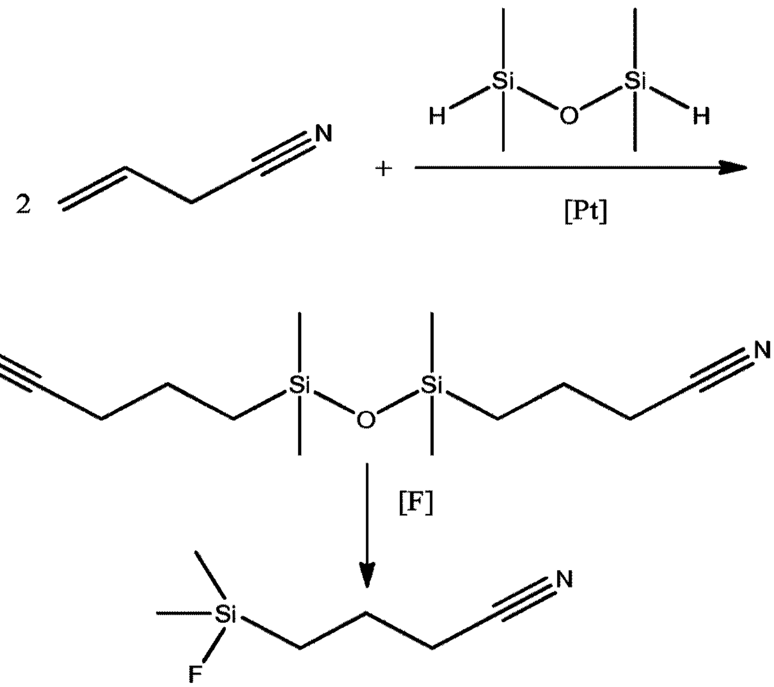

$F1S_3MN$

Scheme 4

Scheme 5 depicts yet another synthesis scheme for $F1S_3MN$. As with Scheme 1, [F] indicates a fluorinating agent, such as HF, NH_4FHF, or other fluorinating agent.

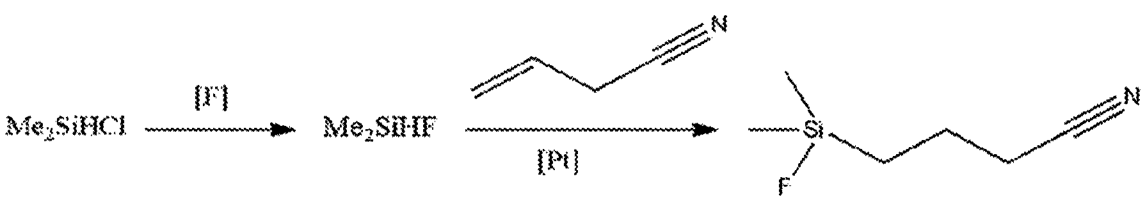

Scheme 5

Synthesis of $F1S_3MN$:

In the preferred route, allyl cyanide is heated to about 100°C with a small amount of Karstedt's catalyst. Dimethylchlorosilane was added dropwise and refluxed 4 hours. After cooling to room temperature, the mixture was fluorinated using 1 mol equivalent of ammonium hydrogen fluoride at room temperature. Cold hexane was added to the mixture, the solid was filtered off, and the solvent evaporated. Calcium oxide was added to the crude product and it was distilled under vacuum between 45-55°C at 0.4 Torr to yield the desired product, $F1S_3MN$.

Synthesis of $F1S_3ME$:

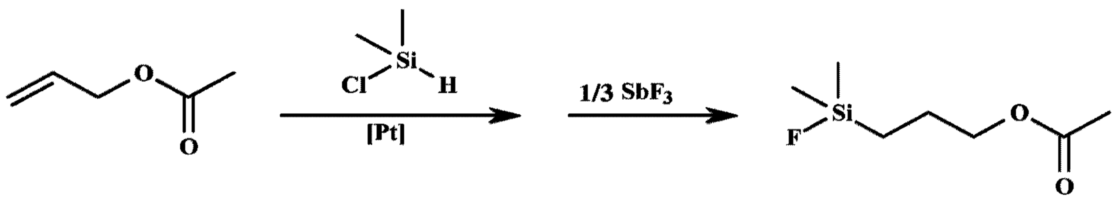

Scheme 6

In the preferred route, allyl acetate is mixed with dimethylchlorosilane and a small amount of Karstedt's catalyst is added. The mixture is left reacting overnight. Next day, the mixture was fluorinated using 0.33 mol equivalent of antimony trifluoride at room temperature overnight with strong stirring. Next day, the solid was filtered off, and the product distilled under vacuum between 25-30 °C at 0.3 Torr to yield the desired product, $F1S_3ME$.

This ester is suitable as an electrochemical solvent in an electrolyte composition. $F1S_3ME$ has good solubility with 1M $LiPF_6$ and dissolved readily at room temperature. Its flash point is acceptable at 66°C, as is its dielectric constant of 6.6. Its CV oxidation/reduction behavior is likewise suitable for lithium ion charge storage cells. Full cell cycling with 80% $F1S_3ME$ electrolyte was stable with good capacity. It retained a very low current density at potentials at or below 5 V at 30°C. $F1S_3ME$ is electrochemically viable by fundamental Pt oxidation and graphite reduction. It displayed normal reduction behavior in on the first cycle and passivation was observed on the second cycle. $F1S_3ME$ cycled well in an 80% electrolyte formulation in a NMC/graphite electrode system through 26 cycles (data not shown).

Synthesis of $DF1S_3DN$:

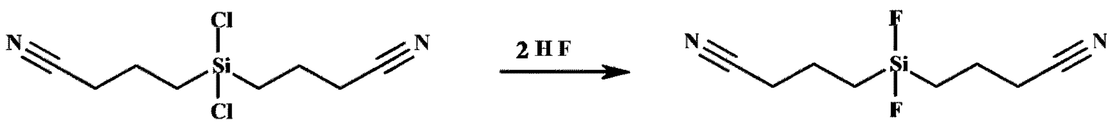

Scheme 7

Bis(cyanopropyl)dichlorosilane was mixed with 2 mol equivalents of aqueous HF at room temperature and left reacting overnight. The crude product was extracted with dichloromethane, the solvent evaporated and the product distilled under vacuum at 165 °C at 0.1 Torr to yield the desired product, DF1S$_3$DN.

Synthesis of 1S$_3$DN:

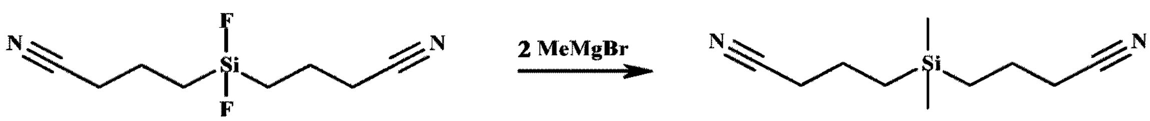

Scheme 8

DF1S$_3$DN was dissolved in THF and cooled with an ice bath, then 2 mol equivalents of methylmagnesium bromide were added and the mixture was left reacting until it slowly reached room temperature. The mixture was quenched with ethanol, the crude product was extracted with dichloromethane, the solvent evaporated and the product distilled under vacuum at 125 °C at 0.2 Torr to yield the desired product, 1S$_3$DN.

Synthesis of TF1S$_3$MN:

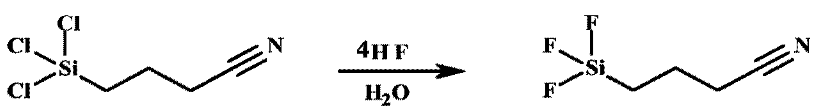

Scheme 9

Cyanopropyltrichlorosilane was cooled in an ice bath and 4 mol equivalents of aqueous HF were added dropwise. The mixture was left reacting no more than 2 hours. The crude product was extracted with dichloromethane, the solvent evaporated and the product distilled under vacuum at 25 °C at 0.2 Torr to yield the desired product, TF1S$_3$MN.

Synthesis of DPF1S$_3$MN:

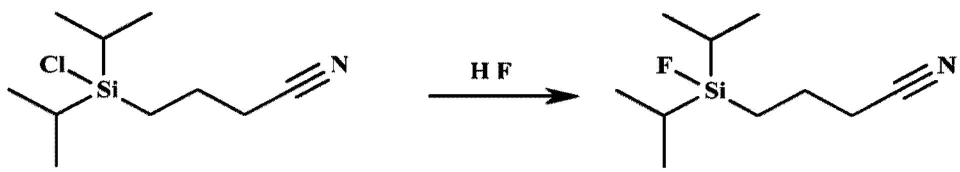

Scheme 10

Bis(isopropyl)cyanopropylchlorosilane was dissolved in THF and cooled in an ice bath, then 1 mol equivalent of aqueous HF was added dropwise and left reacting overnight at room temperature. Next day the solvent was evaporated and the product distilled under vacuum at 60 °C at 0.2 Torr to yield the desired product, DPF1S$_3$MN.

DPF1S$_3$MN was made to explore how larger alkyl groups on the silicon atom impact the physical characteristics and electronic characteristics of the molecule. This compound has good solubility with $LiPF_6$, dissolving readily at room temperature. It displayed stable oxidation behavior in cyclic voltammetry (CV) up to approximately 5 V. Its CV reduction behavior was also good, with passivation on the second cycle. This compound is suitable for electrochemical applications at elevated temperatures (flash point = 118°C) and at potentials up to approximately 5 V. DPF1S$_3$MN is electrochemically viable by fundamental Pt oxidation and graphite reduction.

Synthesis of DF1S$_3$MSO:

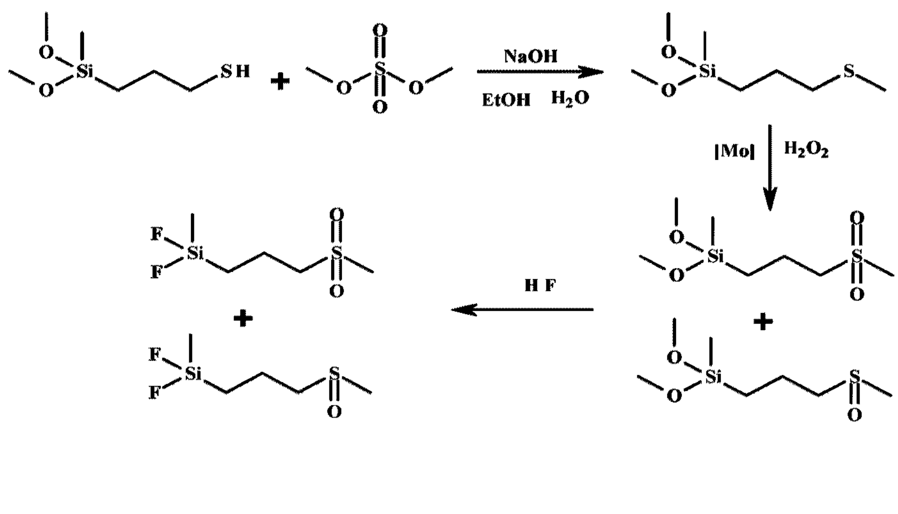

Scheme 11

DF1S3MSO was obtained as byproduct of incomplete oxidation during the synthesis of DF1S3MS according to the procedure mentioned. DF1S3MSO was purified by distillation under vacuum at 40 °C at 0.1Torr.

Synthesis of F1S3MA:

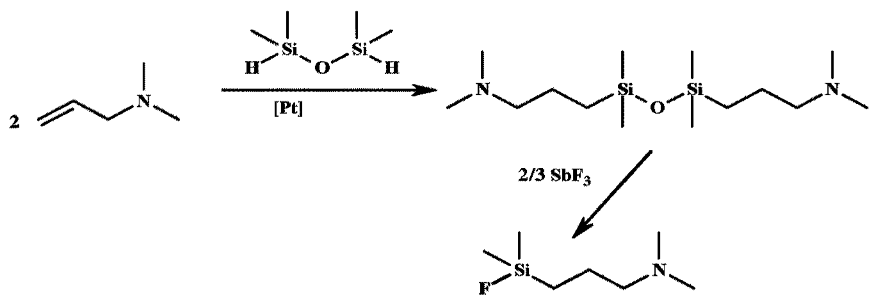

Scheme 12

In this synthesis, 2 mol equivalents of dimethylallylamine is mixed with 1,1,3,3-tetramethyldisiloxane and a small amount of Karstedt's catalyst. The mixture is heated to 100 °C and left reacting overnight. Next day, the mixture was fluorinated using 0.67 mol equivalent of antimony trifluoride at 150°C overnight with strong stirring. Next day, the solid was filtered off, and the product distilled under vacuum between 20-25 °C at 0.2 Torr to yield the desired product, F1S3MA.

Synthesis of F1S3MC:

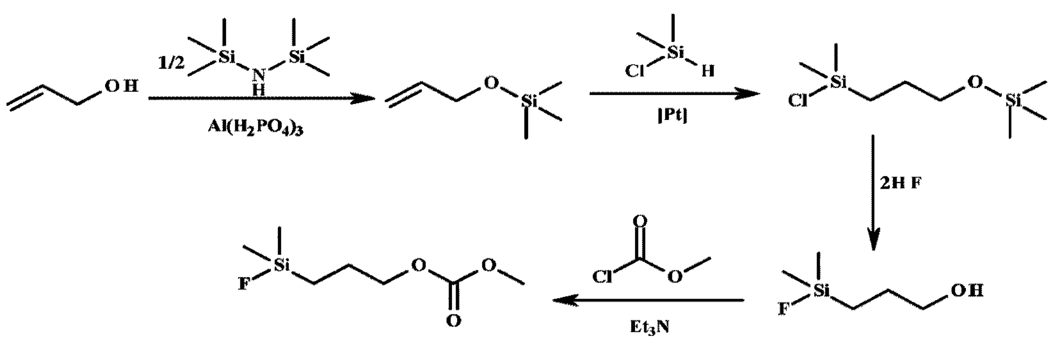

Scheme 13

Allyl alchol was silylated with hexamethyldisilazane, using a catalytic amount of aluminum dihydrogenphosphate at 80°C overnight. The intermediate allyloxytrimethylsilane was distilled to purify it before the hydrosilylation. The hydrosilylation was done overnight with 1 mol equivalent of dimethylchlorosilane and a small amount of Karstedt's catalyst at 80 °C. Next day, the mixture was fluorinated and hydrolyzed using 2 mol equivalent of aqueous hydrofluoric acid at room temperature with strong stirring to get the (3-hydroxypropyl)dimethylfluorosilane, which was distilled before the next step. The last intermediate was dissolved in hexane, 1 mol equivalent of trimethylamine was added, the mixture cooled in an ice bath and methyl chloroformate was added dropwise to the mixture, then it was left reacting overnight at room temperature. Next day the solid was filtered off, the solvent evaporated and the product distilled under vacuum between 28 °C at 0.2 Torr to yield the desired product, $F1S_3MC$.

$F1S_3MC$ was synthesized to compare the electrochemical performance of commonly used carbonates to a silyl analog. The CV oxidation and reduction of $F1S_3MC$ was shown to be suitable for electrochemical application. The synthesis is quite good, yielding $F1S_3MC$ in > 99.8% purity. $F1S_3MC$ dissolved readily in 1M $LiPF_6$ at room temperature. It displayed acceptable cycling at 30°C with good capacity. $F1S_3MC$ also displayed good oxidation stability at potentials up to about 5 V. In CV, reduction showed two peaks in the first cycle (at 1.7 V and 0.6 V) and passivation in the second cycle.

Determination of the Electrochemical Stability of Organosilicon Materials:

Computational chemistry methods were used to calculate electrochemical properties of various organosilicon molecules. We used the GAMESS program developed by the Gordon research group at Iowa State University for the Density Function Theory (DFT) molecular orbital calculations. The HOMO (highest occupied molecular orbital) and LUMO (lowest unoccupied molecular orbital) energy levels, which correlate to the reduction and oxidation potentials of compounds, were calculated at the B3LYP/DZV level.

The oxidative stability of electrolytes containing organosilicon solvents was determined using linear sweep voltammetry (LSV) or cyclic voltammetry (CV) in a 3-electrode cell. A platinum microelectrode was used as the working electrode with lithium metal as both the counter and reference electrode. The potential of the system was increased from the open circuit voltage (OCV) to 6 or 8V (vs. Li/Li^+) at a scan rate of 10 mV/s. The resulting current density (mA/cm^2) was recorded at each potential with a higher current indicating an oxidative reaction (*i.e.*, lower oxidative stability). For the linear sweep voltammetry, 8V was used as a final potential to evaluate the fundamental oxidative stability of the material across a wider voltage range. For the cyclic voltammetry, 6V was used to evaluate the material across multiple scans under potentials more relevant to traditional battery applications. Multiple scans were conducted in the cyclic voltammetry experiments to determine the reversibility/irreversibility of any reactions observed.

The reductive stability of electrolytes containing organosilicon solvents was determined using linear sweep voltammetry (LSV) in a 3-electrode cell. A glassy carbon electrode was used as the working electrode with lithium metal as both the counter and reference electrode. The potential of the system was decreased from the open circuit voltage (OCV, typically 3V) to 0.1V (vs. Li/Li^+) at a scan rate of 10 mV/s. The resulting current density (mA/cm^2) was recorded at each potential with a greater current indicating a reduction reaction (i.e., lower reductive stability). Two scans were conducted to evaluate if the reductive processes were reversible or irreversible (*i.e.*, passivating).

Electrochemical Stability of $F1S_3MN$:

Molecular orbital diagrams for $F1S_3MN$ and $F1S_3M2$, not shown, reveal that the energy difference between the highest occupied molecular orbital (HOMO) and the lowest unoccupied molecular orbital (LUMO) is greater for $F1S_3MN$ (9.07 eV) than for $F1S_3M2$ (8.20 eV). $F1S_3MN$ also has a higher oxidation potential (-8.75 eV) than $F1S_3M2$ (-6.84 eV).

FIGS. 1A and 1B depict the oxidation stability of $F1S_3MN$ with $LiPF_6$, $LiBF_4$, or LiTFSI in current density (mA/cm^2) versus voltage (V vs. Li/Li^+). The oxidation stability was tested at room temperature with a working electrode as Pt, a counter electrode as Li, a reference electrode as Li/Li^+, and a sweep rate of 10 mV/s. FIG. 1B depicts a close-up of the same data shown in FIG. 1A. The $F1S_3MN$-$LiPF_6$ electrolyte exhibited the best oxidation stability, having a current density of 1 mA/cm^2 at 7.3 V compared to a current density of 1 mA/cm^2 at 6.8 V and 6.2 V for $F1S_3MN$-$LiBF_4$ and $F1S_3MN$-LiTFSI, respectively.

FIGS. 2A and 2B depict the reduction stability of $F1S_3MN$ with $LiPF_6$, $LiBF_4$, or LiTFSI in current density (mA/cm^2) versus voltage (V vs. Li/Li^+). The reduction stability was tested at room temperature with a working electrode as Pt, a counter electrode as Li, a reference electrode as Li/Li^+, and a sweep rate of 10 mV/s. FIGS. 2A and 2B are two separate scans. The $F1S_3MN$-$LiPF_6$ electrolyte exhibited the best reduction stability.

FIGS. 3A and 3B depict the oxidation stability of $F1S_3MN$ or $F1S_3M2$ with 1M $LiPF_6$ in current density (mA/cm^2) versus voltage (V vs. Li/Li^+). The oxidation stability was tested at room temperature with a working electrode as Pt, a counter electrode as Li, a reference electrode as Li/Li^+, and a sweep rate of 10 mV/s. FIG. 3B depicts a close-up of the same data shown in FIG. 3A. $F1S_3MN$ demonstrated improved oxidation stability with respect to $F1S_3M2$.

FIG. 4 depicts the reduction stability of $F1S_3MN$ or $F1S_3M2$ with 1M $LiPF_6$ compared to a carbonate control electrolyte with $LiPF_6$ in current density (mA/cm^2) versus voltage (V vs. Li/Li^+) in two separate scans. The reduction stability was tested at room temperature with a working electrode as Pt, a counter electrode as Li, a reference electrode as Li/Li^+, and a sweep rate of 10 mV/s. $F1S_3MN$ demonstrated less resistance to reduction compared to $F1S_3M2$.

Determination of Thermal Stability of neat Solvents & Formulated Electrolytes:

The thermal stability of both the neat organosilicon solvents and the electrolyte compositions were determined as follows: Approximately 0.75 mL of liquid sample was heated in a sealed cell under an argon purge. The Argon purge was carried to an atmospheric sampling mass spectrometer where any gas phase impurities and/or decomposition products can be detected at very low levels using electron impact mass spectrometry (EI-MS). The sample was held for 1 hour at pre-determined temperature levels that are relevant for battery applications (30, 55, 70, 100, 125, 150, 175, and 200°C). The gas phase decomposition products were identified by comparing fragmentation patterns obtained from the EI-MS to NIST standards. Following the heating experiment (and detection/collection of all gas phase products), the remaining liquid sample was analyzed via NMR spectroscopy for a quantitative analysis of the extent of decomposition. Multiple nuclei were examined to fully analyze all components of the system, including the organosilicon solvent, any carbonate co-solvents, all additives, and the lithium salt (if present).

Thermal Stability of $F1S_3MN$:

FIGS. 5A and 5B depict the thermal stability of $F1S_3MN$ with $LiPF_6$. $F1S_3MN$-$LiPF_6$ electrolyte (batch ZP815-01) was exposed to temperatures ranging from 30°C to 175°C and analyzed by electron impact mass spectrometry (EI-MS) and nuclear magnetic resonance spectroscopy (NMR) for gas and liquid decomposition products, respectively. The temperatures at which salient peaks appeared are annotated. $F1S_3MN$ showed no significant gas and/or liquid phase decomposition up to 175°C. Me_2SiF_2 appeared at temperatures of 100-125°C at 81 m/z, and $MeSiF_3$ appeared at temperatures of 150-175°C at 85 m/z. However, the 81 m/z and 85 m/z peaks appeared inconsistently at 100-175°C. Furthermore,

^1H NMR analysis showed no decomposition after heating to 175°C. Therefore, $F1S_3MN$ does not show consistent decomposition up to 175°C. FIG. 5A depicts a close-up of the same data shown in FIG. 5B.

FIG. 6 depicts the thermal stability of $F1S_3M2$ with $LiPF_6$. $F1S_3M2$-$LiPF_6$ electrolyte was exposed to temperatures ranging from 30°C to 150°C and analyzed by mass spectrometry for decomposition products. The temperatures at which salient peaks appeared are annotated. $F1S_3M2$ showed decomposition at temperatures ≥ 125°C. Decomposition products included Me_2SiF_2 and 1,4-dioxane. ^1H NMR analysis showed approximately 6% decomposition at 150°C. These results in combination with those discussed in relation to FIG. 5A and FIG. 5B indicate that $F1S_3MN$ is more thermally stable than $F1S_3M2$.

FIG. 7 depicts the thermal stability of $F1S_3MN$ with LiTFSI. $F1S_3MN$-LiTFSI electrolyte was exposed to temperatures ranging from 30°C to 185°C and analyzed by mass spectrometry for decomposition products. The temperatures at which salient peaks appeared are annotated. Gas phase peaks were observed at temperatures ≥ 150°C. Peaks at 117 and 102 matched patterns observed for $F1S_3MN$-$LiBF_4$ electrolyte and neat solvent (see FIGS. 8 and 9).

FIG. 8 depicts the thermal stability of $F1S_3MN$ with $LiBF_4$. $F1S_3MN$-$LiBF_4$ electrolyte was exposed to temperatures ranging from 30°C to 200°C and analyzed by mass spectrometry for decomposition products. The temperatures at which salient peaks appeared are annotated. Gas phase peaks were observed at temperatures ≥ 175°C. Peaks at 117 and 102 matched patterns observed for neat solvent and $F1S_3MN$-LiTFSI electrolyte (see FIGS. 7 and 9). ^1H NMR analysis showed no fluorinated decomposition products and < 0.5% of a non-fluorinated hydrolysis product.

FIG. 9 depicts the thermal stability of neat $F1S_3MN$. $F1S_3MN$ electrolyte was exposed to temperatures ranging from 30°C to 195°C and analyzed by mass spectrometry for decomposition products. The temperatures at which salient peaks appeared are annotated. Gas phase peaks were observed at temperatures ≥ 150°C. At 150°C, Me_2SiF_2 was observed (96/81 m/z), but other peaks were not associated with this product. ^1H NMR analysis showed no fluorinated decomposition products and < 0.5% hydrolysis.

The above data show that $F1S_3MN$ is the most thermally stable OS solvent with $LiPF_6$.

Synthesis of DF1S3MN:

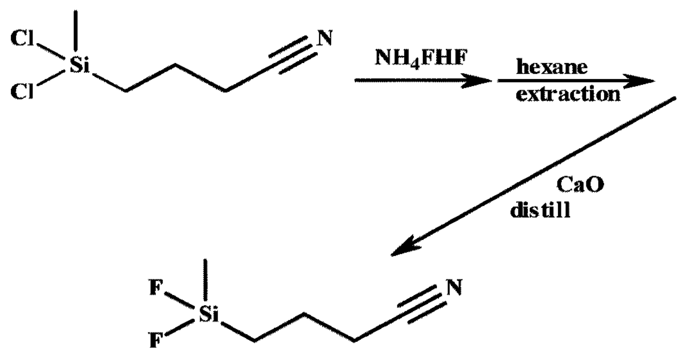

Scheme 14

Commercial 3-cyanopropyldichloromethylsilane (CAS No. 1190-16-5; Sigma Aldrich, St. Louis, MO, US) was fluorinated with ammonium bifluoride at room temperature. Cold hexane was then added to the mixture. The solid was filtered off and the solvent evaporated. Calcium oxide was added to the crude product. The solvent was distilled under vacuum between 35-45°C at 0.4 Torr to yield the desired product in very high purity (~99.8%) and approximately 90% yield.

Synthesis of DF1S2MN:

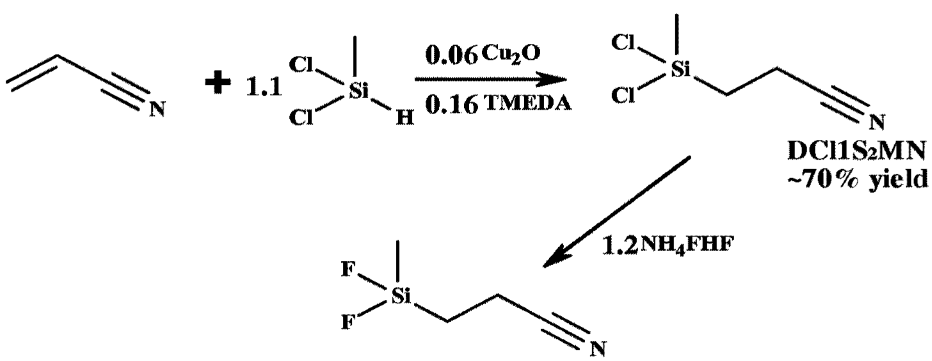

Scheme 15

Acrylonitrile was mixed with N,N,N',N'-tetramethylethylenediamine and copper (I) oxide in a flask and heated to 60°C. Dichloromethylsilane was then added dropwise and refluxed overnight. After cooling to room temperature, the mixture was distilled under vacuum (43°C, 0.2 Torr) to yield the dichloro intermediate (DCl1S_2MN). The intermediate was fluorinated using 1.2 mol equivalents of ammonium hydrogen fluoride at room temperature or 1.2 mol equivalents of sodium hydrogen fluoride at 130°C. Dichloromethane was then added and the solid filtered off. The solvent was evaporated and the crude product was distilled under vacuum. Triethylamine and molecular sieves were added to the product and distilled under vacuum between 25-33°C at 0.1 Torr to yield the desired product at extremely high purity (>99%) at approximately 75% yield.

Thermal Stability of DF1S_3MN:

FIG. 10 depicts the thermal stability of DF1S_3MN with $LiPF_6$. DF1S_3MN-$LiPF_6$ electrolyte (ZP990-01) was exposed to temperatures from 30°C to 150°C and analyzed by electron impact mass spectrometry (EI-MS) and nuclear magnetic resonance spectroscopy (NMR) for gas and liquid decomposition products, respectively. DF1S_3MN showed no significant gas and/or liquid phase decomposition up to 150°C.

Differential Scanning Calorimetry (DSC) Evaluation for Thermal Abuse Tolerance:

DSC measurements were conducted with F1S_3MN and carbonate based electrolytes in the presence of de-lithiated cathode materials to evaluate potential thermal abuse tolerance effects that could translate to safety advantages in a full cell format. Higher onset temperature, lower total heat output and lower peak heat output are all effects that suggest improved thermal abuse behavior in full format cells.

FIG. 11 depicts the thermal stability of F1S_3MN with $LiPF_6$ and various carbonate co-solvents and is compared to a carbonate control electrolyte with $LiPF_6$. Cells containing each electrolyte were charged to 4.25V and then disassembled. The lithium nickel cobalt aluminum oxide (NCA) cathode was rinsed with diethylene carbonate and allowed to dry. Each sample containing 5 mg of active material and 2 mg of fresh electrolyte was hermetically sealed into a stainless steel DSC pan. DSC scans at a rate of 2 °C/min showed that the carbonate control electrolyte reacted at a much lower onset temperature than any of the organosilicon electrolyte blends. Additionally, the electrolyte where organosilicon is substituted for EMC has a much lower peak heat output than the control electrolyte.

Preparation of Electrolytes:

Blending of electrolytes is completed inside a moisture-free (< 5ppm) and oxygen-free (< 20ppm) argon glove box. All electrolyte components, including solvents, salts, and additives have been properly dried before blending and are stored in the glove box. Solvent moisture is monitored periodically by Karl Fischer measurement to ensure moisture levels are maintained at < 20ppm. Generally, solvents are weighed first into a separate vial and mixed until homogeneous. 70% of the solvent is added to a volumetric flask. Lithium (or other) salt is added slowly and stirred by magnetic stir bar until completed dissolved. Any other additives (*i.e.* VC, LiBOB) are then added slowly and stirred until the solution is homogeneous. The stir bar is removed and a portion of the remaining solvent is added to complete the volumetric requirement. The stir bar is placed back into the volumetric flask and the electrolyte is stirred until homogeneous. After blending is complete the electrolyte is dispensed into a dried vial or alternate container for storage.

Performance of $F1S_3MN$ in Lithium Ion Cells:

FIG. 12 depicts the discharge capacity at 30°C of cells containing various electrolyte solvents. Three different electrolyte solvents were tested in Lithium Ion cells over a series of cycles at different C-rates in a 2032-size coin cell assembly (assembly stack as in FIG. 13) containing a graphite anode, a lithium nickel cobalt aluminum oxide (NCA) cathode, and "2500"-type separator from Celgard, LLC (Charlotte, NC). The three electrolyte solvents were: (1) control EPA6 carbonate electrolyte comprising 1:1 by volume ethylene carbonate (EC) and diethyl carbonate (DEC) (triangles); (2) an $F1S_3MN$-based electrolyte comprising 79% $F1S_3MN$, 20% EC, 1 M $LiPF_6$, and solid electrolyte interphase (SEI)-forming additives (squares); and (3) an $F1S_3M2$-based electrolyte, comprising 79% $F1S_3M2$, 20% EC, 1 M $LiPF_6$, and SEI-forming additives (circles). As shown in FIG. 12, the $F1S_3MN$-based electrolyte is equivalent to EPA6 at the 4C rate.

FIG. 14 depicts the discharge capacity at 55°C of cells containing the same electrolytes as shown in, and described for FIG. 12. The cells were assembled in the same manner and cycled at a C/2 rate. As shown in FIG. 14, the $F1S_3MN$-based solvent had improved cycling stability at 55°C compared to both the carbonate control and the $F1S_3M2$-based electrolyte.

Performance of $F1S_3MN$ and $DF1S_2MN$ in Electrical Double-Layer Capacitors Cells:

Symmetric electrical double layer capacitors (EDLC) were assembled into CR2032 coin cells as depicted in FIG 15. A glass fiber separator (AP40, Merck Millipore) was sandwiched between two pieces of AC cloth electrode, with 100 μL electrolyte added to the separator. Tetraethylammonium tetrafluoroborate (TEA-BF_4, Alfa Aesar, 99%) and tetrabutylphosphonium hexafluorophosphate (TBP-PF_6, Sigma Aldrich, ≥99.0%) were used as the salts. Organosilicon solvents of $F1S_3MN$ (99.4%) and $DF1S_2MN$ (99.8%) were made by Silatronix. Acetonitrile (AN, Sigma Aldrich, anhydrous, 99.8%) was used as a co-solvent.

Zorflex FM10 100% activated carbon (AC) cloth from Calgon carbon was used for both electrodes. FM10 has 1000-2000 m^2/g surface area, 0.5 mm thickness, and 120 g/m^2 area density. The AC cloth was punched to 15 mm diameter discs, and used directly as electrodes without any binder or conductive additives.

The performance of EDLC cells was tested by cyclic voltammetry (CV) using a Biologic BMP300 potentiostat. The temperature as control in an oven with variation as $\pm 0.1\,^{0}C$. The cyclic voltammetry (CV) responses of the EDLC cells was conducted between 0 and 3 V at a scan rate of 10 mV/s. A normalized specific capacitance, C, was derived according to the following equation [1,2]:

$$C = \frac{i}{mv}$$

where i is the current, v is the scan rate, m is the mass of one electrode.

FIG. 16 shows the cyclic voltammograms of EDLC cells with OS electrolytes containing TEA-BF_4 salt. Electrolyte ZX1193 included 1.0M TEA-BF_4 dissolved in 70 volume percent $DF1S_2MN$ and 30 volume percent acetonitrile. Electrolyte ZX1190 included 0.8M TEA-BF_4 dissolved into blended $DF1S_2MN$ and acetonitrile solvents, 60:40 by volume. The EDLC cells with both electrolyte formulations showed the regular and symmetric features to the 0 horizontal axis, indicating a non-redox or faradic properties of the cell.

FIG. 17 shows the cyclic voltammograms of EDLC cells with ZX1170 electrolyte and ZX1184 electrolyte containing TBP-PF_6 salt. Electrolyte ZX1170 has 1.2M TBP-PF_6 dissolved into $F1S_3MN$, and electrolyte ZX1184 has 1.2M TBP-PF_6 dissolved into $DF1S_2MN$. The non-redox or faradic properties can also be observed from the EDLC cells with both electrolyte ZX1170 and ZX1184 formulations.

1ND1N Synthesis:

Scheme 16 depicts a synthesis scheme for 1ND1N. 1ND1N cannot be chemically dried with sodium (Na), calcium oxide (CaO), or calcium hydride (CaH_2).

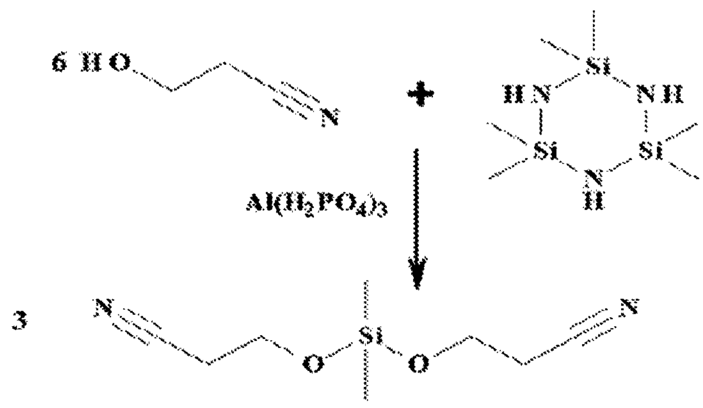

Scheme 16

Electrochemical Stability of 1ND1N:

The molecular orbital diagram for 1ND1N and 1ND1, not shown, reveal the energy difference between the highest occupied molecular orbital (HOMO) and the lowest unoccupied molecular orbital (LUMO) for 1ND1N is 7.88 eV (LUMO = 0.21 eV; HOMO = -7.88 eV) and for 1ND1 is 8.36 eV (LUMO = 1.63 eV; HOMO = -6.73 eV). 1ND1N has great oxidation stability but lower reduction resistance than 1ND1.

FIG. 18 depicts the oxidation stability of 1ND1N with 1M $LiPF_6$ or 1M LiTFSI in current density (mA/cm^2) versus voltage (V vs. Li/Li^+). The oxidation stability was tested at room temperature with a working electrode as Pt, a counter electrode as Li, a reference electrode as Li/Li^+, and a sweep rate of 10 mV/s.

FIG. 19 depicts the reduction stability of 1ND1N with 1M $LiPF_6$ or 1M LiTFSI in current density (mA/cm^2) versus voltage (V vs. Li/Li^+). The reduction stability was tested at room temperature with a working electrode as Pt, a counter electrode as Li, a reference electrode as Li/Li^+, and a sweep rate of 10 mV/s. Two separate scans for each electrolyte are shown.

FIGS. 20A and 20B depict current density (mA/cm^2) versus voltage (V vs. Li/Li^+) for cycling scans with 1ND1N and 1M $LiPF_6$ or 1M LiTFSI from 0 to 6 V and from 6 to 0 V. FIG. 20A depicts a first cycle. FIG. 20B depicts a second cycle.

FIGS. 21A and 21B depict the oxidation stability of $F1S_3MN$ or 1ND1N with 1M $LiPF_6$ in current density (mA/cm^2) versus voltage (V vs. Li/Li^+). The oxidation stability was tested at room temperature with a working electrode as Pt, a counter electrode as Li, a reference electrode as Li/Li^+, and a sweep rate of 10 mV/s. FIG. 21B depicts a close-up of the same data shown in FIG. 21A. The $F1S_3MN$-$LiPF_6$ electrolyte had a current density of 1 mA/cm^2 at 7.3 V, and the 1ND1N-$LiPF_6$ electrolyte had a current density of 1 mA/cm^2 at 7.2 V.

FIGS. 22A and 22B depict the oxidation stability of $F1S_3MN$ or 1ND1N with 1M LiTFSI in current density (mA/cm^2) versus voltage (V vs. Li/Li^+). The oxidation stability was tested at room temperature with a working electrode as Pt, a counter electrode as Li, a reference electrode as Li/Li^+, and a sweep rate of 10 mV/s. FIG. 22B depicts a close-up of the same data shown in FIG. 22A. The $F1S_3MN$-LiTFSI electrolyte had a current density of 1 mA/cm^2 at 6.2 V, and the 1ND1N-LiTFSI electrolyte had a current density of 1 mA/cm^2 at 6.5 V.

Thermal Stability of 1ND1N:

FIG. 23 depicts the thermal stability of neat 1ND1N. 1ND1N was exposed to temperatures ranging from 30°C to 189°C and analyzed by mass spectrometry for decomposition products. 1ND1N showed no liquid or gas phase decomposition products up to 189°C. ^1H NMR showed ~%5 decomposition.

FIG. 24 depicts the thermal stability of 1ND1N with $LiPF_6$. 1ND1N-$LiPF_6$ electrolyte was exposed to temperatures ranging from 30°C to 150°C and analyzed by mass spectrometry for decomposition products. The temperatures at which salient peaks appeared are annotated. 1ND1N showed gas phase decomposition ≥ 70°C, but no vigorous reaction was observed up to 150°C. Me_2SiF_2 (81 m/z) (96 g/mol) and a peak at 52/53 m/z suspected as being acrylonitrile (53 g/mol) appeared at a temperatures of 125-150°C. No 1,4-dioxane gas was observed at 150°C. ^1H NMR analysis showed that 50.6% 1ND1N remained at 125°C and 58% remained at 150°C. At 125°C, presence of 39.7% fluorinated product F1NM1N (vs. 2.3% in unheated sample, 1.6% Me_2SiF_2 (vs. 0% in unheated sample), and 2.95 % hydrolysis (vs. 5.5% in unheated sample) was observed. At 150°C, presence of 41% fluorinated product F1NM1N (vs. 2.3% in unheated sample), 1.7% Me_2SiF_2 (vs. 0% in unheated sample), and 5.0 % hydrolysis (vs. 5.5% in unheated sample) was observed.

To identify the peaks observed at 52/53 m/z upon heating 1ND1N-$LiPF_6$ at 125-150°C, the mass spectrum profile for heated 1ND1N-$LiPF_6$ was compared with the mass spectrum profiles of National Institute of Standards and Technology (NIST) standards for 2-propenenitrile and hydrogen cyanide. FIG. 25A depicts a close-up of the mass spectrum profile as described with respect to FIG. 24 from 24-30 m/z. FIG. 25B depicts a close-up of the mass spectrum profile as described with respect to FIG. 24 from 49-55 m/z. The temperatures at which salient peaks in FIGS. 25A and 25B appeared are annotated. The peaks at 51, 52, and 53 m/z in FIG. 25B indicate that acrylonitrile is likely present. The presence of HCN cannot be definitively confirmed or disconfirmed due to the presence of peaks at 26 and 27 m/z in the NIST spectra. The spectrum in FIG. 25A shows a greater peak intensity at 26 m/z compared to 27 m/z, which supports the presence of acrylonitrile. However, the magnitude of the peak at 27 m/z is greater than expected for acrylonitrile alone.

FIG. 26 depicts the thermal stability of 1ND1N with LiTFSI, vinylene carbonate (VC) and lithium bis(oxalato)borate (LiBOB). 1ND1N-LiTFSI-VC-LiBOB was exposed to temperatures ranging from 30°C to 185°C and analyzed by mass spectrometry for decomposition products. 1ND1N-LiTFSI-VC-LiBOB showed no gas phase decomposition products up to 185°C. ^{1}H NMR showed an increase in hydrolysis from 3% (in the unheated sample) to 18.7% (after heating), which was likely due to a delay before the NMR analysis was performed.

FIG. 27 depicts the thermal stability of 1ND1N with $LiBF_4$. 1ND1N-$LiBF_4$ was exposed to temperatures ranging from 30°C to 125°C and analyzed by mass spectrometry for decomposition products. The temperatures at which salient peaks appeared are annotated. Gas phase products evolved at $\geq$ 30°C. As expected, Me_2SiF_2 (81 m/z) (96 g/mol) was observed. No acrylonitrile was observed. ^{1}H NMR showed 3.7% hydrolysis and 34.2% fluorinated products (3 sets of peaks). ^{19}F NMR showed that all F in the system was bonded to Si. No BF_4 remained. There was insufficient F to fully decompose 1ND1N (~5M 1ND1N versus 4 M F).

While no acrylonitrile was observed by mass spectrometry in heated 1ND1N-$LiBF_4$ samples, it was observed in unheated control (70 ppm). This indicates 1ND1N is not stable with $LiBF_4$ at room temperature. NMR analysis revealed that heating does little to increase decomposition, as shown in the following table:

	^{1}H (MeSi peak)	
	hydrolysis	fluorination
Before Heating	3%	43%
After Heating	4%	34%

Performance of 1ND1N in Cells:

FIG. 28 depicts the discharge capacity of cells containing various electrolytes at a variety of C-rates. The electrolyte solvents were: (1) 1ND1N; (2) 1ND1N with 20% ethylene carbonate (EC) co-solvent (1ND1N_EC); and (3) 1ND2 with 20% EC co-solvent (1ND2_EC). All formulations also contained SEI-forming additives and 1 M $LiPF_6$ salt. As shown in FIG. 28, 20% EC co-solvent improved the performance of 1ND1N. With 20% EC co-solvent, 1ND1N showed diminished performance compared to 1ND2 at all C-rates.

FIG. 29 depicts the discharge capacity of cells containing various other electrolyte solvents. The electrolyte solvents were: (1) 1ND1N with 20% EC co-solvent, 1 M $LiPF_6$ and SEI-forming additives (1ND1N-EC- $LiPF_6$, shown as 1ND1N_EC in FIG. 29); (2) 1ND1N with 20% EC co-solvent, 1 M LiTFSI and SEI-forming additives (1ND1N-EC-LiTFSI, shown as 1ND1N_T in FIG. 29); and (3) 1ND2 with 20% EC co-solvent, 1 M $LiPF_6$ and SEI-forming additives (1ND2-EC-$LiPF_6$, shown as CP597-07 in FIG. 29). The 1ND1N-EC-$LiPF_6$ combination and the 1ND1N-EC-LiTFSI combination showed performance comparable to the 1ND2-EC-$LiPF_6$ combination.

FIGS. 30A and 30B depict the discharge capacity of cells containing a 1ND1N-$LiPF_6$-based electrolyte or a 1ND1N-LiTFSI-based electrolyte, respectively, at a variety of C-rates. For each experiment, a CR2032 coin cell with a Saft America (Cockeysville, MD) NCA cathode, a graphite anode, and a 2500 separator from Celgard, LLC (Charlotte, NC) was used. The cells were charged with a constant-current/constant-voltage (CCCV) procedure at C/5, C/2, 1C or 2C rates to 4.1 V. The cells were discharged each cycle to 3.0 V with a constant current at the same rate that they were charged. In FIG. 30A, the 1ND1N-$LiPF_6$-based electrolyte solution included 1 M $LiPF_6$ and 1ND1N (batch ZP780-01), and the charging/discharging was performed at 30°C or 55°C. In FIG. 30B, the 1ND1N-LiTFSI-based electrolyte solution included 1 M LiTFSI and 1ND1N, batch (ZT781-01), and the charging/discharging was performed at 30°C, 55°C, or 70°C. As shown in FIGS. 30A and 38B, the 1ND1N-LiTFSI-based electrolyte displayed better rate capability than the 1ND1N-$LiPF_6$-based electrolyte.

Physical Properties of OS Solvents and Electrolyte Solutions:

Table 1, above, shows physical properties of selected organosilicon (OS) compounds ($1S_3MN$, $F1S_3MN$, $F1S_3cMN$, $DF1S_3MN$, $DF1S_2MN$, and $F1S_3M2$) as neat solvents and formulated electrolyte solutions. Table 2, above, shows physical properties of neat 1ND2, 1ND1, 1ND1N $F1S_3MN$, $DPF1S_3MN$, $F1S_3MC$, $F1S_3ME$, $F1S_3MA$, $F1S_3MS$, 1NMS,

$F1S_3M2$, and $F1S_{3c}MN$ and various electrolyte compositions containing them. In both tables, the conductivity has units of mS/cm, the viscosity has units of cP, and the flash point is in degrees Celsius.

Proton (^1H) NMR spectra taken in $CDCl_3$ for 1ND1N, 1ND1N, $DF1S_2MN$, $DF1S_3MN$, $F1S_3cMN$, and $1S_3MN$ are presented in Figs. 31-36, respectively. For selected compounds containing a fluorine atom, ^{19}F- NMR data were collected in $CDCl_3$ and DMSO-d_6. The results are tabulated below:

<u>^{19}F-NMR in $CDCl_3$</u>

$F1S_3MN$	-162.3 ppm, $^1J(^{19}F,^{29}Si)$=280Hz
iso$F1S_3MN$	-166.6 ppm, $^1J(^{19}F,^{29}Si)$=284Hz
$DF1S_3MN$	-135.3 ppm, $^1J(^{19}F,^{29}Si)$=296Hz
$TF1S_3MN$	-136.8 ppm, $^1J(^{19}F,^{29}Si)$=280Hz
$DF1S_2MN$	-135.2 ppm, $^1J(^{19}F,^{29}Si)$=296Hz

<u>^{19}F-NMR in DMSO-d_6</u>

$F1S_3MN$	-159.2 ppm, $^1J(^{19}F,^{29}Si)$=279Hz

Thermal Stability of OS Electrolyte Solutions:

FIGS. 37 and 38 depict the gas phase decomposition of $F1S_3MC$, $F1S_3cMN$, $1S_3DN$ $DF1S_2MN$, $TF1S_2MN$ and $TF1S_3MN$ with 1M $LiPF_6$. Each electrolyte was exposed to temperatures ranging from 30°C to 175°C (60 min at each step) and analyzed by electron impact mass spectrometry (EI-MS) and nuclear magnetic resonance spectroscopy (NMR) for gas and liquid decomposition products, respectively. No significant gas and/or liquid phase decomposition was noted up to 175°C.

Conclusions:

$F1S_3MN$ and 1ND1N are both suitable for use as electrolyte solvents in Li-ion batteries. $F1S_3MN$ and $DF1S_2MN$ have demonstrated function as electrolyte solvents in EDLC devices. $F1S_3MN$ shows very high thermal stability (measured by ^1H NMR) with all salts tested. $F1S_3MN$ shows the highest thermal stability of any OS with $LiPF_6$ (175°C), with no observed decomposition. $F1S_3MN$ does produce gas phase products as neat solvent, with $LiBF_4$, and with LiTFSI. These gas phase products can be attributed to low levels of $F1S_3MN$ evaporation. $F1S_3MN$ shows increased voltage stability (higher oxidation potential with wide window) compared to F1S_3M2. F1S_3MN provides equivalent performance as EPA6 up to a rate of 4C. LiBOB has limited solubility in F1S_3MN (<0.03M) without co-solvent, but LiBOB solubility improves (>0.1M) with use of co-solvent (i.e. 20% EC). The decomposition products of F1S_3MN are Me_2SiF_2 and $MeSiF_3$, both of which are gases.

1ND1N shows no gas phase decomposition as a neat solvent or in combination with LiTFSI electrolyte up to 185-190°C. The combination of 1ND1N with LiTFSI electrolyte shows promise up to 70°C and higher. 1ND1N with $LiPF_6$ is more thermally stable than either 1ND1 or 1ND2 with $LiPF_6$. It forms acrylonitrile above 125°C. Like other non-spacer compounds, 1ND1N reacts at room temperature with $LiBF_4$. However, there is insufficient F to fully decompose the 1ND1N, and it does not form acrylonitrile. The rate performance of 1ND1N is slightly lower than 1ND2.

F1S_3ME, DPF1S_3MN and F1S_3MC are all suitable for use as electrolyte solvents in Li-ion batteries. F1S_3MC, F1S_{3c}MN, 1S_3DN, DF1S_2MN, TF1S_2MN, and TF1S_3MN demonstrate thermal stability with $LiPF_6$ (175°C), with no observed decomposition.

CLAIMS

1. A compound selected from the group consisting of:

$$(R)_{4-a}\text{—}Si\text{—}(Sp\text{—}Y)_a\text{—}Z_b \quad \text{(Formula I)}$$

wherein:

"a" is an integer from 2 to 4; "b" is an integer from 0 to (3 x a);

"Z," which is absent when "b" = 0, is selected from the group consisting of "R" and

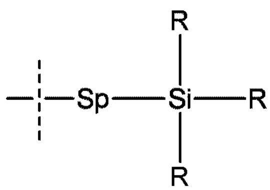

(Formula II);

where each "R" is independently selected from the group consisting of halogen, C_{1-6} linear or branched alkyl, alkenyl, or alkynyl and C_{1-6} linear or branched halo-alkyl, halo-alkenyl, or halo-alkynyl, wherein at least one "R" is fluorine;

each "Sp" in Formulas I and II is independently selected from the group consisting of C_{1-15} linear or branched alkylenyl and C_{1-15} linear or branched halo-alkylenyl; and

each "Y" in Formula I is independently selected from the group consisting of:

Date Reçue/Date Received 2023-01-30

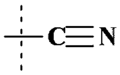, 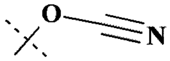, 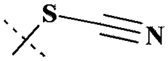, 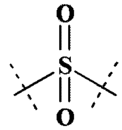, 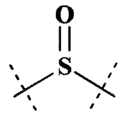,

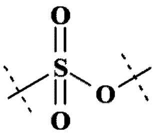, 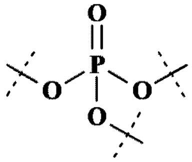, 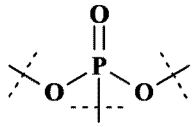. 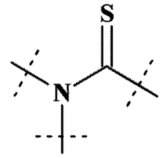,

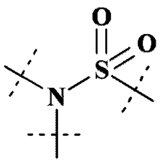, 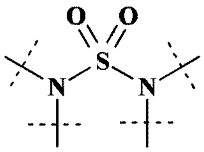, 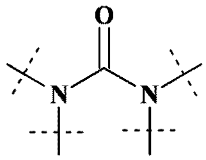, 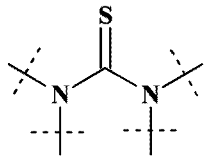,

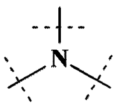, 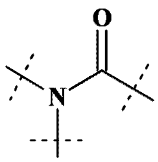, 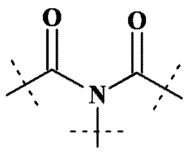, 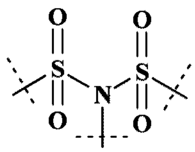, 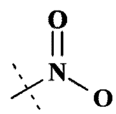,

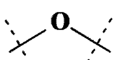, 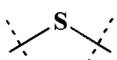, 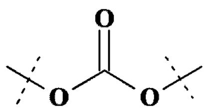, 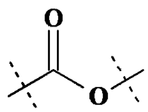, 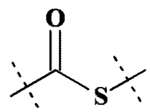,

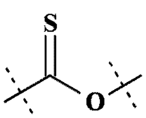, 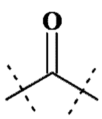, 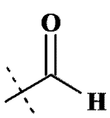, 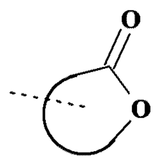, 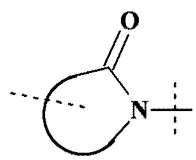,

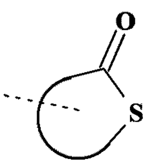, 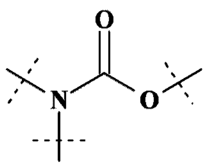, 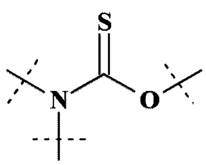, 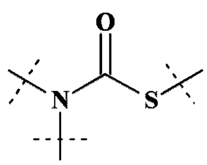,

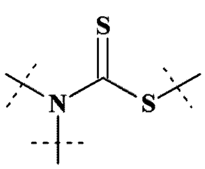, and 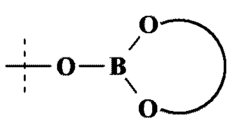,

wherein a curved bond denotes a C_{2-6} alkylene bridging moiety.

Date Reçue/Date Received 2023-01-30

2. The compound of claim 1, wherein each "Y" is independently an organic polar group selected from the group consisting of:

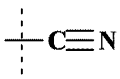

,
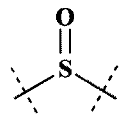

, and
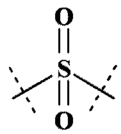

.

3. The compound of claim 2, wherein each "R" is independently selected from the group consisting of fluorine and C_{1-6} linear or branched fluoro-alkyl, fluoro-alkenyl, and fluoro-alkynyl; and

each "Sp" in Formulas I and II is independently selected from the group consisting of C_{1-15} linear or branched fluoro-alkylenyl.

4. The compound of claim 1, wherein "a" is 2, and "b" is 0 to 6.

5. The compound according to claim 4, wherein "b" is 1 and "Z" is "R".

6. The compound according to claim 4, wherein at least one "R" is fluorine, and each "Sp" is independently selected from the group consisting of C_{1-6} linear alkylene.

7. The compound of claim 1, wherein "a" is 3, and "b" is 0 to 9.

8. The compound according to claim 7, wherein "b" is 1 and "Z" is "R".

9. The compound according to claim 7, wherein at least one "R" is fluorine, and each "Sp" is independently selected from the group consisting of C_{1-6} linear alkylene.

Date Reçue/Date Received 2023-01-30

10. The compound of claim 1, wherein “a” is 4, and “b” is 0 to 12.

11. The compound according to claim 10, wherein “b” is 1 and “Z” is “R”.

12. The compound according to claim 10, wherein at least one “R” is fluorine, and each “Sp” is independently selected from the group consisting of C_{1-6} linear alkylene.

13. An electrolyte composition comprising a compound as recited in any one of claims 1-3, in combination with a salt.

14. The electrolyte composition of claim 13, wherein the salt is a lithium-containing salt.

15. An electrochemical device comprising an electrolyte composition as recited in claim 13.

Date Reçue/Date Received 2023-01-30

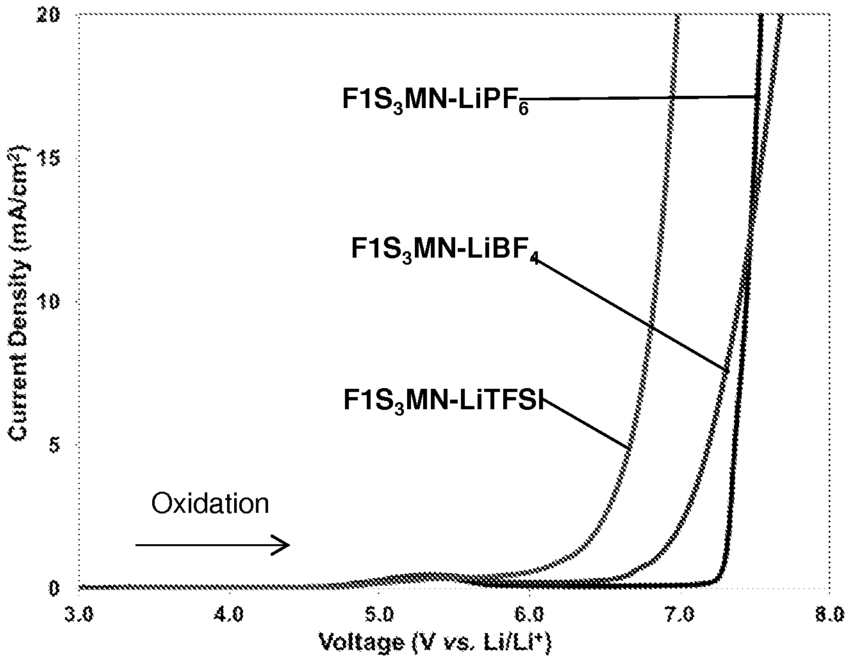
F1S3MN-LiPF6
F1S3MN-LiBF4
F1S3MN-LiTFSI
Oxidation
Current Density (mA/cm2)
Voltage (V vs. Li/Li+)
20
15
10
5
0
3.0
4.0
5.0
6.0
7.0
8.0

FIG. 1A

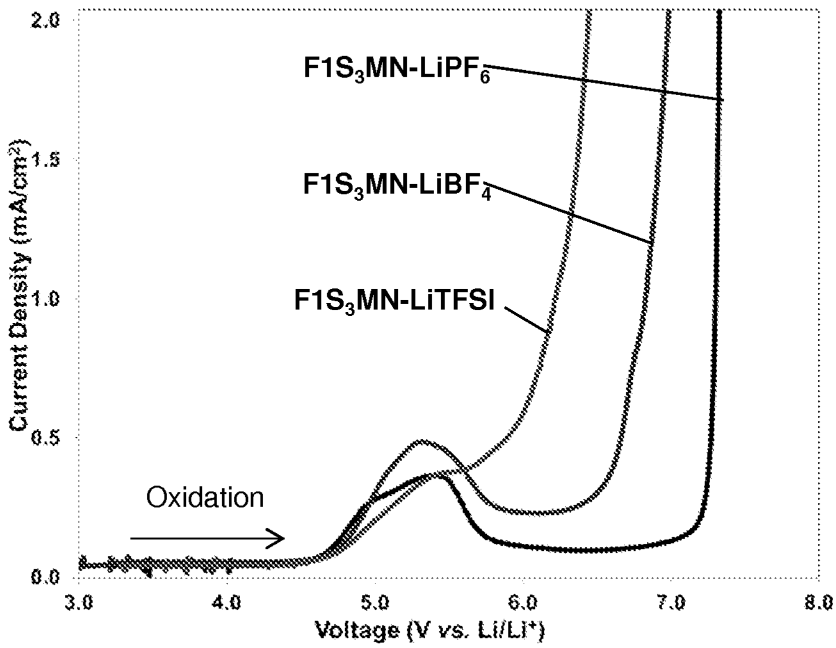
F1S3MN-LiPF6
F1S3MN-LiBF4
F1S3MN-LiTFSI
Oxidation
Current Density (mA/cm2)
Voltage (V vs. Li/Li+)
2.0
1.5
1.0
0.5
0.0
3.0
4.0
5.0
6.0
7.0
8.0

FIG. 1B

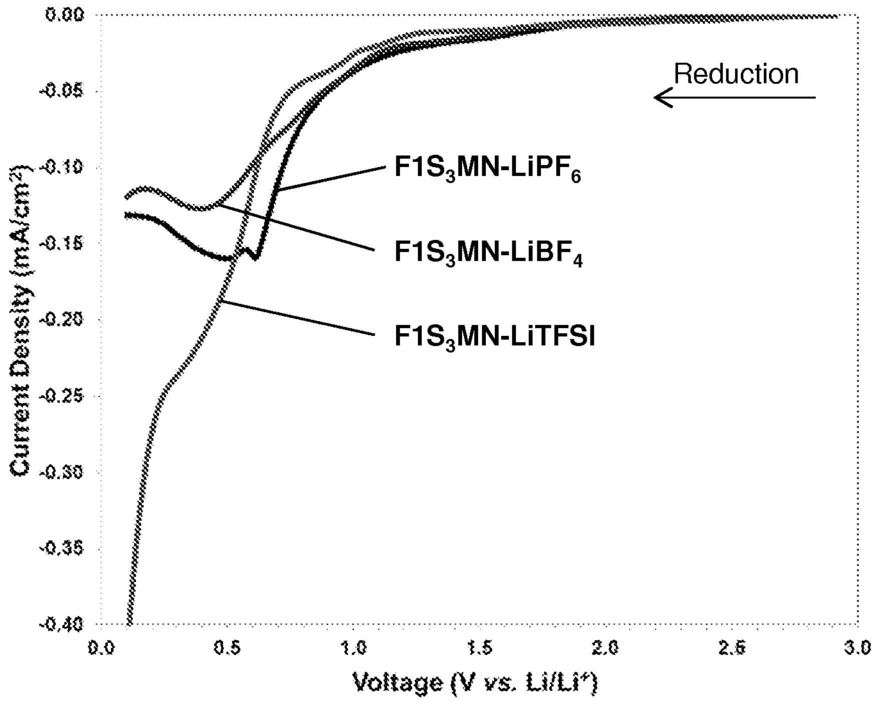
0.00
-0.05
-0.10
-0.15
-0.20
-0.25
-0.30
-0.35
-0.40
0.0
0.5
1.0
1.5
2.0
2.5
3.0
Current Density (mA/cm²)
Voltage (V vs. Li/Li⁺)
Reduction
F1S3MN-LiPF6
F1S3MN-LiBF4
F1S3MN-LiTFSI

FIG. 2A

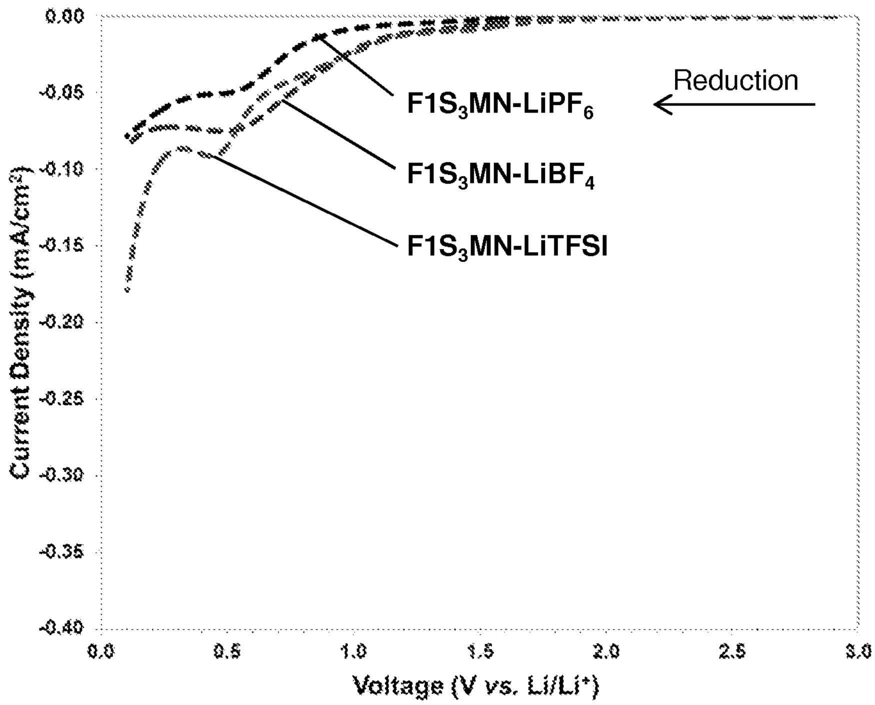
0.00
-0.05
-0.10
-0.15
-0.20
-0.25
-0.30
-0.35
-0.40
0.0
0.5
1.0
1.5
2.0
2.5
3.0
Current Density (mA/cm²)
Voltage (V vs. Li/Li⁺)
Reduction
F1S3MN-LiPF6
F1S3MN-LiBF4
F1S3MN-LiTFSI

FIG. 2B

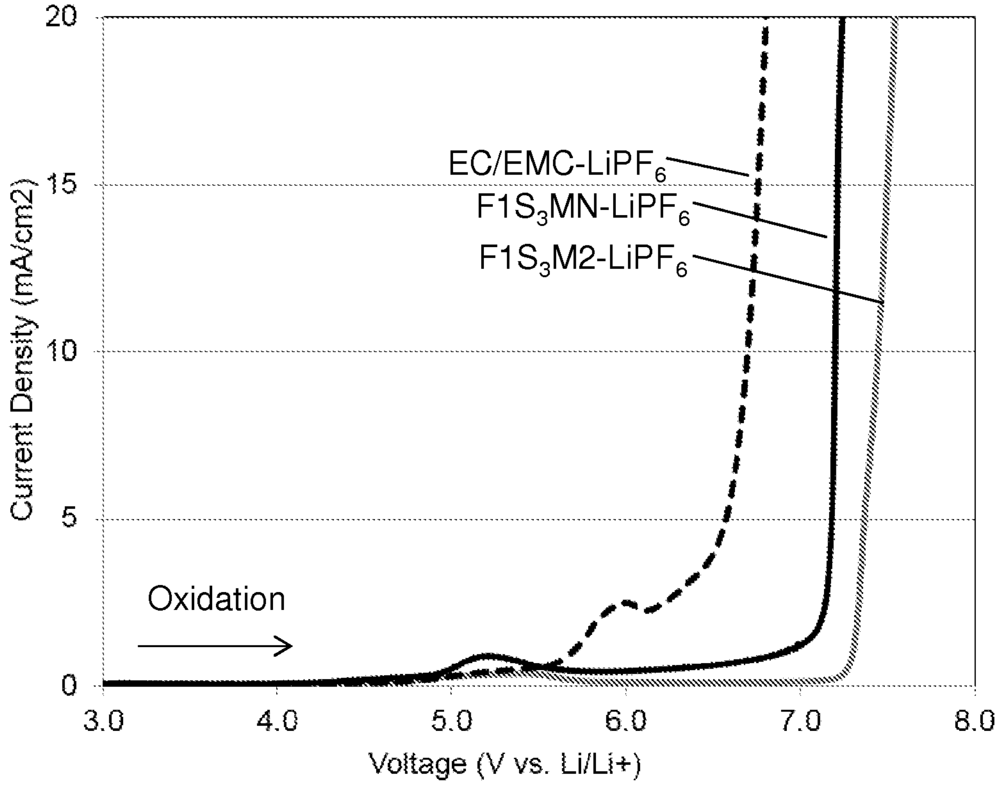
20
15
10
5
0
3.0
4.0
5.0
6.0
7.0
8.0
Current Density (mA/cm2)
Voltage (V vs. Li/Li+)
EC/EMC-LiPF6
F1S3MN-LiPF6
F1S3M2-LiPF6
Oxidation

FIG. 3A

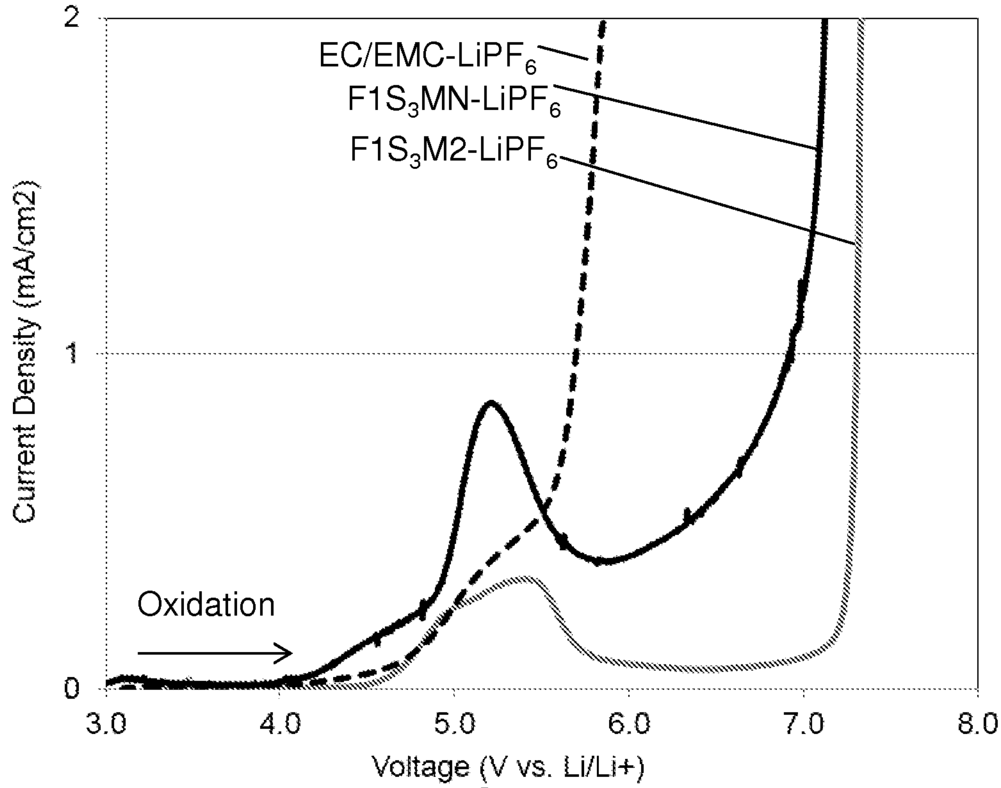
2
1
0
3.0
4.0
5.0
6.0
7.0
8.0
Current Density (mA/cm2)
Voltage (V vs. Li/Li+)
EC/EMC-LiPF6
F1S3MN-LiPF6
F1S3M2-LiPF6
Oxidation

FIG. 3B

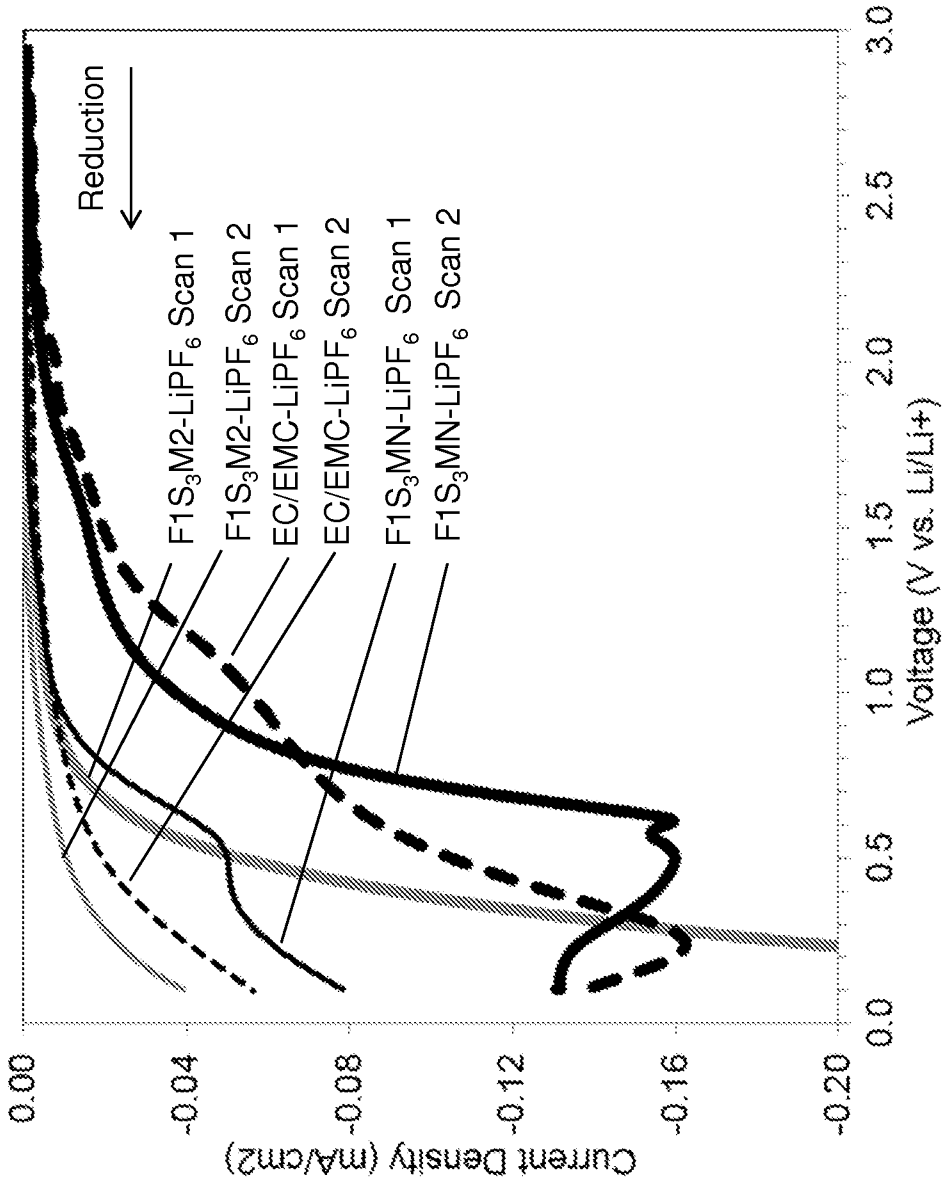
Current Density (mA/cm2)
0.00
-0.04
-0.08
-0.12
-0.16
-0.20
Voltage (V vs. Li/Li+)
0.0
0.5
1.0
1.5
2.0
2.5
3.0
Reduction
F1S3M2-LiPF6 Scan 1
F1S3M2-LiPF6 Scan 2
EC/EMC-LiPF6 Scan 1
EC/EMC-LiPF6 Scan 2
F1S3MN-LiPF6 Scan 1
F1S3MN-LiPF6 Scan 2

FIG. 4

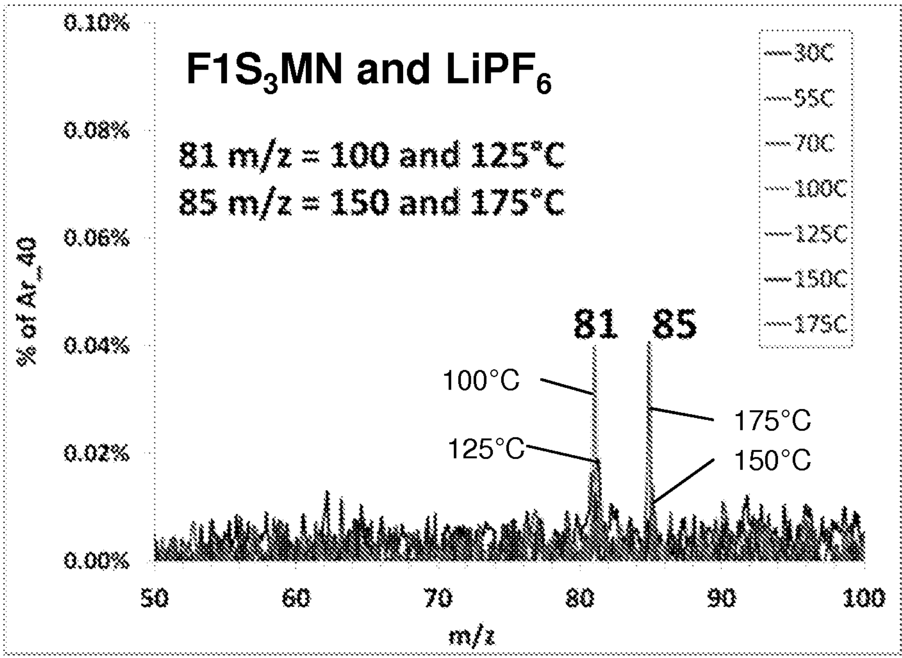
F1S3MN and LiPF6
81 m/z = 100 and 125°C
85 m/z = 150 and 175°C
81
85
100°C
125°C
175°C
150°C
% of Ar_40
0.10%
0.08%
0.06%
0.04%
0.02%
0.00%
50
60
70
80
90
100
m/z
30C
55C
70C
100C
125C
150C
175C

FIG. 5A

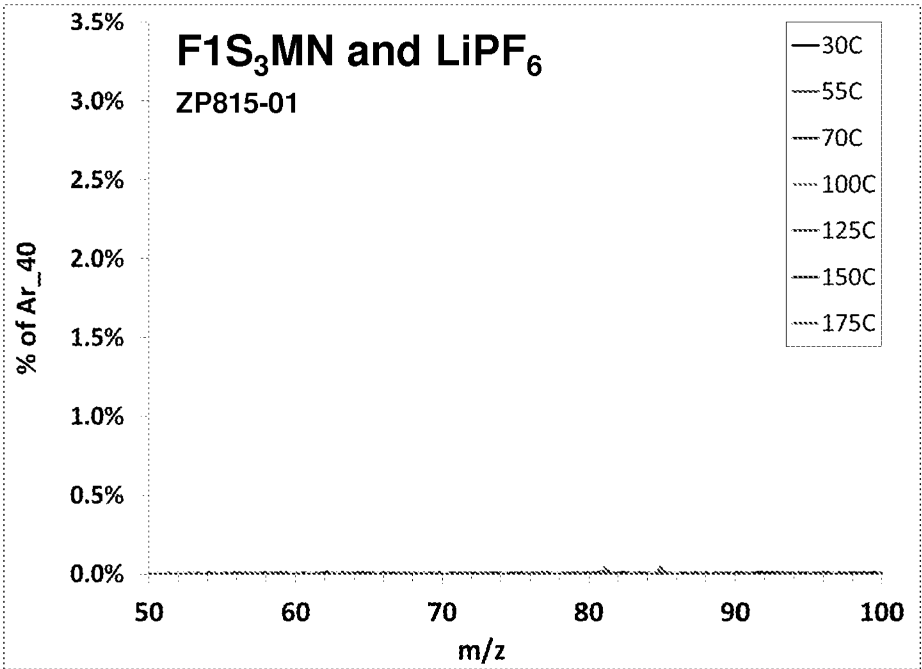
F1S3MN and LiPF6
ZP815-01
% of Ar_40
3.5%
3.0%
2.5%
2.0%
1.5%
1.0%
0.5%
0.0%
50
60
70
80
90
100
m/z
30C
55C
70C
100C
125C
150C
175C

FIG. 5B

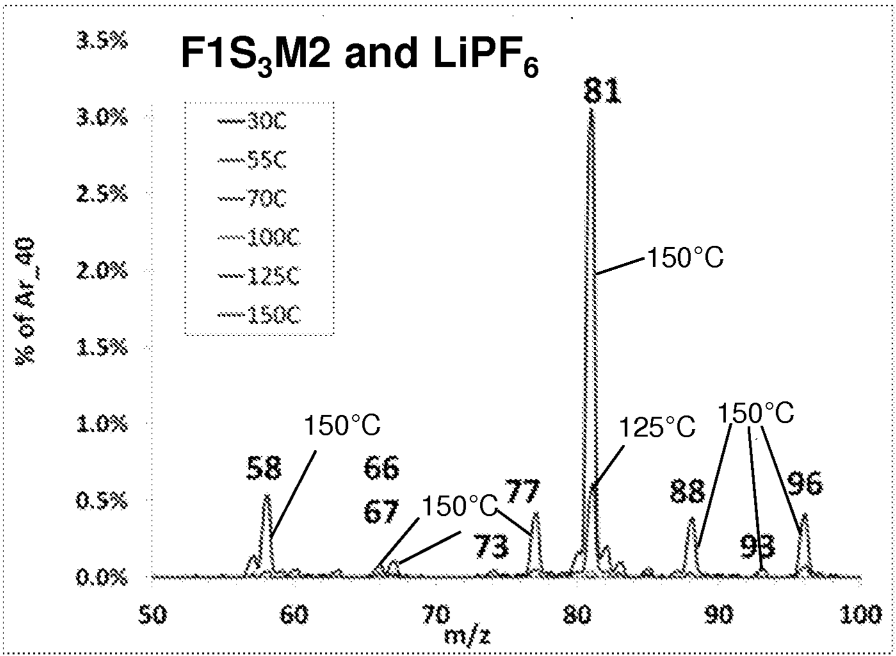
F1S3M2 and LiPF6
3.5%
3.0%
2.5%
2.0%
1.5%
1.0%
0.5%
0.0%
% of Ar_40
30C
55C
70C
100C
125C
150C
81
150°C
125°C
150°C
58
150°C
66
67
150°C
77
73
88
93
96
50
60
70
80
90
100
m/z

FIG. 6

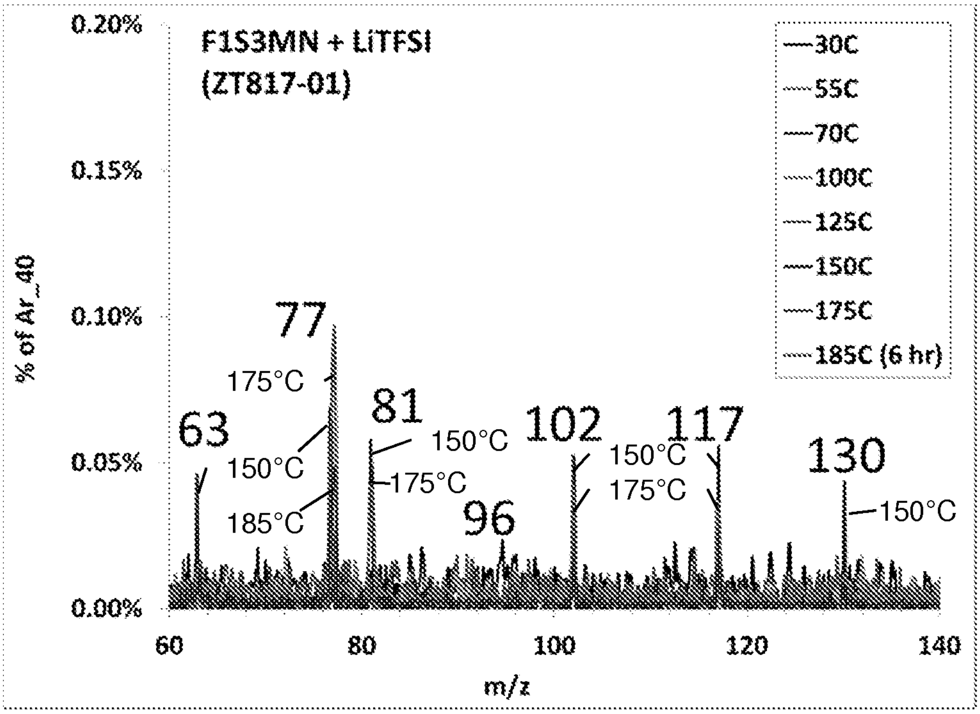
F1S3MN + LiTFSI
(ZT817-01)
0.20%
0.15%
0.10%
0.05%
0.00%
% of Ar_40
60
80
100
120
140
m/z
30C
55C
70C
100C
125C
150C
175C
185C (6 hr)
77
175°C
150°C
185°C
63
81
150°C
175°C
96
102
150°C
175°C
117
130
150°C

FIG. 7

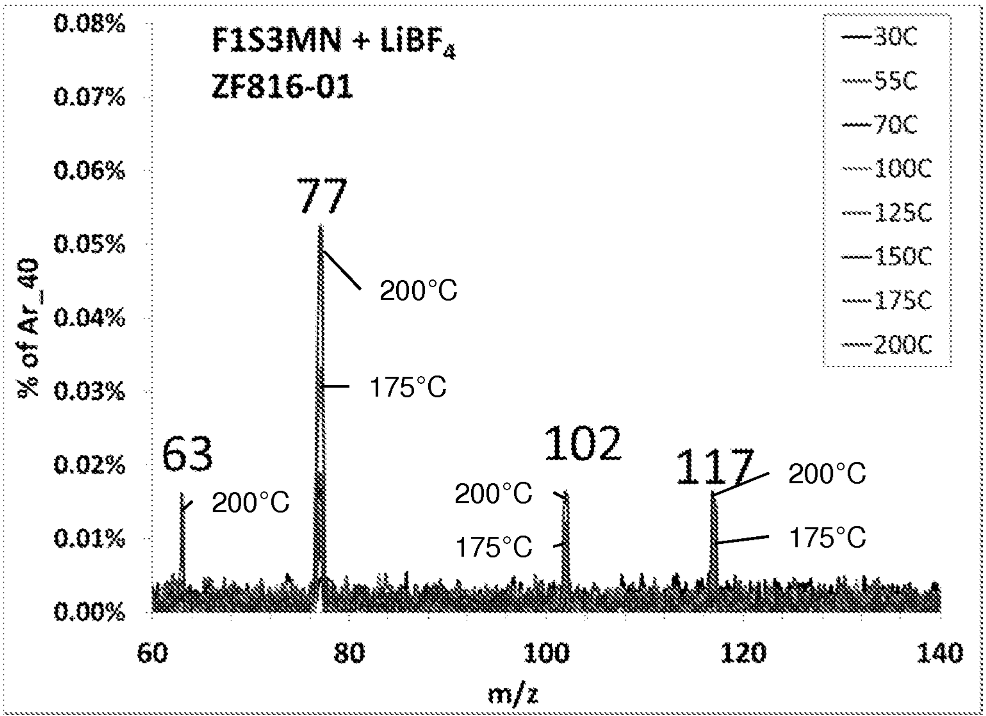
F1S3MN + LiBF4
ZF816-01
0.08%
0.07%
0.06%
0.05%
0.04%
0.03%
0.02%
0.01%
0.00%
% of Ar_40
60
80
100
120
140
m/z
30C
55C
70C
100C
125C
150C
175C
200C
77
200°C
175°C
63
200°C
102
200°C
175°C
117
200°C
175°C

FIG. 8

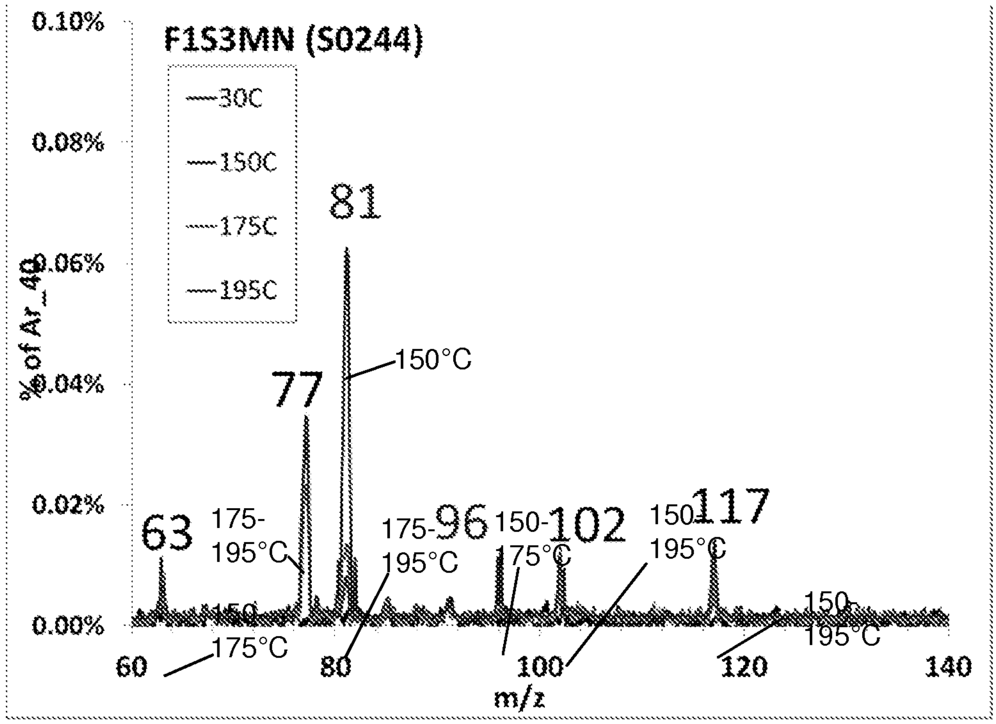
F1S3MN (S0244)
30C
150C
175C
195C
% of Ar_40
0.10%
0.08%
0.06%
0.04%
0.02%
0.00%
81
77
63
96
102
117
150°C
175-195°C
175-195°C
150-175°C
150-195°C
150-195°C
150-175°C
60
80
100
120
140
m/z

FIG. 9

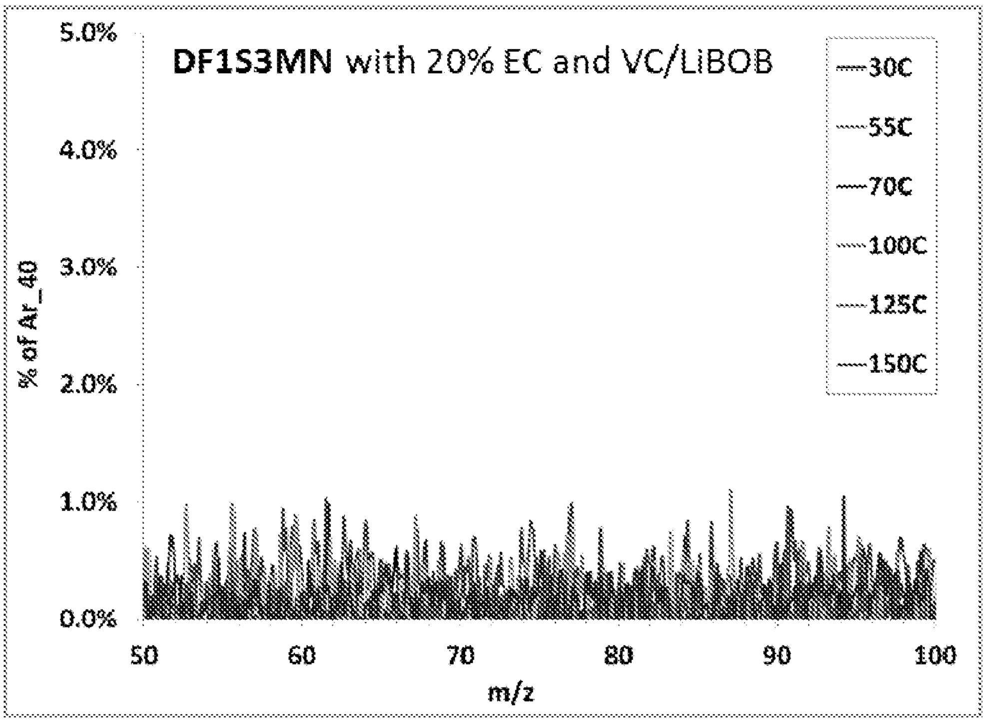
DF1S3MN with 20% EC and VC/LiBOB
30C
55C
70C
100C
125C
150C
% of Ar_40
5.0%
4.0%
3.0%
2.0%
1.0%
0.0%
50
60
70
80
90
100
m/z

FIG. 10

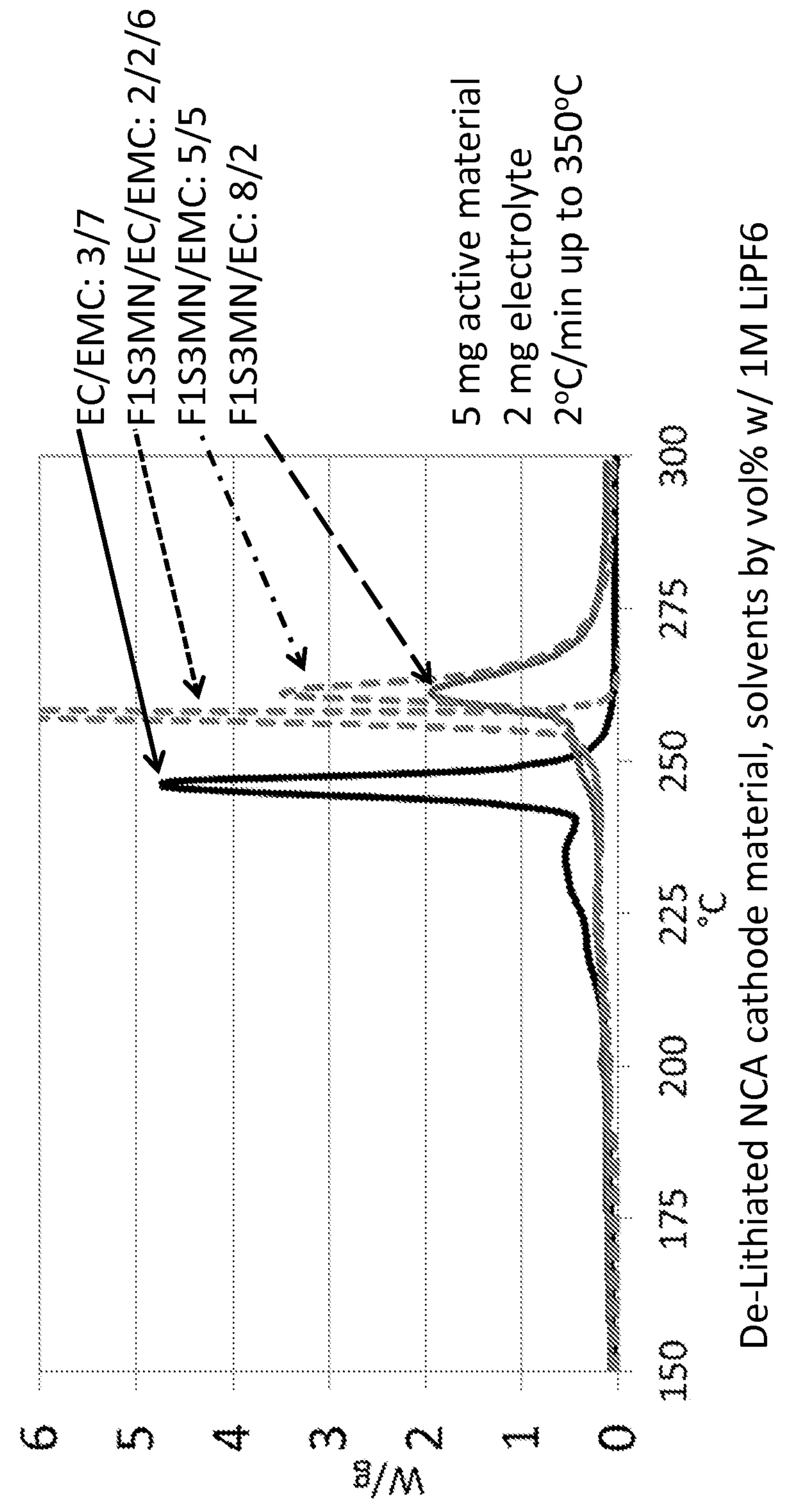
EC/EMC: 3/7
F1S3MN/EC/EMC: 2/2/6
F1S3MN/EMC: 5/5
F1S3MN/EC: 8/2
5 mg active material
2 mg electrolyte
2°C/min up to 350°C
W/g
0
1
2
3
4
5
6
150
175
200
225
250
275
300
°C
De-Lithiated NCA cathode material, solvents by vol% w/ 1M LiPF6

FIG. 11

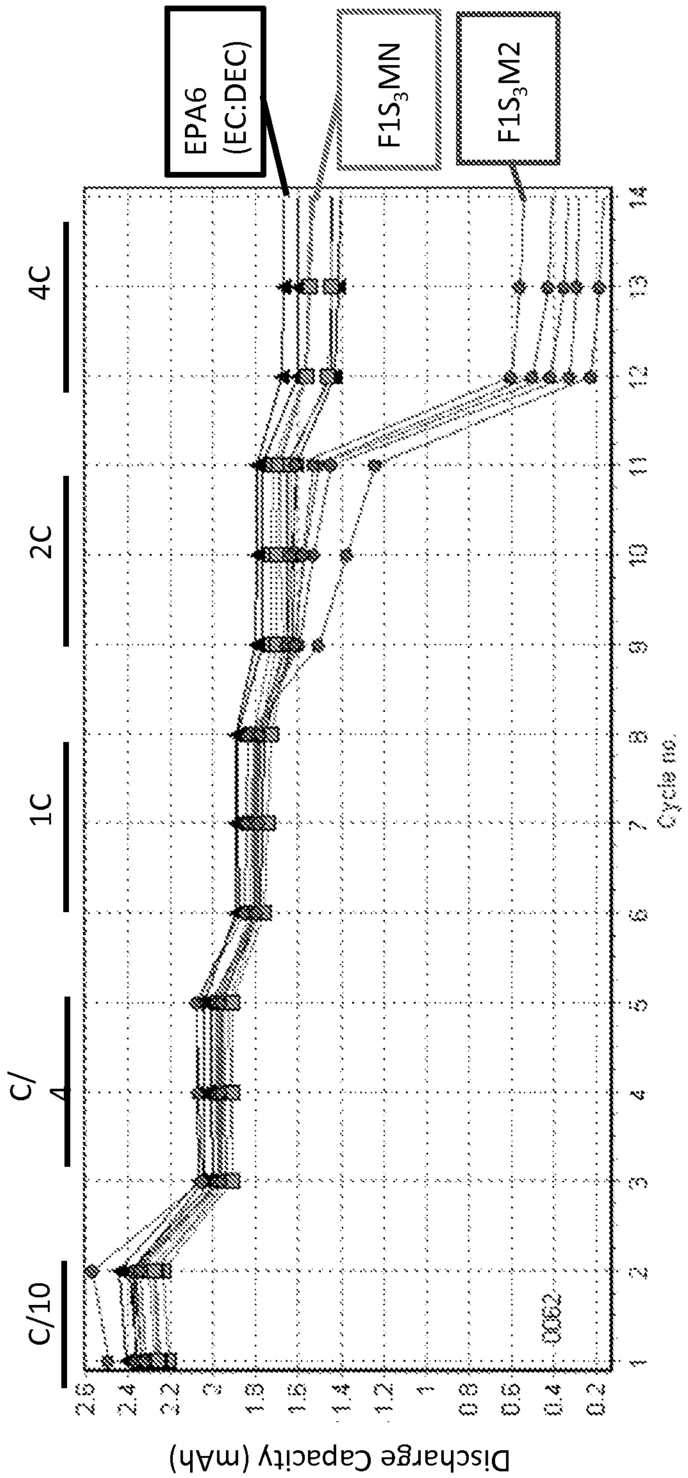
EPA6 (EC:DEC)
F1S3MN
F1S3M2
C/10
C/4
1C
2C
4C
Discharge Capacity (mAh)
Cycle no.
2.6
2.4
2.2
2
1.8
1.6
1.4
1.2
1
0.8
0.6
0.4
0.2
1
2
3
4
5
6
7
8
9
10
11
12
13
14

FIG. 12

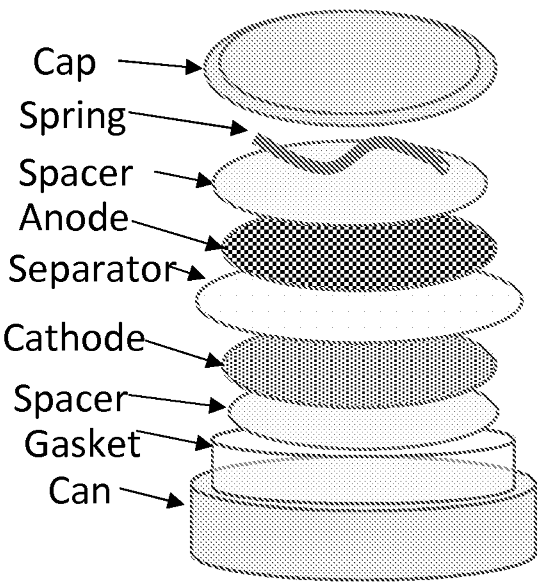
Cap
Spring
Spacer
Anode
Separator
Cathode
Spacer
Gasket
Can

FIG. 13

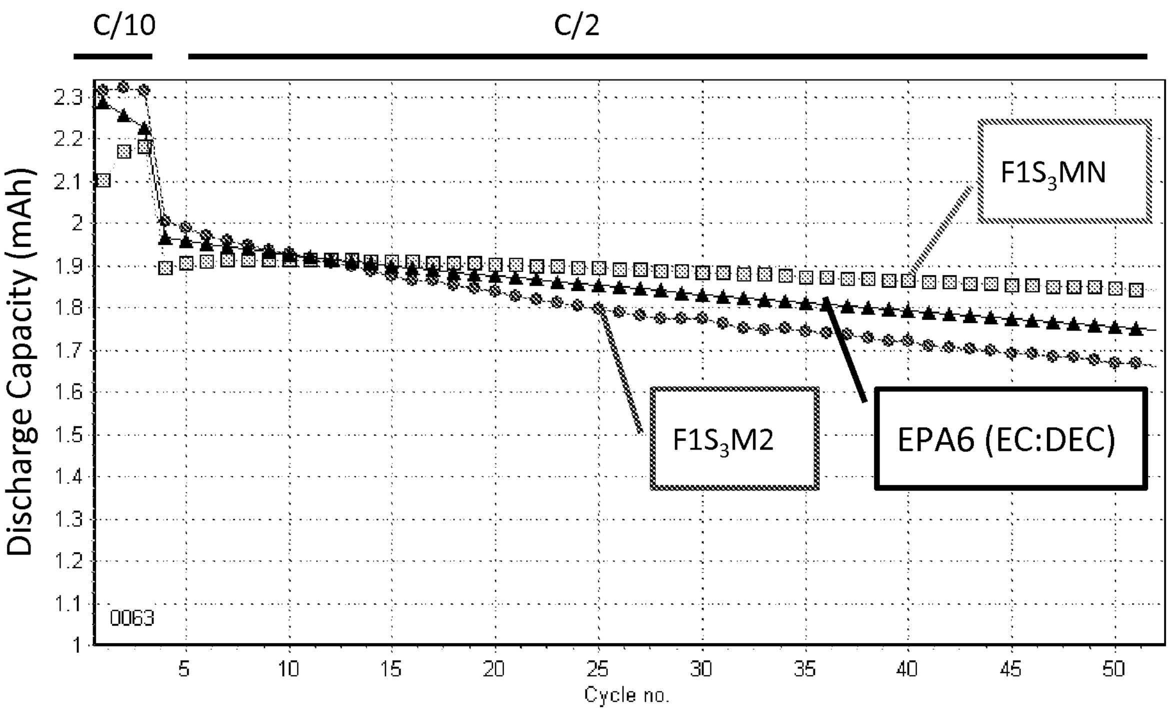
C/10
C/2
Discharge Capacity (mAh)
2.3
2.2
2.1
2
1.9
1.8
1.7
1.6
1.5
1.4
1.3
1.2
1.1
1
5
10
15
20
25
30
35
40
45
50
Cycle no.
0063
F1S3MN
F1S3M2
EPA6 (EC:DEC)

FIG. 14

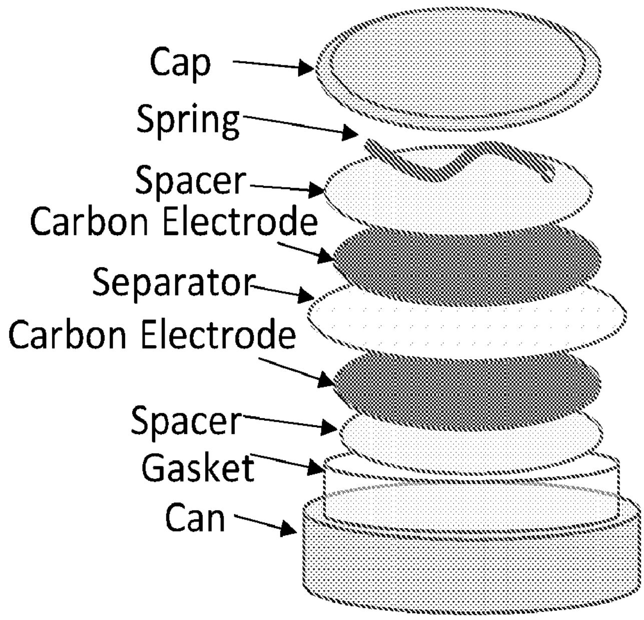
Cap
Spring
Spacer
Carbon Electrode
Separator
Carbon Electrode
Spacer
Gasket
Can

FIG. 15

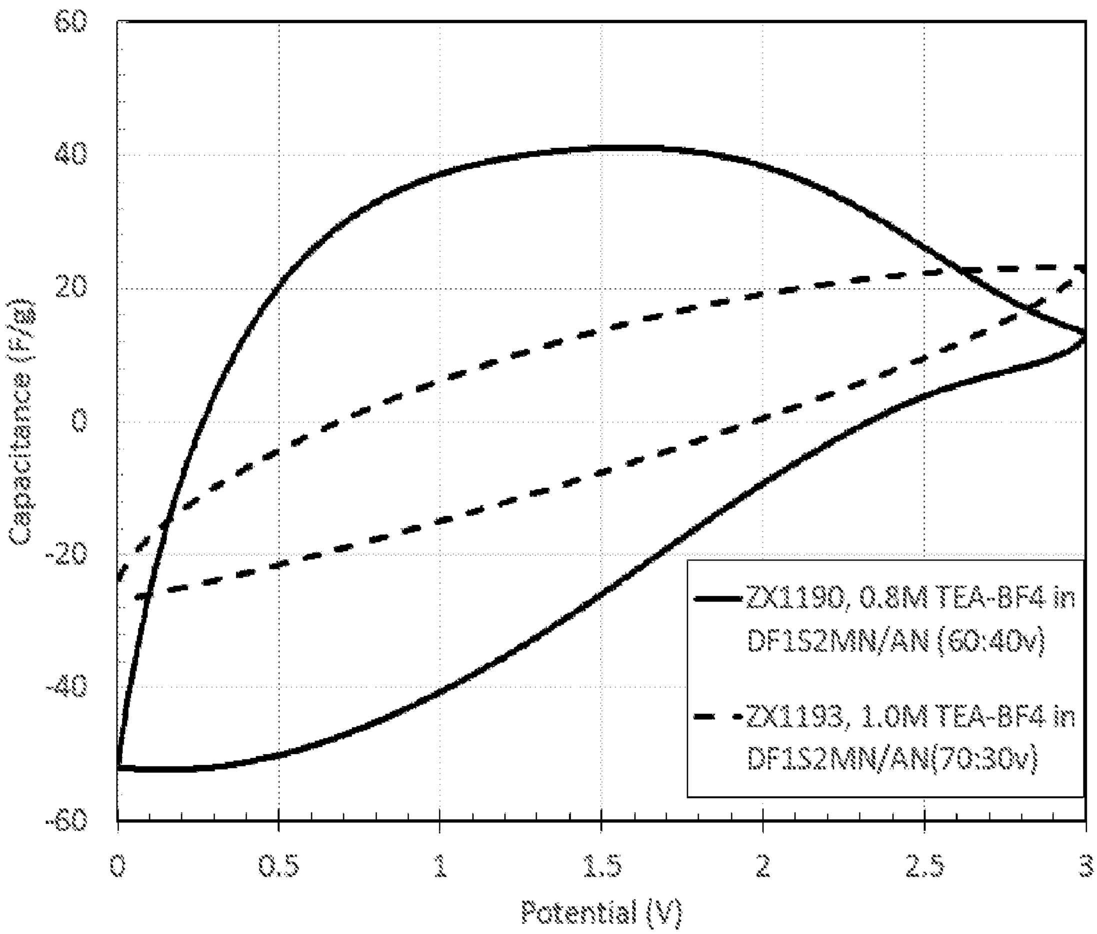
60
40
20
0
-20
-40
-60
Capacitance (F/g)
0
0.5
1
1.5
2
2.5
3
Potential (V)
ZX1190, 0.8M TEA-BF4 in DF1S2MN/AN (60:40v)
ZX1193, 1.0M TEA-BF4 in DF1S2MN/AN(70:30v)

FIG. 16

13/31

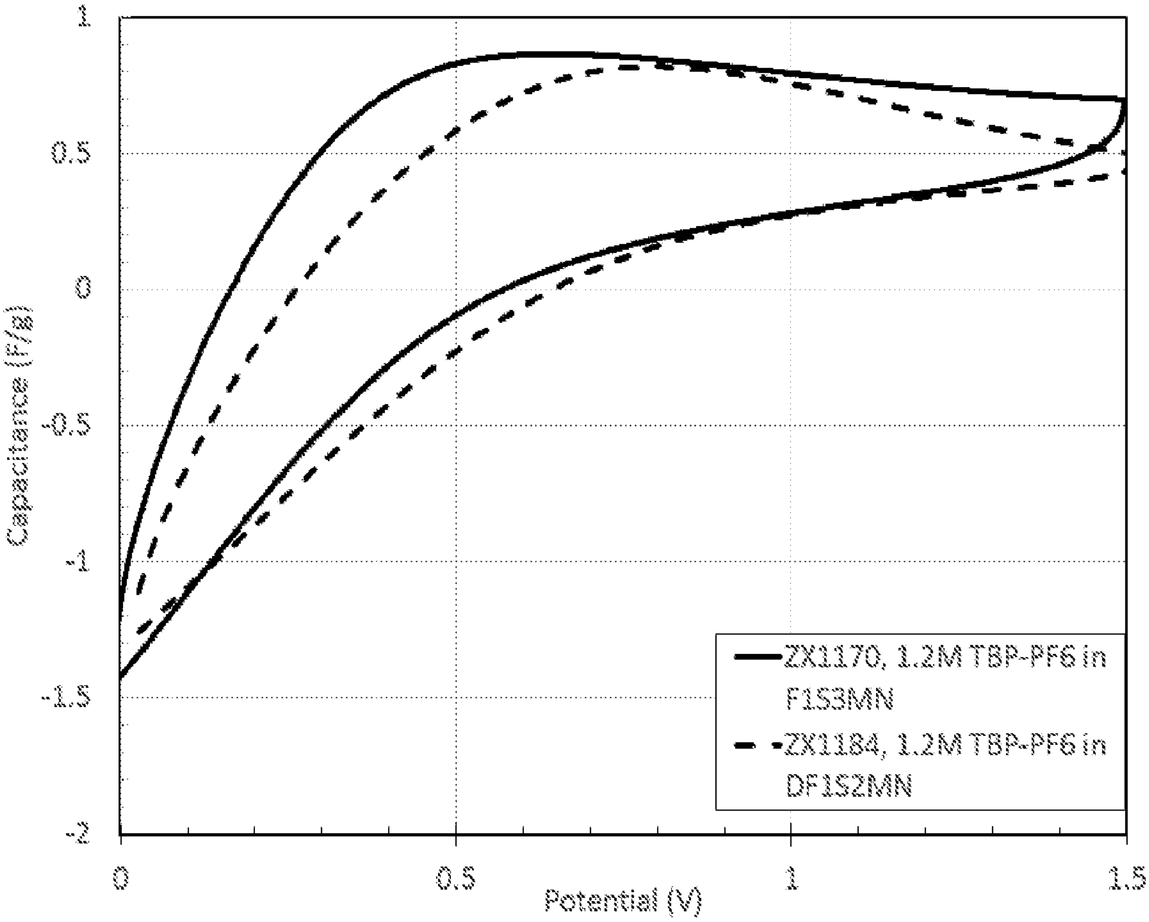
1
0.5
0
-0.5
-1
-1.5
-2
Capacitance (F/g)
0
0.5
1
1.5
Potential (V)
ZX1170, 1.2M TBP-PF6 in F1S3MN
ZX1184, 1.2M TBP-PF6 in DF1S2MN

FIG. 17

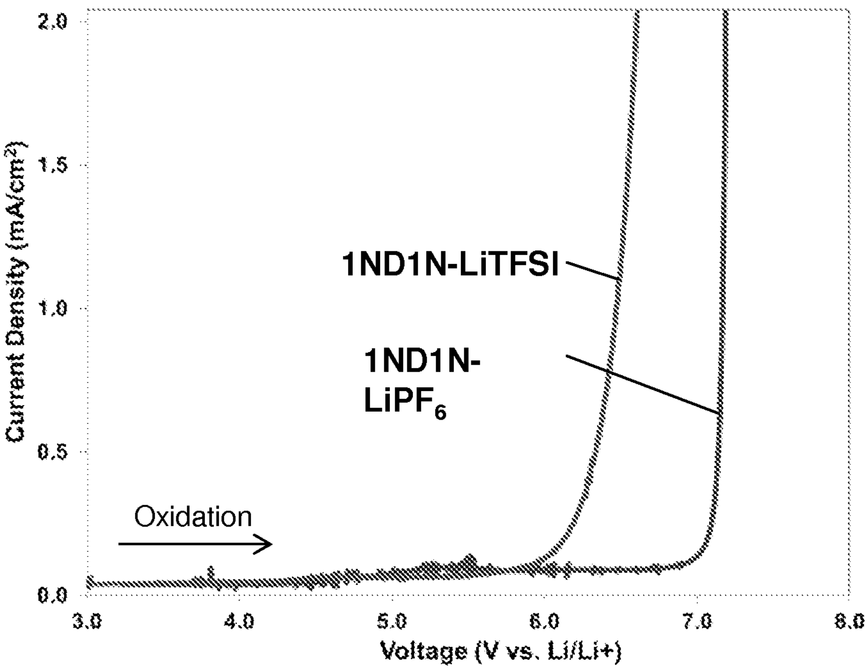
2.0
1.5
1.0
0.5
0.0
Current Density (mA/cm^2)
1ND1N-LiTFSI
1ND1N-
$LiPF_6$
Oxidation
3.0
4.0
5.0
6.0
7.0
8.0
Voltage (V vs. Li/Li+)

FIG. 18

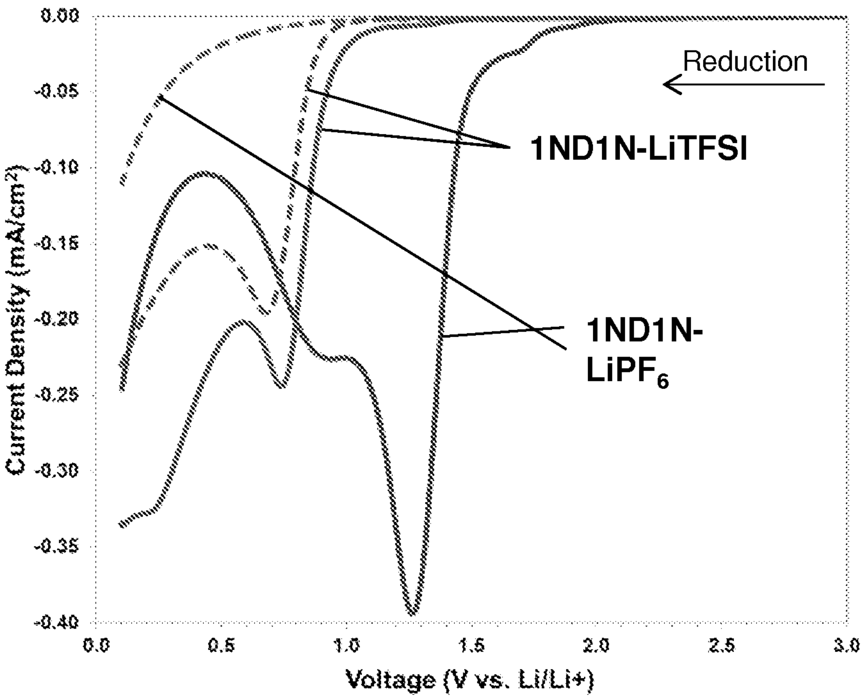
0.00
-0.05
-0.10
-0.15
-0.20
-0.25
-0.30
-0.35
-0.40
Current Density (mA/cm^2)
Reduction
1ND1N-LiTFSI
1ND1N-
$LiPF_6$
0.0
0.5
1.0
1.5
2.0
2.5
3.0
Voltage (V vs. Li/Li+)

FIG. 19

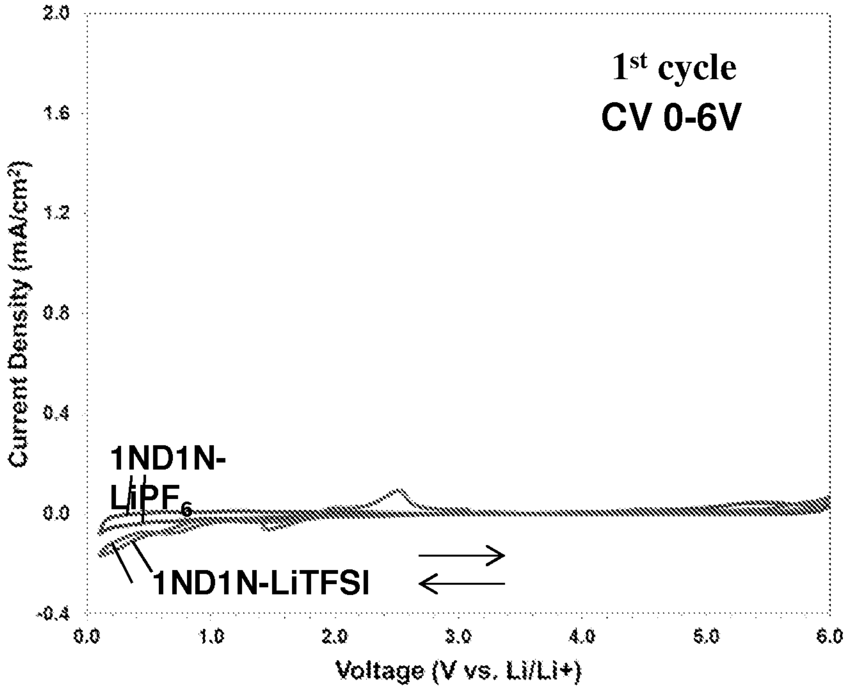

FIG. 20A

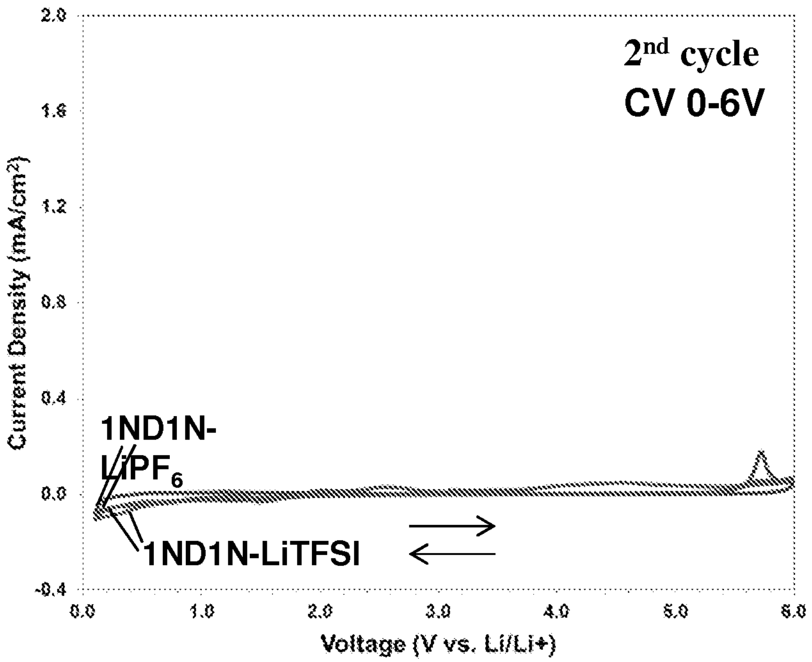

FIG. 20B

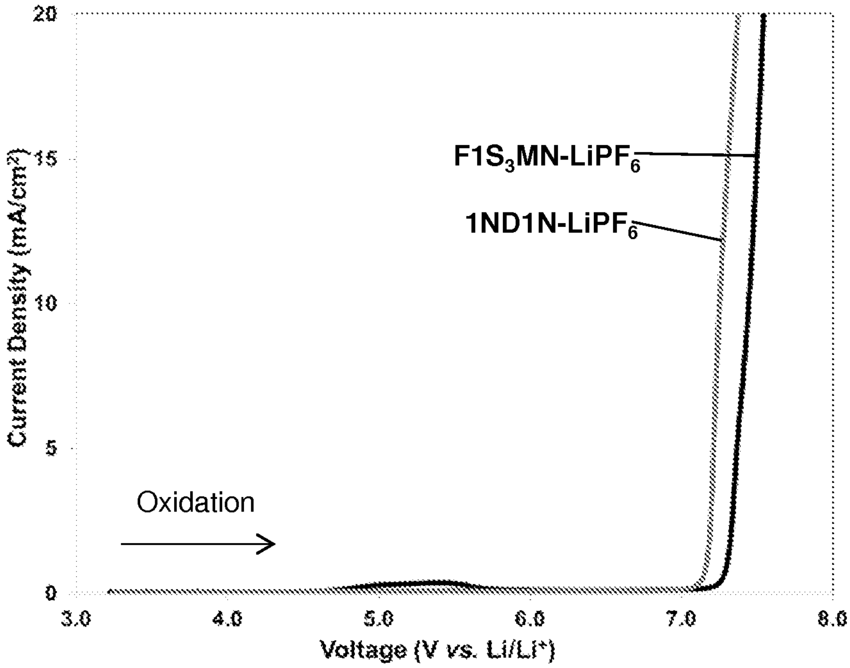

FIG. 21A

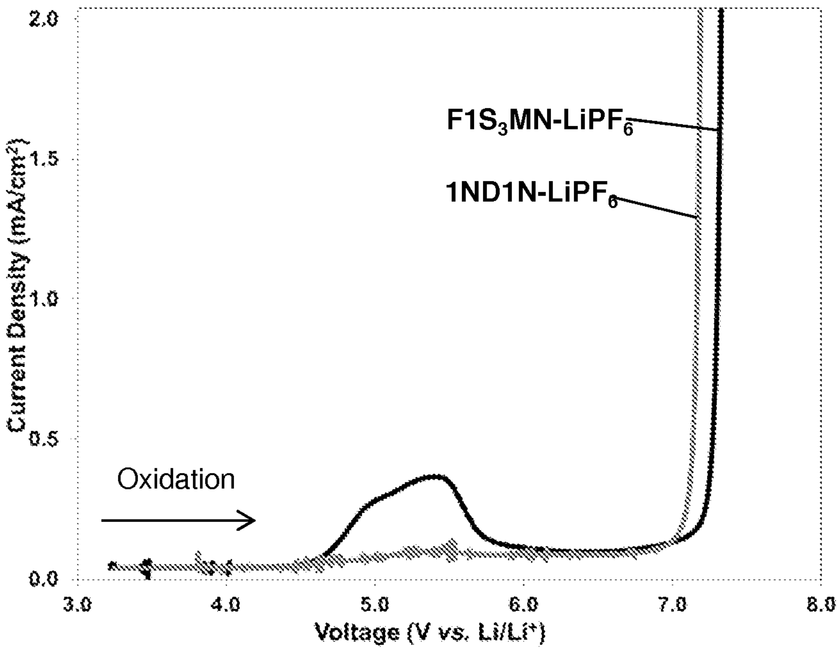

FIG. 21B

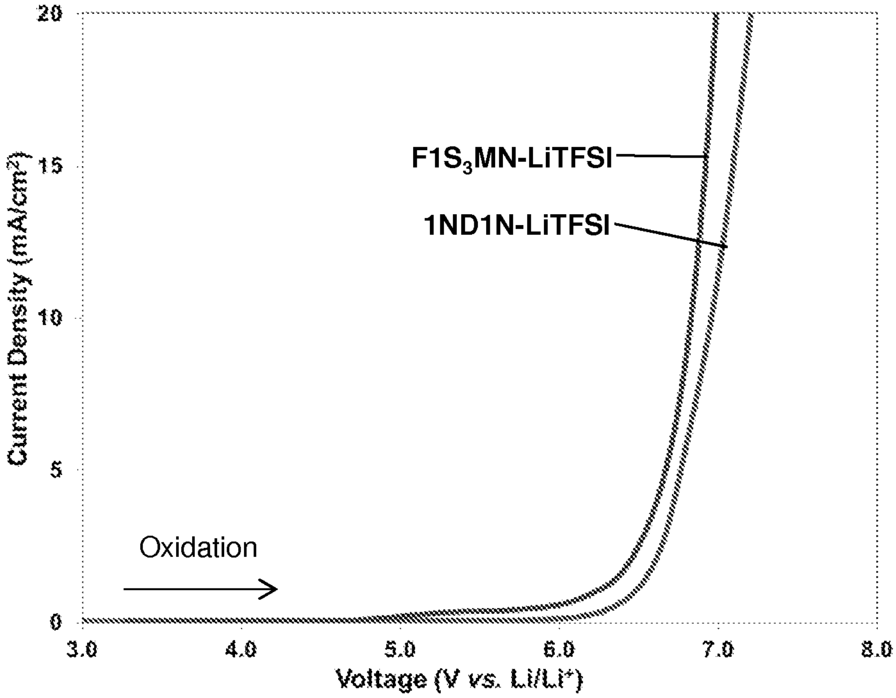

FIG. 22A

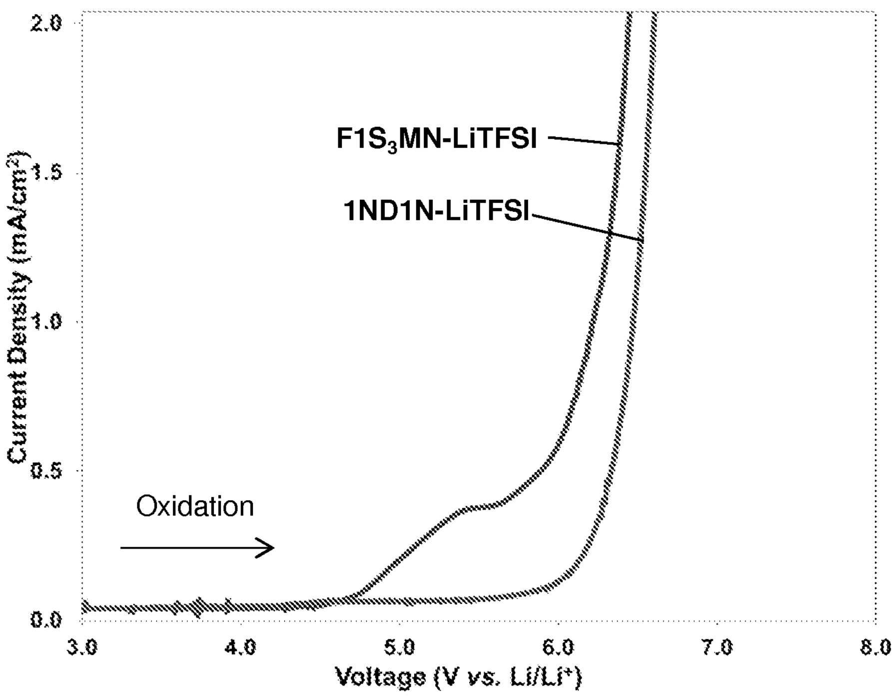

FIG. 22B

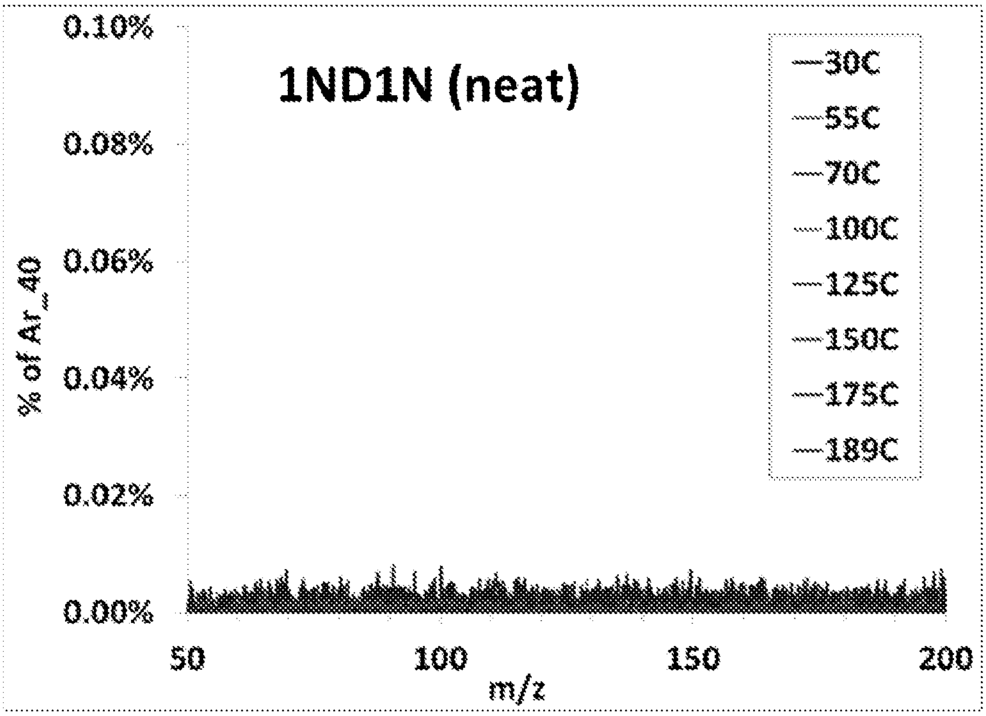
1ND1N (neat)
0.10%
0.08%
0.06%
0.04%
0.02%
0.00%
% of Ar_40
50
100
150
200
m/z
30C
55C
70C
100C
125C
150C
175C
189C

FIG. 23

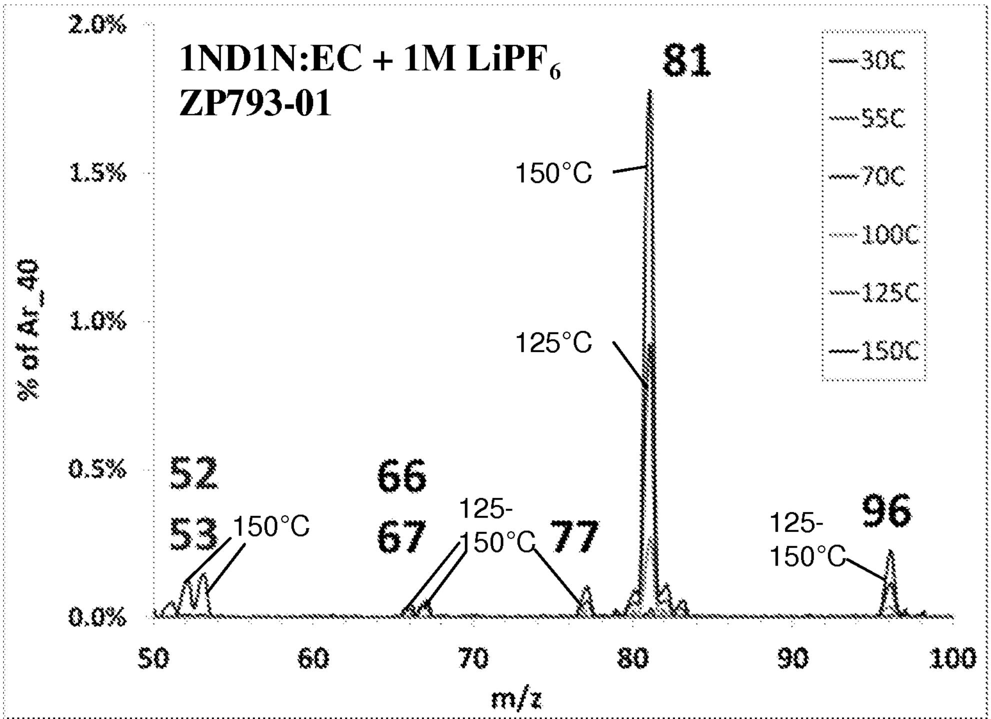
1ND1N:EC + 1M LiPF6
ZP793-01
81
150°C
125°C
52
53
150°C
66
67
125-
150°C
77
125-
150°C
96
2.0%
1.5%
1.0%
0.5%
0.0%
% of Ar_40
50
60
70
80
90
100
m/z
30C
55C
70C
100C
125C
150C

FIG. 24

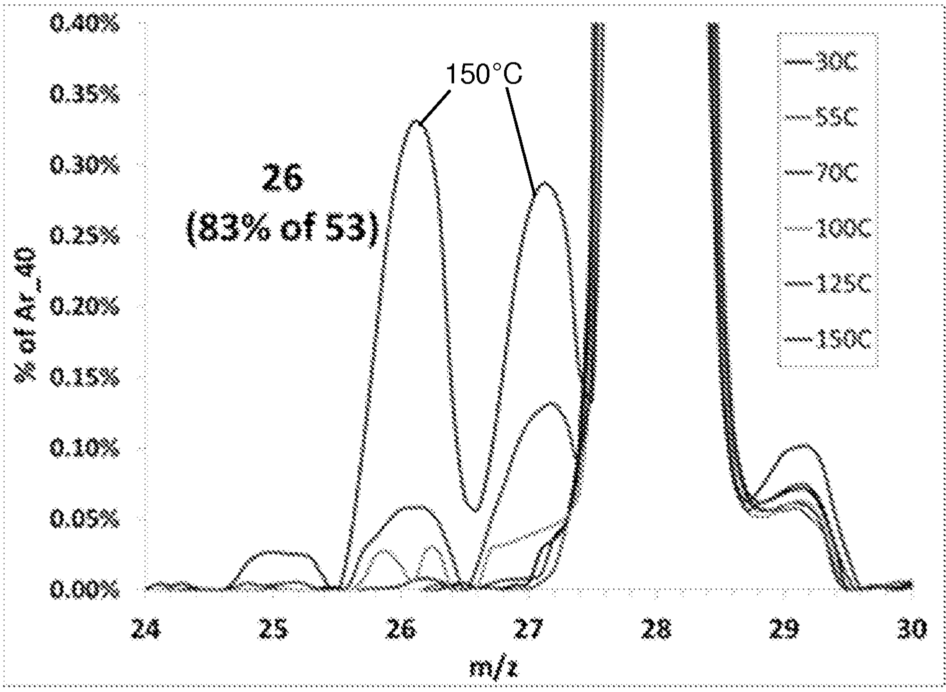

FIG. 25A

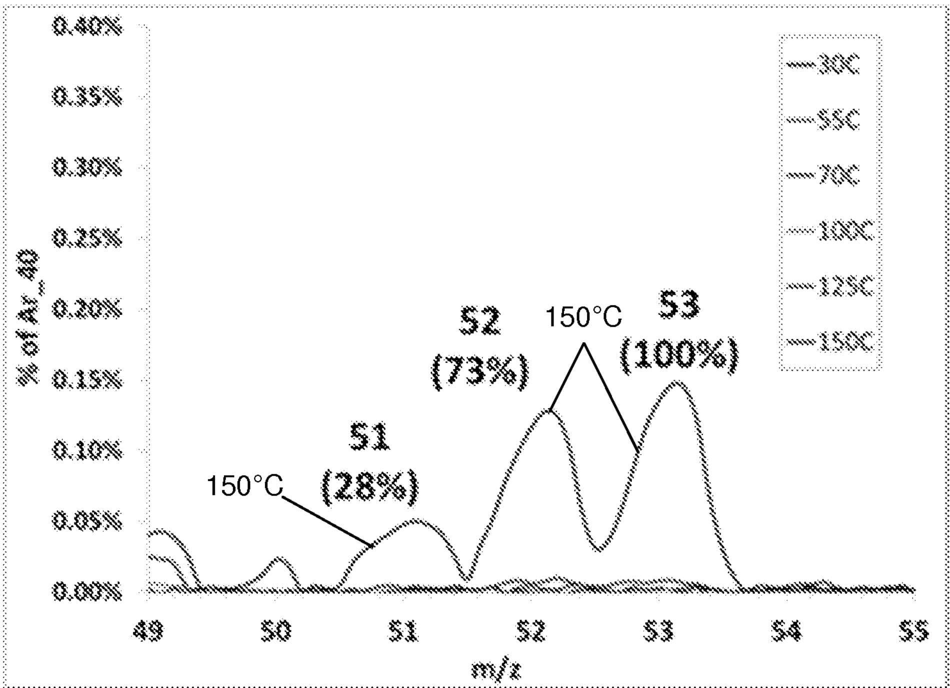

FIG. 25B

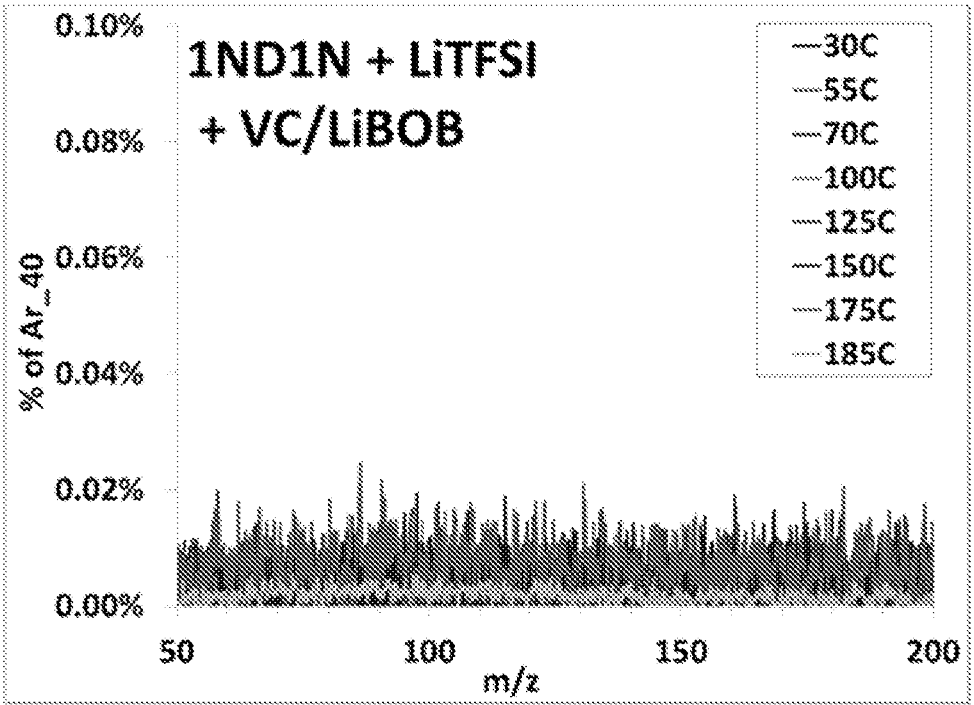
1ND1N + LiTFSI
+ VC/LiBOB
30C
55C
70C
100C
125C
150C
175C
185C
0.10%
0.08%
0.06%
0.04%
0.02%
0.00%
% of Ar_40
50
100
150
200
m/z

FIG. 26

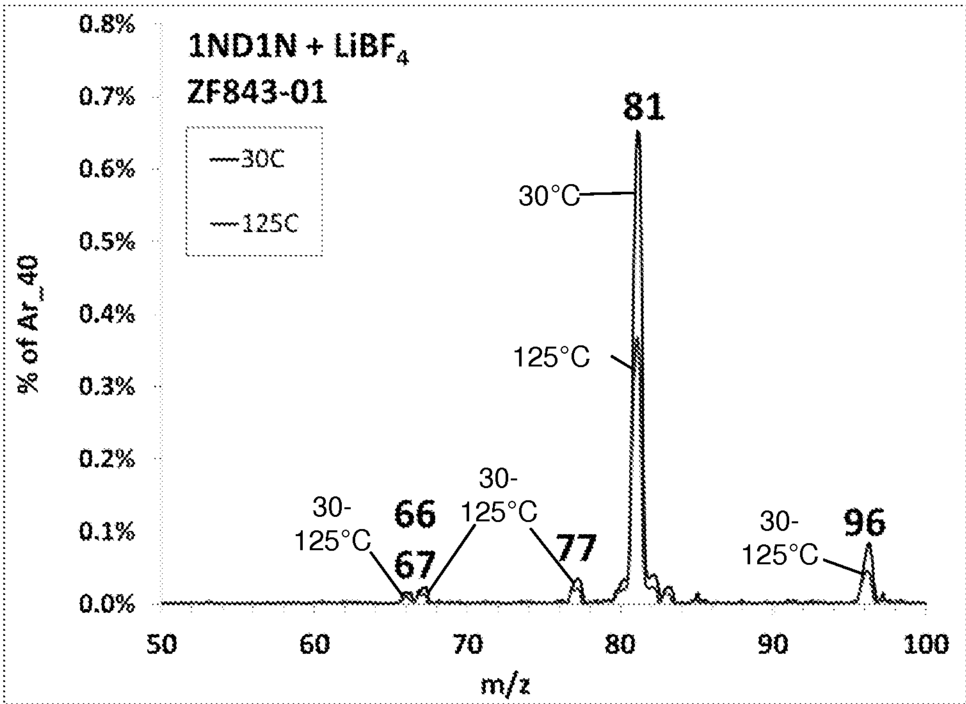
1ND1N + LiBF4
ZF843-01
30C
125C
81
30°C
125°C
30-
125°C
66
67
30-
125°C
77
30-
125°C
96
0.8%
0.7%
0.6%
0.5%
0.4%
0.3%
0.2%
0.1%
0.0%
% of Ar_40
50
60
70
80
90
100
m/z

FIG. 27

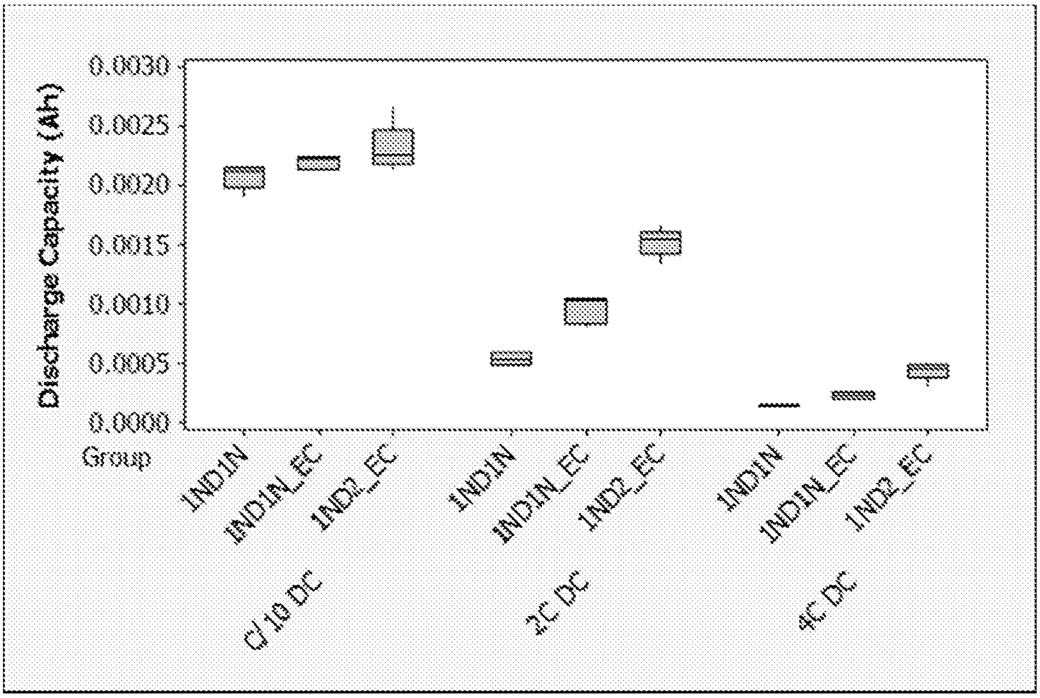
Discharge Capacity (Ah)
0.0030
0.0025
0.0020
0.0015
0.0010
0.0005
0.0000
Group
1ND1N
1ND1N_EC
1ND2_EC
1ND1N
1ND1N_EC
1ND2_EC
1ND1N
1ND1N_EC
1ND2_EC
c/ 10 DC
2C DC
4C DC

FIG. 28

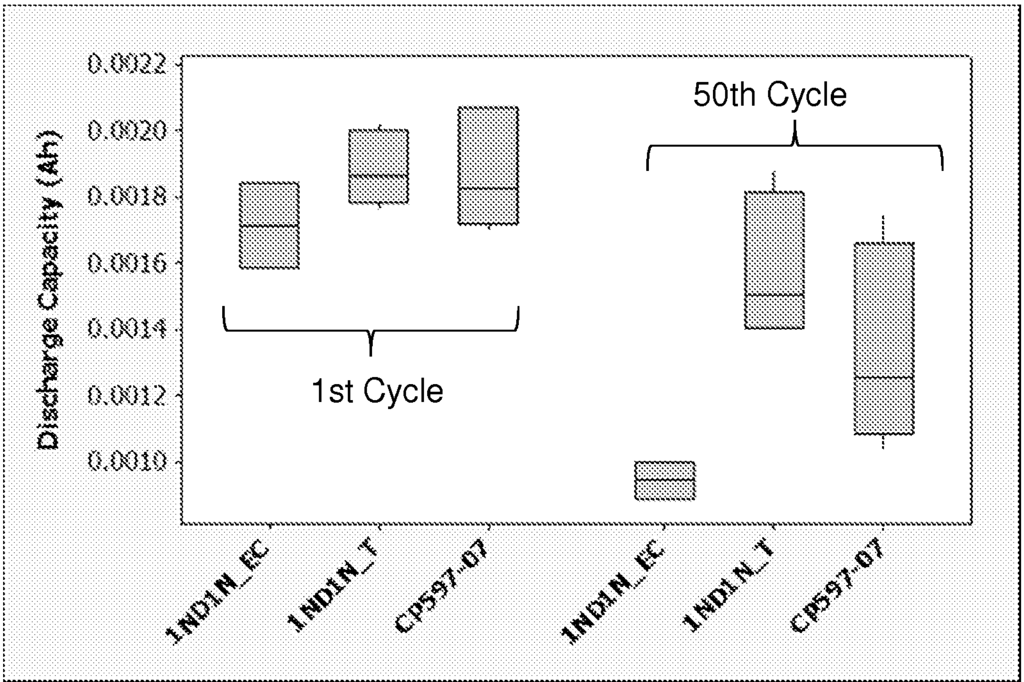
Discharge Capacity (Ah)
0.0022
0.0020
0.0018
0.0016
0.0014
0.0012
0.0010
50th Cycle
1st Cycle
1ND1N_EC
1ND1N_T
CP597-07
1ND1N_EC
1ND1N_T
CP597-07

FIG. 29

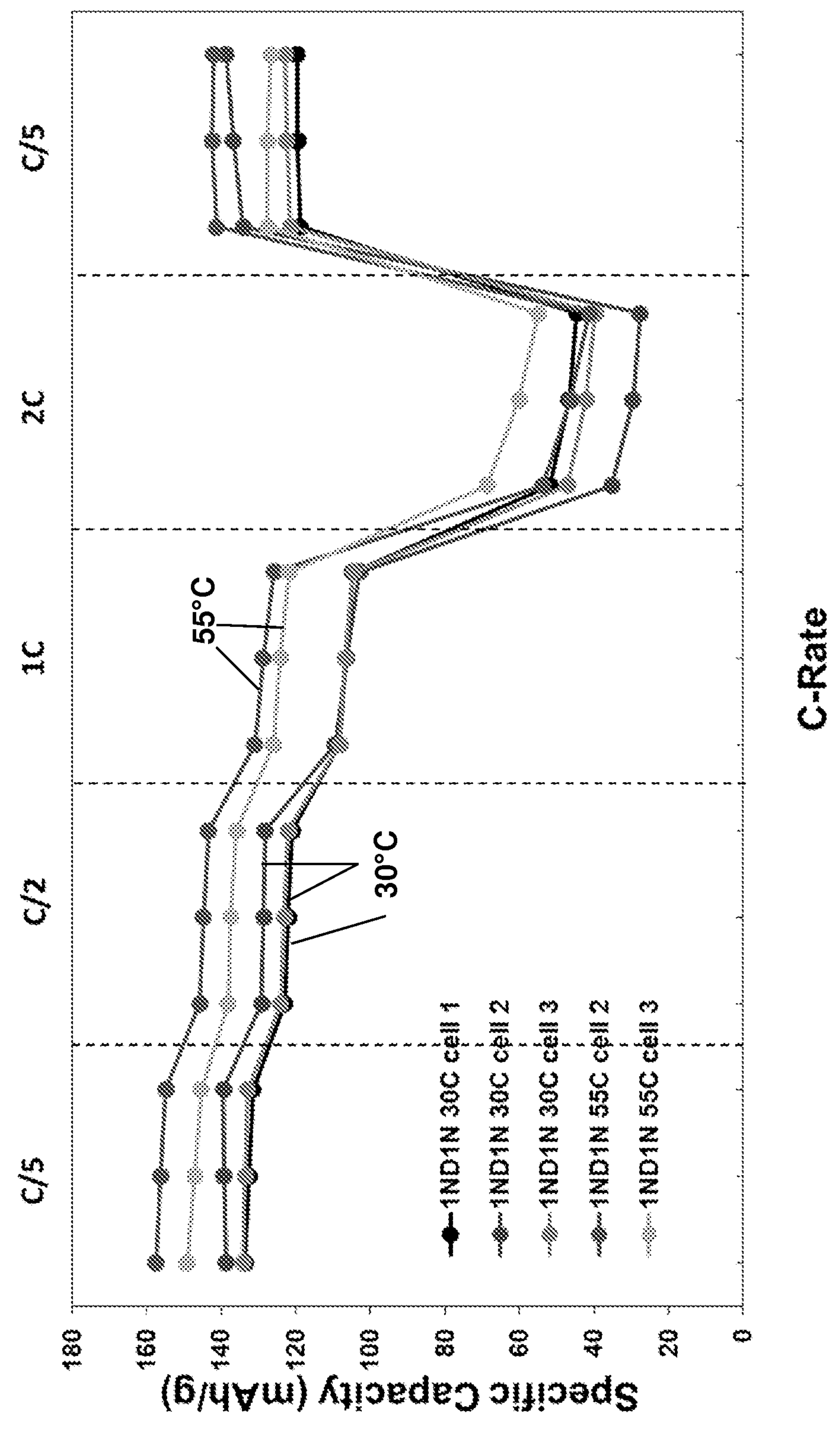
Specific Capacity (mAh/g)
180
160
140
120
100
80
60
40
20
0
C/5
C/2
1C
2C
C/5
55°C
30°C
1ND1N 30C cell 1
1ND1N 30C cell 2
1ND1N 30C cell 3
1ND1N 55C cell 2
1ND1N 55C cell 3
C-Rate

FIG. 30A

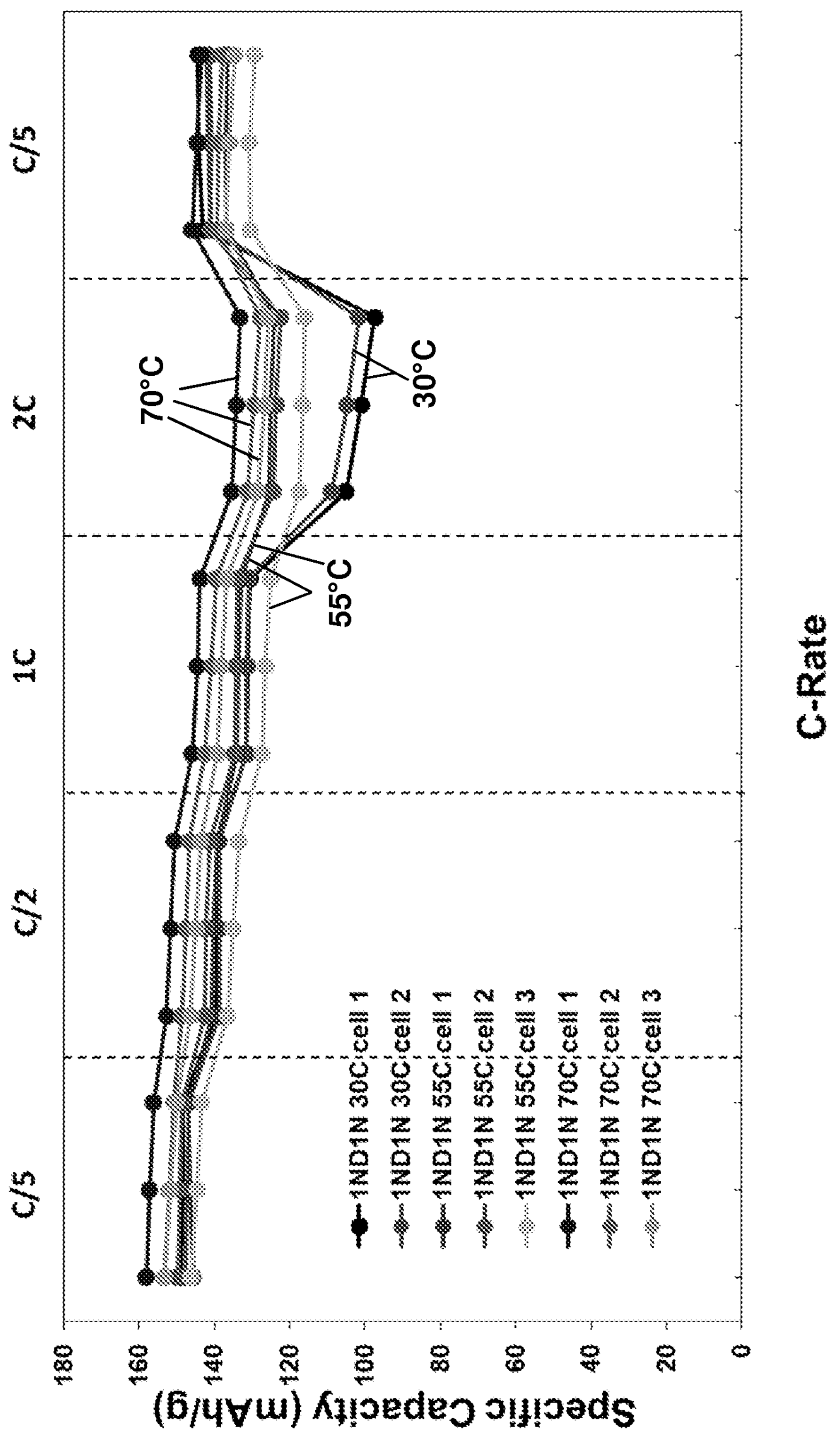
C/5
C/2
1C
2C
C/5
70°C
55°C
30°C
1ND1N 30C cell 1
1ND1N 30C cell 2
1ND1N 55C cell 1
1ND1N 55C cell 2
1ND1N 55C cell 3
1ND1N 70C cell 1
1ND1N 70C cell 2
1ND1N 70C cell 3
180
160
140
120
100
80
60
40
20
0
Specific Capacity (mAh/g)
C-Rate

FIG. 30B

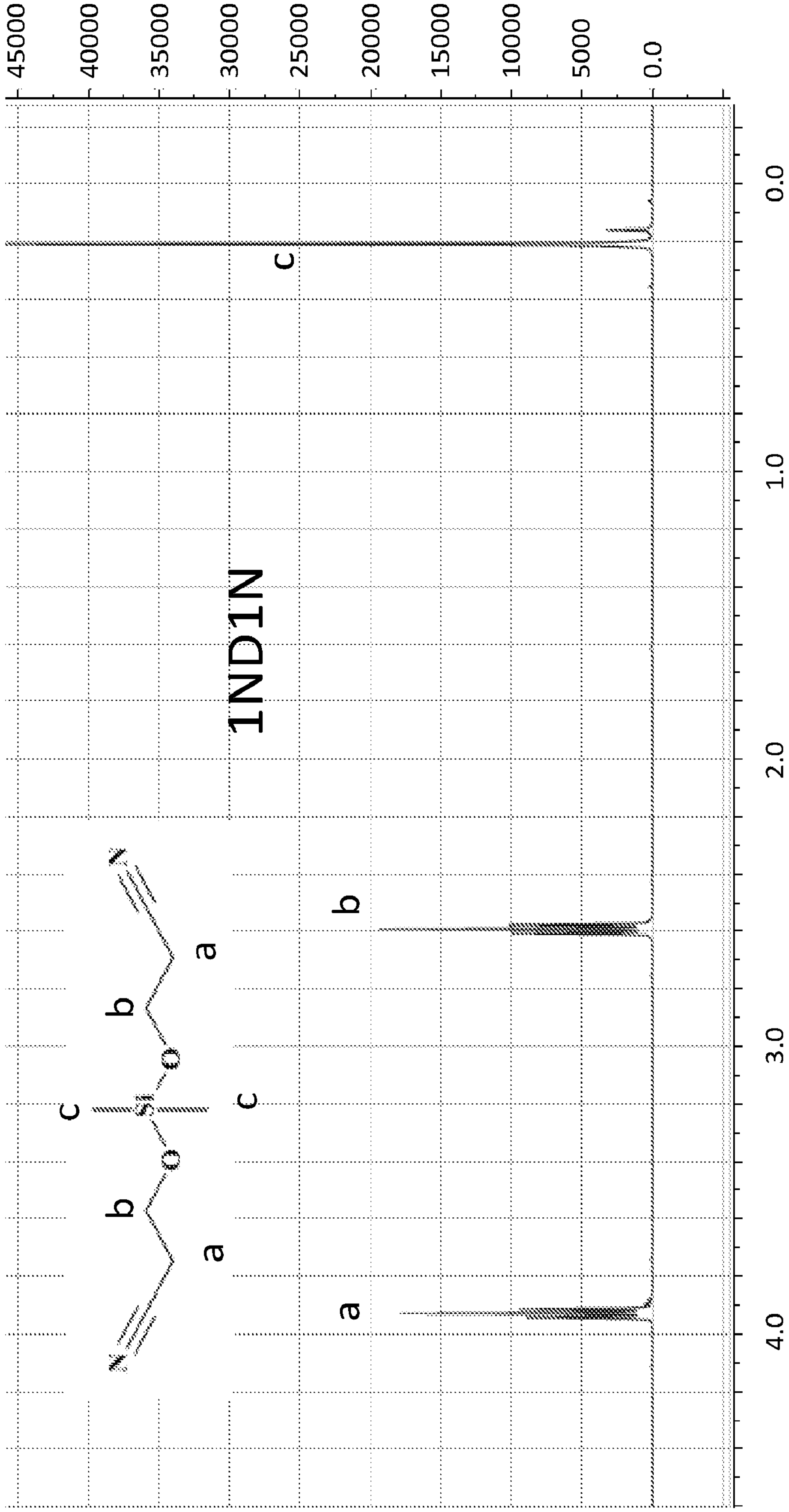
45000
40000
35000
30000
25000
20000
15000
10000
5000
0.0
0.0
1.0
2.0
3.0
4.0
1ND1N
a
b
c
c
b
a
a
b
c

FIG. 31

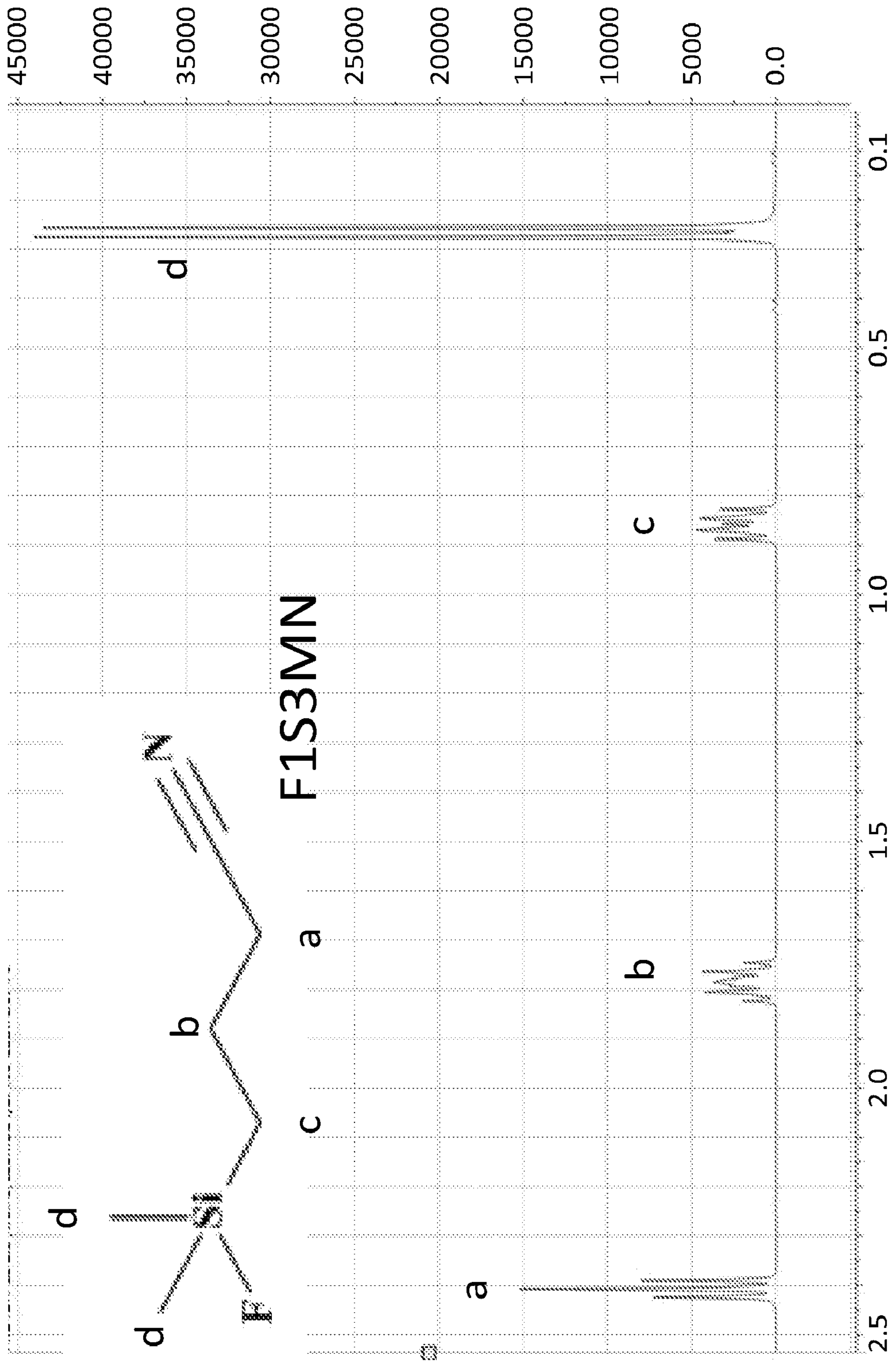
F1S3MN
Si
F
N
a
b
c
d
45000
40000
35000
30000
25000
20000
15000
10000
5000
0.0
0.1
0.5
1.0
1.5
2.0
2.5

FIG. 32

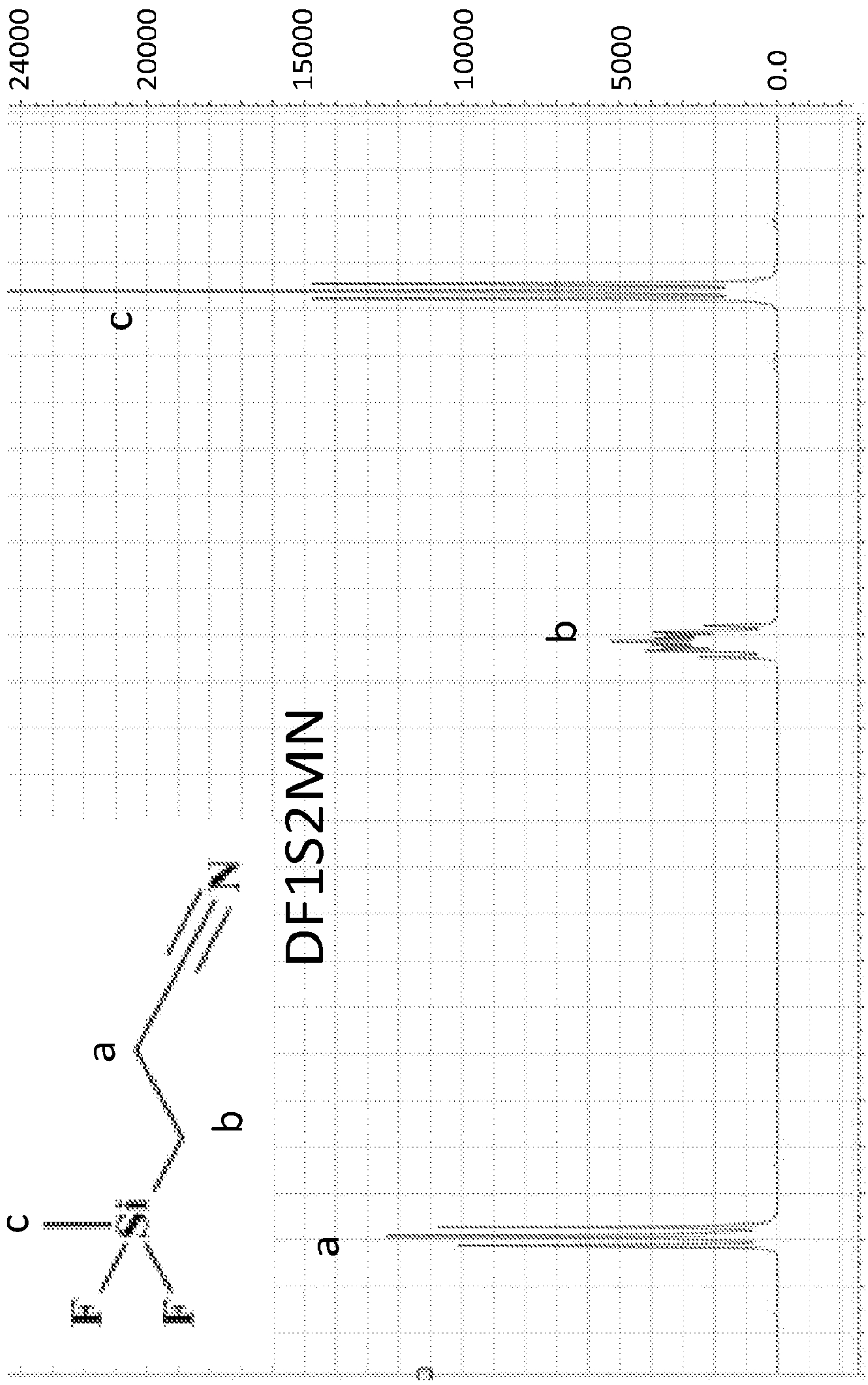
24000
20000
15000
10000
5000
0.0
0.1
0.5
1.0
1.5
2.0
2.5
c
b
a
DF1S2MN
F
Si
N

FIG. 33

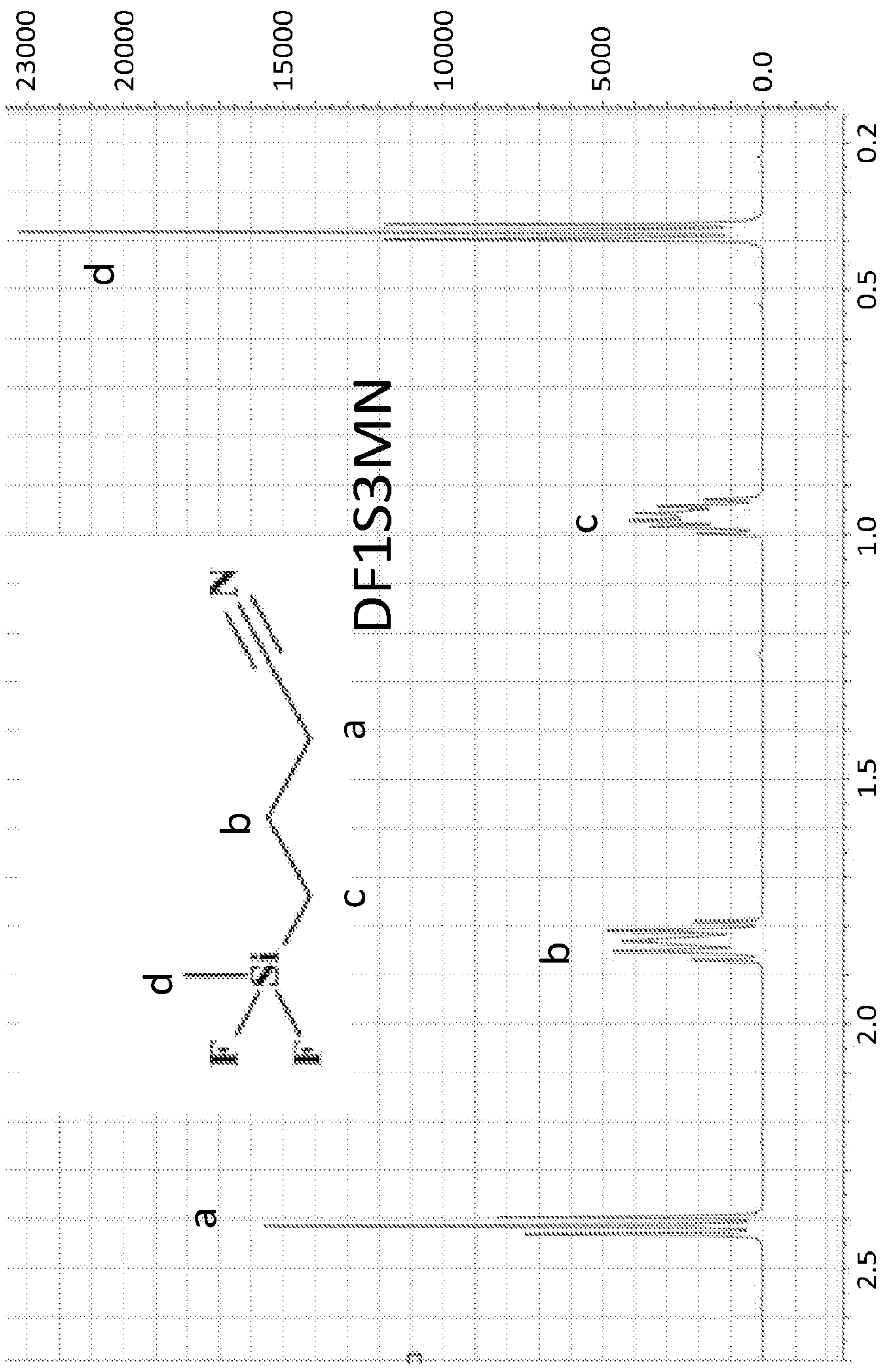
DF1S3MN
d
c
b
a
Si
F
F
N
23000
20000
15000
10000
5000
0.0
0.2
0.5
1.0
1.5
2.0
2.5

FIG. 34

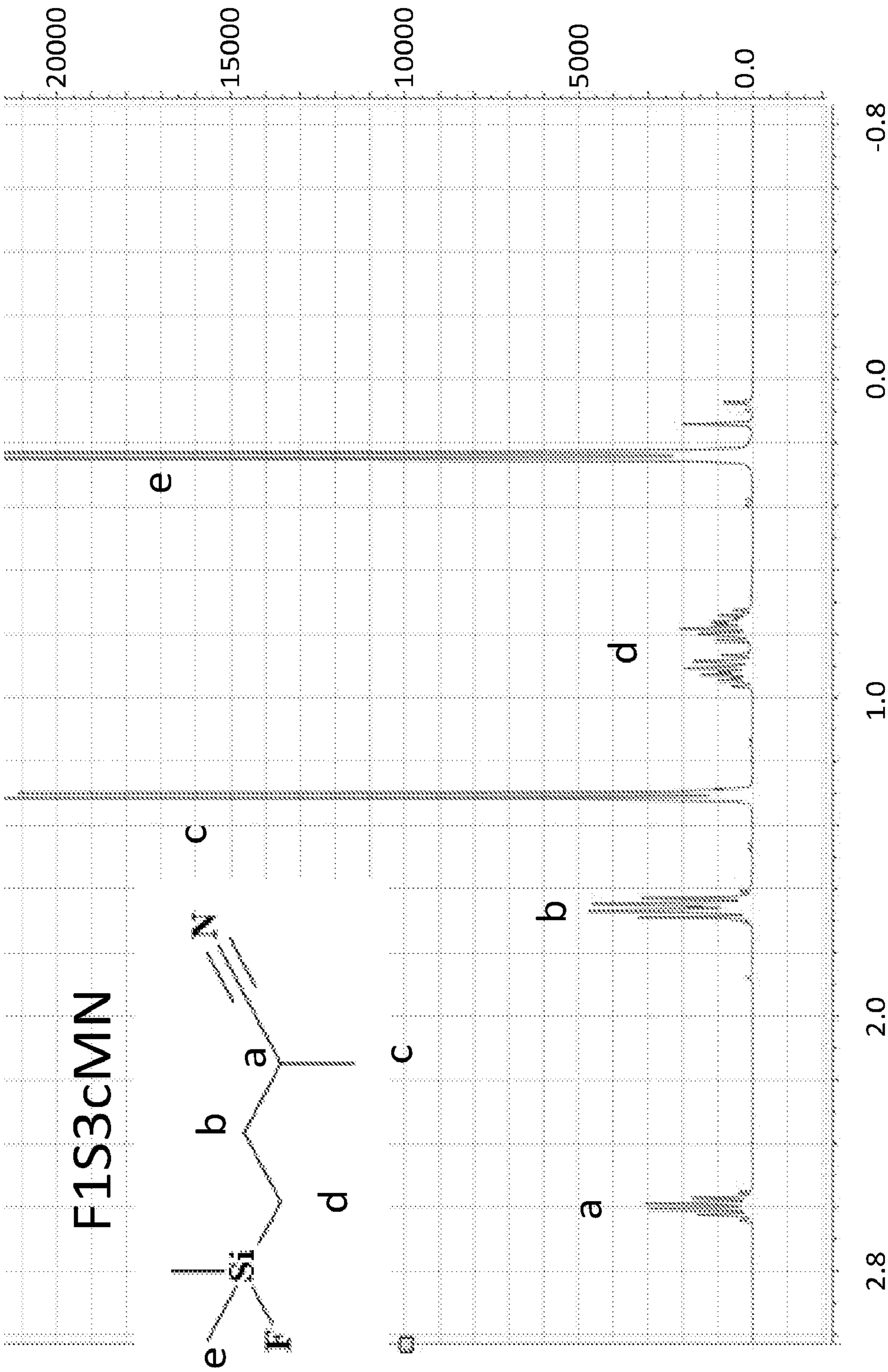

FIG. 35

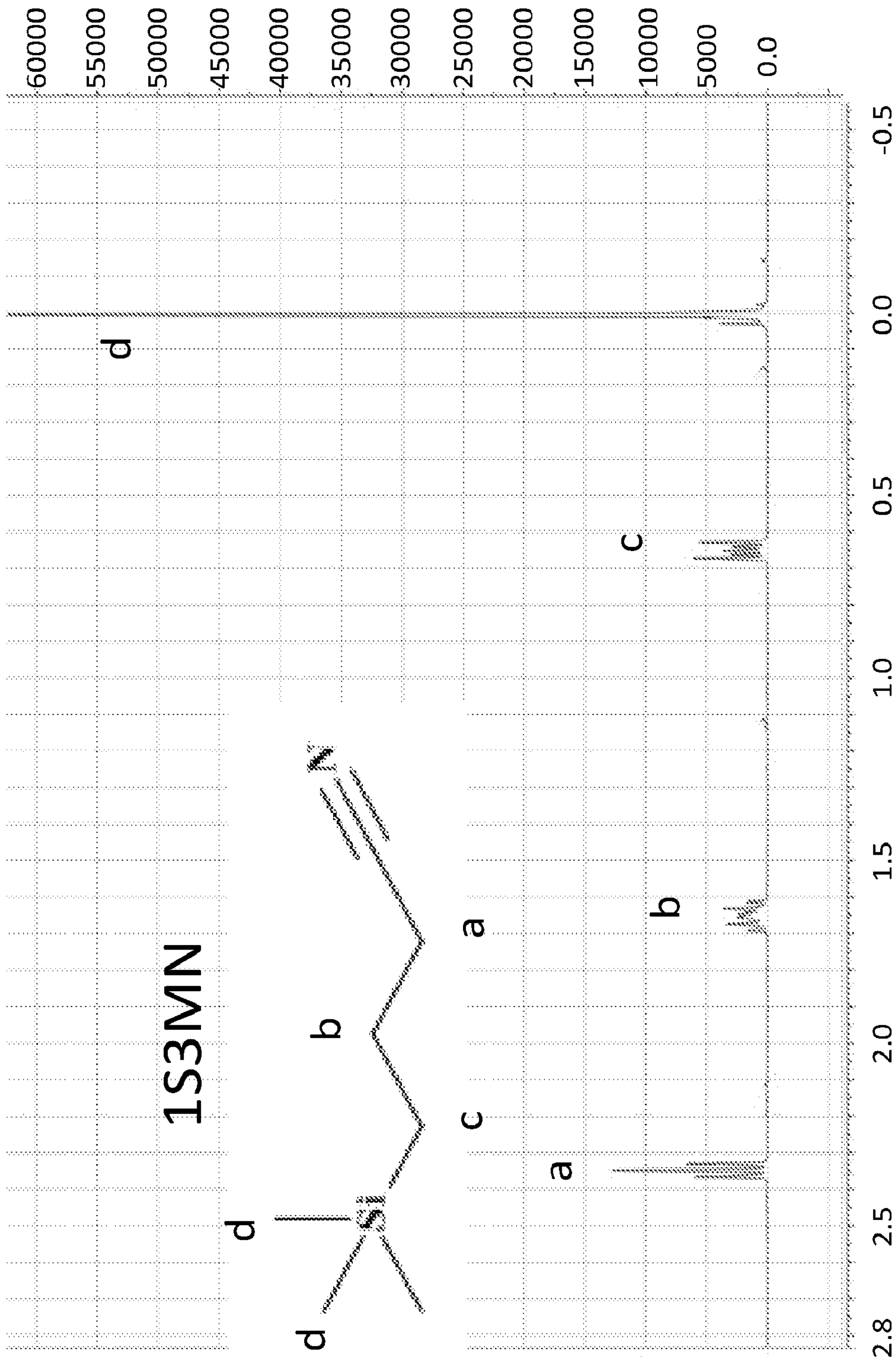
1S3MN
Si
a
b
c
d
60000
55000
50000
45000
40000
35000
30000
25000
20000
15000
10000
5000
0.0
-0.5
0.0
0.5
1.0
1.5
2.0
2.5
2.8

FIG. 36

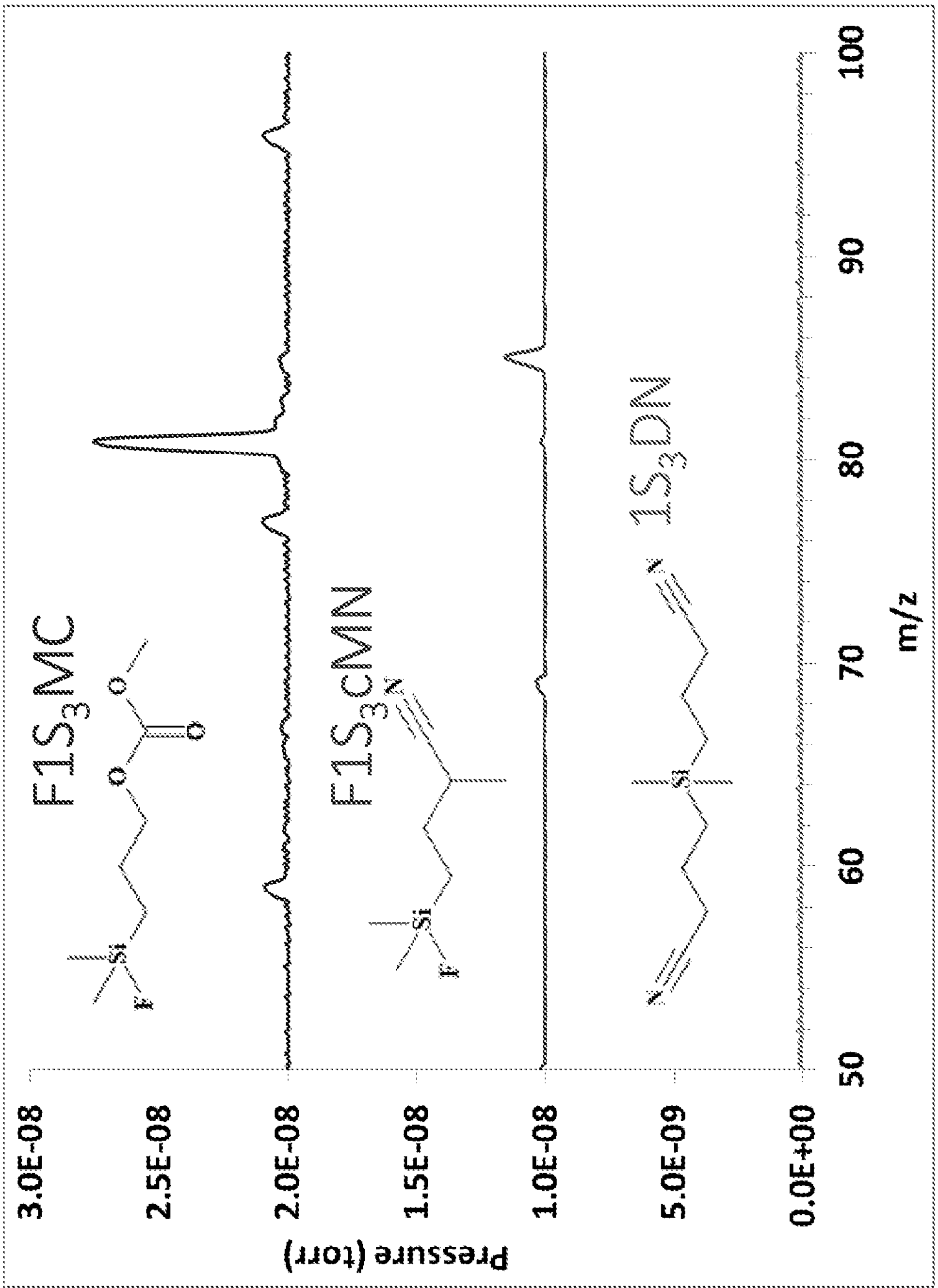
F1S3MC
F1S3cMN
1S3DN
Pressure (torr)
3.0E-08
2.5E-08
2.0E-08
1.5E-08
1.0E-08
5.0E-09
0.0E+00
50
60
70
80
90
100
m/z
Si
F
O
N

FIG. 37

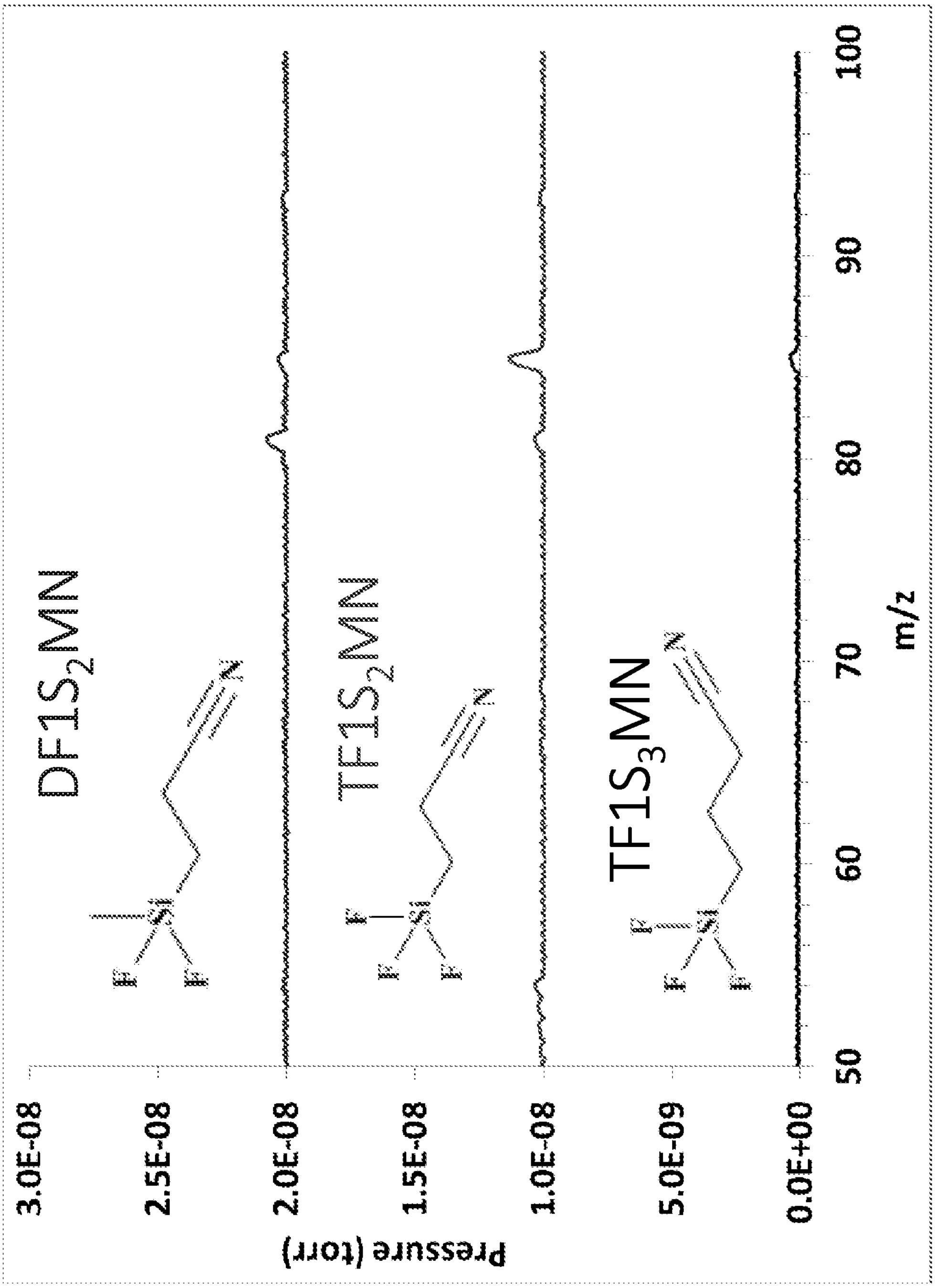
Pressure (torr)
3.0E-08
2.5E-08
2.0E-08
1.5E-08
1.0E-08
5.0E-09
0.0E+00
50
60
70
80
90
100
m/z
DF1S$_2$MN
TF1S$_2$MN
TF1S$_3$MN

FIG. 38

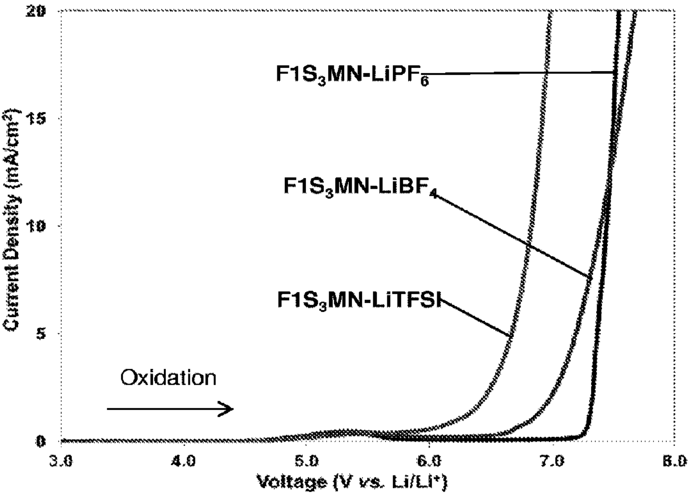

20
15
10
5
0
3.0
4.0
5.0
6.0
7.0
8.0
Current Density (mA/cm^2)
Voltage (V vs. Li/Li$^+$)
F1S$_3$MN-LiPF$_6$
F1S$_3$MN-LiBF$_4$
F1S$_3$MN-LiTFSI
Oxidation